Doctoral Thesis

Coexistence of Wireless Communication and Non-communication Systems

Shota YAMASHITA

Graduate School of Informatics, Kyoto University

March 2018

Preface

This thesis aims to efficiently utilize radio spectrum and tackles coexistence problems of wireless communication and non-communication systems on the assumption that both systems use the same spectrum channel. As the coexistence problem, this thesis presents two main topics. One topic is a microwave power transmission (MPT) system to a wireless local area network (WLAN) station for the batteryless operation of the WLAN station. The other topic is a database-driven spectrum sharing system for the fifth generation (5G) mobile networks.

The first topic focuses on the co-channel operation of MPT and IEEE 802.11-based data transmission. To avoid harmful interference to the WLAN station, where the harmful interference is caused by exposure of the station to microwave radiation for MPT, this work proposes two schemes. One scheme is a scheduling scheme, which allocates time for MPT and IEEE 802.11-based data transmission. In this scheme, on the basis of the time information within data and beacon frame transmissions, microwaves for MPT are transmitted except when these frames are transmitted. The other scheme is a rate adaptive scheme (RAS) based on exposure assessment with a rectenna output, where the rectenna is the element that has been installed in the device powered with MPT. The devices, on which this scheme is implemented, determine the next PHY data rate using historical information (e.g., data frame loss ratio) corresponding to the assessment result. These proposed schemes are verified by performing experiments with commercial WLAN devices in a radio frequency anechoic chamber.

The second topic focuses on the operation of a secondary user (SU) with communication capability in the channel allocated to a primary user (PU) with non-communication capability such as a radar system. On the constraint that a PU does not experience harmful interference from SUs, this thesis adopts a primary exclusive region (PER), within which SUs are prohibited to transmit, and describes two types of the works related to PER design. One is to present a framework for updating a PER and to design a circular PER centered at a PU. The other is to design a complex-shaped PER by introducing two spatial grids, i.e., polar and square grids. In both cases, the aggregate interference is analyzed on the assumption that SUs are distributed following a Poisson point process. Numerical results show that the more detailed database information, which is related to a PU and SU, leads to a smaller PER.

The chapters of this thesis are listed as follows. Chapters 2 explains the related technologies of this work such as MPT, WLAN, and stochastic geometry. Chapters 3 and 4 describe the first topic related to the MPT system to a single WLAN station. Chapter 3 proposes a scheduling scheme that allocates time for MPT and WLAN data transmissions. Chapter 4 proposes a RAS based on exposure assessment with rectenna output for a WLAN station exposed to microwave radiation for MPT. To verify the proposed schemes, these chapters perform the experiments that microwaves are intermittently transmitted to an IEEE 802.11g-based commercial WLAN device. Chapters 5 and 6 describe the second topic related to the spectrum sharing system with a spectrum database. Chapter 5 presents a framework for updating a circular PER with stochastic geometry approach. Chapter 6 presents a stochastic geometry analysis for a spatial grid-based spectrum database system and designs a complex-shaped PER. These chapters present stochastic geometry analysis of the aggregate interference at a PU, and then designs a PER by solving an optimization problem.

Acknowledgements

First of all, I would like to express my sincere gratitude to my supervisor, Professor Masahiro Morikura, for his continuous support and guidance in my research. Without his persistent help and constant encouragement, this work would have never been completed.

I would like to express my great gratitude to Associate Professor Koji Yamamoto and Assistant Professor Takayuki Nishio, who are members of Integrated-Media Communications Laboratory of Graduate School of Informatics, Kyoto University. Their constructive feedbacks and discussions have helped my work.

I would like to express my deep appreciation to Professor Hiroshi Harada and Professor Eiji Oki of Graduate School of Informatics, Kyoto University for valuable advice and incisive comments. Their advice and comments have been a great help in improving this thesis.

I would like to express my appreciation to the people related to the experiments of Chapters 3 and 4. Professor Naoki Shinohara of Research Institute for Sustainable Humanosphere, Kyoto University, gave me technical advice and comments about microwave power transmission. Mr. Takuya Ichihara, Mr. Yong Huang, Mr. Norikatsu Imoto, and Mr. Koichi Sakaguchi helped me to perform the experiments.

I would like to thank to laboratory secretaries and student members of Integrated-Media Communications Laboratory of Graduate School of Informatics, Kyoto University.

Finally, I would like to thank my parents and family for their support and encouragement throughout my work.

Contents

List of Figures

List of Tables

Notations

Notation	Description
$\mathbb{R}$	Real numbers
$\emptyset$	Empty set
$\setminus$	Difference of sets
$b(x, r)$	Closed disk centered at x with radius r
$\|x\|$	Euclidean distance between origin and $x \in \mathbb{R}^2$
$\|B\|$	Area of compact set $B \subset \mathbb{R}^2$
$N(B)$	Number of points on compact set $B \subset \mathbb{R}^2$
$\mathbb{E}_X(f(X))$	Mean of function $f(X)$ of random variable X defined as $\mathbb{E}_X(f(X)) = \int_{-\infty}^{\infty} f(x)p_X(x)\,\mathrm{d}x$, where p_X is probability density function of X
$\mathbb{P}(A)$	Probability of event A occurring
$M_X(s)$	Moment generating function of random variable X defined as $M_X(s) = \mathbb{E}_X(\mathrm{e}^{sX})$
$\kappa_n(X)$	nth cumulant of random variable X defined as $\kappa_n(X) = \frac{\mathrm{d}^n}{\mathrm{d}s^n} \ln M_X(s)\big\|_{s=0}$

Abbreviations

Abbreviation	Description
5G	fifth generation
ACK	acknowledgment
AP	access point
ATP	allowable transmission probability
BPSK	binary phase shift keying
CCDF	complementary cumulative distribution function
CF	characteristic function
CSMA/CA	carrier sense multiple access with collision avoidance
DR	data receiver
DT	data transmitter
DTIM	delivery traffic indication map
EIRP	equivalent isotropically radiated power
ES	energy source
GD	gamma distribution
IPOPT	interior point optimizer
ISM	industry-science-medical
IoT	Internet of Things
LBT	listen-before-talk
LSA	lisences shared access
LT	Laplace transform
LTEA	long-term evolution advanced
MAC	medium access control
MGF	moment generating function
MPT	microwave power transmission

OFDM	orthogonal frequency division multiplexing
OP	outage probability
PDF	probability density function
PER	primary exclusive region
PGFL	probability generating functional
PHY	physical
PMSE	Programme Making and Special Events
PPP	Poisson point process
PR	primary receiver
PU	primary user
QAM	quadrature amplitude modulation
QPSK	quadrature phase shift keying
RAS	rate adaptation scheme
SINR	signal-to-interference-plus-noise power ratio
SLND	shifted log-normal distribution
SNR	signal-to-noise power ratio
SS	sensor station
ST	secondary transmitter
SU	secondary user
TD-LTE	time-division long-term evolution
UDP	user datagram protocol
WLAN	wireless local area network
WSN	wireless sensor network

Chapter 1

Introduction

1.1 Background

Wireless communication technologies have rapidly and dramatically evolved in the last few decades, and everybody benefits from them. Recently, next-generation wireless communication technologies have been discussed. For example, the fifth generation (5G) mobile communication systems aim to achieve the objectives such as higher system capacity, higher data rate, and massive device connectivity [1, 2].

As these technologies evolve, the shortage of the wireless spectrum, over which one wireless device transmits data to another device, becomes a problem [3]. In general, when multiple wireless devices use the same spectrum channel simultaneously, co-channel interference occurs. Specifically, the aggregate interference at a receiver increases, signal-to-interference-plus-noise power ratio (SINR) becomes below the desired value, and then the receiver fails to receive the signal destined for itself. To avoid co-channel interference, for example, the carrier sense multiple access with collision avoidance (CSMA/CA) protocol is employed in a wireless local area network (WLAN) [4]; however, the conventional scheme cannot support a huge number of wireless devices.

To overcome this problem, it is required not only to exploit spectrum resources such as a millimeter-wave band [5] but also to efficiently use current spectrum resources with cognitive radio technologies [6]. This thesis aims to efficiently utilize radio spectrum and tackles coexistence problems of wireless communication and non-communication systems on the assumption that both systems use the same spectrum channel.

As the coexistence of wireless communication and non-communication systems, this thesis presents two main topics related to future wireless communication technologies. One topic is a microwave power transmission (MPT) system to a WLAN station. The other topic is a database-driven spectrum sharing system for 5G mobile networks. The overviews of these topics are described in the following two sections.

1.2 Microwave Power Transmission to WLAN Station

This topic focuses on the co-channel operation of MPT and IEEE 802.11-based data transmission. MPT is a wireless power transmission technology in which electric power is transmitted via microwaves [7]. MPT enables to transmit power over long distances, as compared with other wireless power transmission methods, such as electromagnetic induction, magnetic resonance, and other components. However, MPT uses radio spectrum obviously, and in the co-channel operation of MPT and data transmission, the influence of MPT on data transmission has to be considered.

The purpose of using MPT is to realize the batteryless operation of a wireless device. Achieving this allows the elimination of power cables and a reduction in battery replacement costs. These cost reduction requrements increase in wireless sensor network (WSN) systems such as medical care and disaster alarm systems [8, 9], where WSN systems utilize sensing information collected from a large number of wireless sensors [10].

In [11], the authors conducted experiments in which microwave power with a frequency of 2.4 GHz was transmitted to an IEEE 802.11g-based WLAN station in co-channel or adjacent channel environments. From the experiment results, two requirements for the coexistence of MPT and IEEE 802.11g-based communication were mentioned as follows.

- MPT and wireless communication should not be performed simultaneously. Even when the authors performed adjacent channel operation of MPT and WLAN communications, the WLAN station could not transmit data frames when microwave power was transmitted. This is because the station is deterred from transmitting data frames due to the carrier sense mechanism. Thus, the authors suggested that the station should share the timing information of MPT and should attempt to transmit data frames except when microwave power is transmitted. Especially, the authors suggested that MPT to the station should be stopped when an access point (AP) broadcasts beacon frames.

- Even when microwave power was intermittently transmitted, throughput degradation could happen due to a rate adaptation scheme (RAS) of the WLAN protocol. Exposure of the WLAN station to microwave radiation for MPT leads to the selection of a lower physical (PHY) layer data rate, the use of which is maintained even after exposure to the microwave radiation is discontinued. The reduction in the PHY data rate occurs because the station attempts to continue data transmission during exposure to the microwave radiation. However, the station does not receive acknowledgment (ACK) frames due to the high interference power at the station. Hence, a low PHY data rate is selected with a RAS, which is implemented on the station. Note that this problem occurs even when the station employs the carrier sense mechanism.

As described in the preface, this thesis proposes two schemes to avoid harmful interference to the WLAN station. One is a scheduling scheme that allocates time for MPT and IEEE 802.11-based data transmission. The other is a RAS based on exposure assessment with rectenna output, where the rectenna is the element that has been installed in the device powered with MPT. The two proposed schemes are independently designed to solve the problems related to MPT to WLAN station, and can be used simultaneously. On the one hand, the scheduling scheme is proposed for completely stopping microwave transmission for MPT in the time duration during which a WLAN station transmits. On the other hand, the rate adaptation scheme is proposed for solving the throughput degradation from exposure of a transmitting WLAN station to microwave radiation for MPT.

This work assumes that the coexistence system of MPT and WLAN is applied in the indoor scenario. This is because the power transmission range of MPT is about 10 m, while the communication range of WLAN is more than 100 m. Short-distance WSNs with an Internet of Things (IoT) gateway have been proposed [12], and if their communication range is about 10 m, MPT can be applied to the WSN node. In addition, MPT can be employed to sensor nodes that have been powered with energy harvesting technologies.

This work uses an IEEE 802.11g-based WLAN device in the experiments without loss of generality, considering that the proposed schemes are for IEEE 802.11 series WLAN devices powered with MPT. Note that the big goal of this thesis is to transmit microwave power to IEEE 802.11ah-based wireless sensors [13] in the co-channel operation. IEEE 802.11ah-based wireless sensors operate at 900-MHz bands, whereas IEEE 802.11g-based wireless sensors operate at 2.4-GHz bands. However, there have been no devices that communicate over IEEE 802.11ah-based WLANs at present. Therefore, this thesis considers the use of an IEEE 802.11g-based wireless sensor instead of an IEEE 802.11ah-based wireless sensor because IEEE 802.11ah employs the same CSMA/CA protocol as IEEE 802.11g.

1.3 Database-driven Spectrum Sharing System for 5G Mobile Networks

This topic focuses on a database-driven spectrum sharing system and on the operation of a secondary user (SU), which is a communication system, in the channel allocated to a primary user (PU), which is a non-communication system, such as a radar system. Database-driven spectrum sharing [14–16] is a promising cognitive radio technique in which SUs opportunistically operates in the spectrum allocated to a PU. The overview of this technique is as follows. Firstly, a spectrum database collects the PU's usage information regarding the licensed bands in each region. Then, the database establishes a spectrum sharing policy for the SU such that the SU unlicensed operation will not interfere with the PU operation. Finally, an SU queries the database, providing its location and operates in the channel determined by the policy.

In the database-driven spectrum sharing system, even when the SU follows the spectrum sharing policy, the PU rarely experience harmful interference. This occurs owing to unpredictable propagation paths from changes in the geological and building environment. To reduce the probability that a PU experiences harmful interference, the spectrum sharing policy should be modified to limit the number of transmitting SUs; however, an efficient spatial reuse of the licensed bands cannot be achieved.

As the spectrum sharing policy, this thesis adopts a primary exclusive region (PER) [17, 18] around a PU, within which the SUs are forbidden to transmit. Reducing the PER area improves the spatial reuse of the shared channel because the region area where the SU can operate the licensed spectrum increases. In addition, this thesis establishes the PER centered at the fixed-location primary receiver (PR), and prohibits secondary transmitters (STs) around the PR to transmit.

In [19–21], a circular PER has been considered, and the radius of the PER has been optimized to minimize the area of the PER or to maximize the transmission capacity of the secondary network, under an outage constraint for the PU. In [22], the non-circular PER that consists of multiple sectors has been considered, the radius of each sector has been optimized to maximize the number of transmitting STs under the outage constraint. These works have used stochastic geometry to analyze the aggregate interference or SINR at a PR. Stochastic geometry is a powerful tool that enables the analysis of the aggregate interference in wireless networks with random topologies [23–25]. However, a practical PER should be designed, based on the local information, which includes the PR antenna pattern, and the ST density and transmission power. More detailed information is expected to result in a smaller PER.

As described in the preface, this thesis addresses twofold to design and to update a PER. One is to present a framework for updating a PER and to design a circular PER centered at a PR. The other is to design a complex-shaped PER by introducing a spatial grid.

A PER is designed by using an optimization problem under the constraint related to the target PU outage probability (OP), which is defined as the probability that the aggregated interference at a PR from all transmitting STs exceeds a maximum tolerable interference threshold. Certainly, a PU demands that the target PU OP is zero; however, to acheve zero PU OP technically, a huge PER is required. On the basis of this fact, in the numerical evaluation, this thesis provides the target PU OP as a parameter. Qualitatively, as the target is reduced, a larger PER is required for reducing a PU OP, i.e., the number of transmitting STs is reduced for satisfying the target PU OP.

This pargraph explains a maximum tolerable interference threshold in the PU OP definition. Qualitatively, as the threshold is reduced, a larger PER is established due to an increase in a PU OP, i.e., the number of transmitting STs is reduced for satisfying the target PU OP. In the numerical evaluation, this thesis assumes a virtual PU and verifies a established PER for a certain threshold. When the PU is a radar system, the threshold is expected to be a very low value based on the maximum allowable interference level of the radar, and then a established PER becomes a very huge area.

This paragraph specifies the SU. STs are randomly distributed around a PR. When STs are permitted to transmit, the STs transmit at any time with fixed power, i.e., the period during which STs do not transmit due to a medium access control (MAC) protocol is ignored. An example of the SUs is a WLAN system. In this system, a cell consisting of an AP and stations is assumed to be a single ST. In addition, AP and stations are assumed to have full buffer, and the period during which the ST do not transmit is negligible.

1.4 Related Works

1.4.1 Batteryless Sensors and MPT

There are many studies on batteryless wireless sensors and MPT. Energy management requirements for batteryless wireless sensors are described in [26, 27]. In [26], adaptive sleep control by using historical data to achieve a long lifetime was proposed. In [27], the necessity of power management for sensors in a WSN was discussed. In [28], the authors conducted experiments related to transmitting microwave power to ZigBee devices and succeeded in both powering the devices and wireless communications. In [7, 29], the authors investigated the use of MPT for powering multiple stations. In [7], the authors conducted experiments in which microwave power was transmitted to several stations with time sharing using a phased array antenna. In contrast, in [29], the authors conducted experiments in which microwave power was transmitted to all stations simultaneously using multiple antennas for MPT while reducing the impact of standing waves caused by multiple reflections and interference.

1.4.2 Rate Adaptation Schemes

In most RASs, by using data related to previous transmission results, e.g., historical data of the data frame loss ratio, the PHY data rate for data transmission is selected. The purpose of using the historical data is to estimate current link quality, which depends on the distance between a data transmitter and a data receiver and on interference power at the data receiver. To match the link quality, the PHY data rate is selected, i.e., such that data frames transmitted at the selected PHY data rate are successfully received by the data receiver. Related to the estimation of the link quality, many previous studies have attempted to propose RASs, e.g., ARF [30], RBAR [31], Onoe [32], and Sample Rate [33]. In addition, some conventional RASs employ loss differentiation mechanisms that diagnose the cause of data frame loss as collision or link quality degradation, e.g., LD-ARF [34], CARA [35], LDRA [36], and ERA [37]. However, these conventional schemes are designed without the assumption that high interference power at the station causes PHY data rate reduction.

Some previous studies have proposed RASs capable of assessing whether a WLAN station is exposed to microwave radiation from devices using Bluetooth, ZigBee, or from microwave ovens. SGRA [38] and ARES [39] attempt to assess whether a WLAN station is exposed to microwave radiation based on both the signal-to-noise power ratio (SNR) and the data frame loss ratio. However, because of the exposure assessment based on the data frame loss ratio, when the data receiver experiences strong SNR degradation, the station erroneously detects that it is exposed to microwave radiation for MPT even when this is not the case. The cause of this is that the data frame loss ratio increases, not only because of exposure of the station to microwave radiation for MPT, but also because of SNR degradation at the data receiver. The increase in the data frame loss ratio with SNR degradation is experimentally demonstrated in [40].

1.4.3 Spectrum Sharing Systems

The use of a database to enable the secondary use of the licensed spectrum has been studied with the aim of utilizing TV white space [14, 15, 41]. The TV system considered in previous studies and the radar system considered in this work differ in terms of whether a PR receives the PU's signals intermittently or continuously. For example, when TV receivers around an SU do not receive TV signals transmitted in the TV band, the SU can use the TV band without interfering with the TV receivers. On the other hand, even when a radar receiver does not receive radar signals transmitted in the radar band, the SUs around the radar receiver should be careful about using the radar band because the radar receiver may detect signals transmitted from the SUs as radar signals.

Other researchers [17, 19, 42] have been designed a circular PER on the assumption that the PU is a TV system; thus, the system models considered in these studies differ from that considered in this work as described in the previous paragraph. A Monte Carlo simulation was used in [19, 42] to design a circular PER, whereas this work designs a PER not by using Monte Carlo simulation but by stochastic geometry approach. In [17, 19, 42], the power levels of the STs are assumed to be constant, whereas this thesis considers the case in which the power levels of the STs vary discretely on the basis of power control.

In a Finnish trial [43–45], a time-division long-term evolution (TD-LTE) mobile communication system uses the 2.3 GHz band, where the 2.3 GHz band has been allocated for Programme Making and Special Events (PMSE) system under the European lisences shared access (LSA) framework, i.e., the TD-LTE system is an SU and the PMSE system is a PU. In the LSA framework, a government assigns private users to spectrum licenses with an upper limit on the number of licensed users [46]. In this trial, when the PU requests the LSA repository that the PU newly uses a certain LSA band at a certain location, immediately the SU at the location is prohibitted to use the LSA band, i.e., the SU evacuates the LSA band to the PU. In this trial, two problems are pointed out. One is that, when an SU is a real-time streaming application, the SU network throughput dramatically degrades during the evacuation process. The other is that the border between the PU and the SU is not clear and should be defined carefully. Towards the second problem, this work contributes to quantitatively designing a PER by using stochastic geometry analysis.

1.5 Chapter Overview of This Thesis

Fig. 1.1 shows the chapter overview of this thesis. The main theme of this thesis is the coexistence of wireless communication and non-communication systems. This

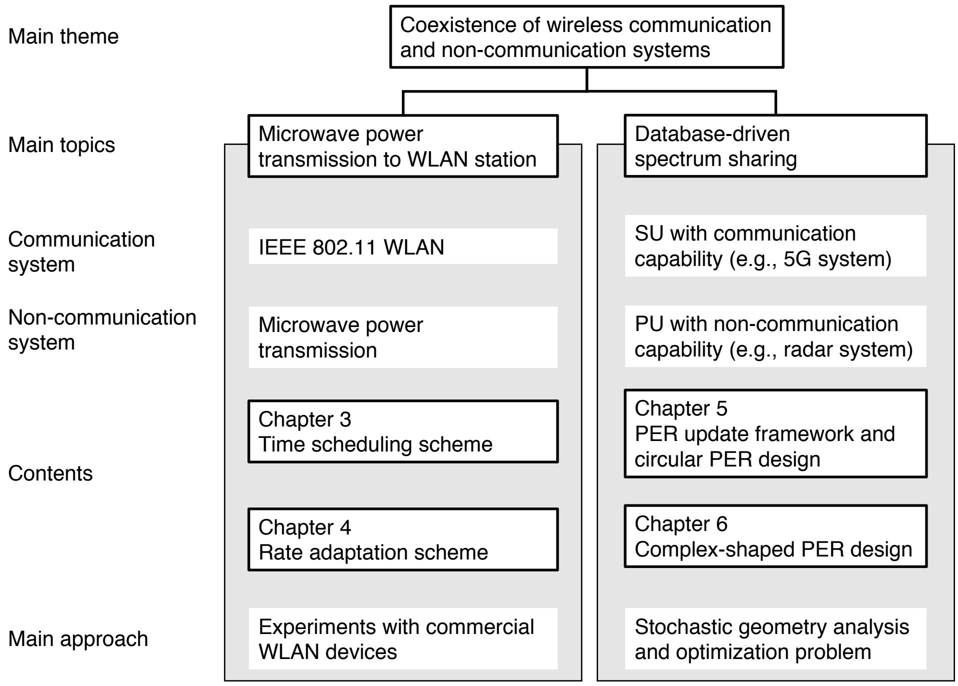

Figure 1.1: Chapter overview.

thesis consists of two main topics, i.e., MPT to WLAN station and Database-driven spectrum sharing. The first topic is tackled in Chapters 3 and 4, and the second topic is tackled in Chapters 5 and 6.

1.6 Contributions of This Thesis

The contribution of the first topic, i.e., an MPT system to a WLAN station, is to perform the experiments with commercial WLAN devices. In the proposed scheduling scheme, microwaves are opportunistically transmitted to a WLAN device, and the device is not modified. In addition, the RAS can be implemented on a WLAN device only by modifying the device driver, and the basic operation of WLAN such as the CSMA/CA protocol remains.

The contributions of the second topic, i.e., a database-driven spectrum sharing system, are twofold. The first contribution is to design a PER using the results of stochastic geometry analysis, which is appropriate to discuss random wireless networks without some case studies. The second contribution is to quantitatively evaluate the impact of the details of database information on a PER.

Chapter 2

Related Technologies

2.1 Microwave Power Transmission

MPT is a wireless power transmission technology where power is wirelessly transmitted through microwaves in the industry-science-medical (ISM) band, e.g., 920 MHz, 2.4 GHz, and 5 GHz bands [7]. The device powered with MPT has a element called "rectenna", which consists of an antenna and rectifier and converts microwave power to direct current.

In MPT, the received power can be obtained simply. It is assumed that there are transmission and reception antennas with gain G_{t} and G_{r}, respectively, and that the distance between these antennas is denoted by d. These antennas have line-of-sight and face each other. From the transmission antenna, microwave power with power P_{t} and frequency f is transmitted to the reception antenna. In free space, by referring to the Friis transmission equation [47], the received power at the reception antenna P_{r} can be obtained as

$$P_{\mathrm{r}} = G_{\mathrm{r}} G_{\mathrm{t}} P_{\mathrm{t}} \left(\frac{c}{4\pi d f} \right)^2, \tag{2.1}$$

where c is the speed of light.

The reason why this thesis focuses on MPT is two fold. First, MPT enables transmitting microwave power far away compared with other wireless power transmission technologies, which utilize electric resonance, electromagnetic induction, and other components [7]. In the technologies, the power transmission range is limited by coil and electrode sizes. Second, MPT enables transmitting arbitrary power actively compared with energy harvesting technologies [48]. The technologies convert light and vibration energy to electric energy using a solar cell and piezoelectric element. The technologies are passive, and the amount of received power depends on the ambient environment.

2.2 Wireless Local Area Network

2.2.1 IEEE 802.11g

IEEE 802.11g is one of IEEE WLAN standards that was developed in the task group g of the 802.11 working group and that was published in 2003 [4]. IEEE 802.11g adopts the orthogonal frequency division multiplexing (OFDM) modulation scheme, and realizes a maximum PHY data rate of 54 Mbit/s, while maintaining backward compatibility with IEEE 802.11b. In IEEE 802.11g, all frames are transmitted in 2.4 GHz ISM band following the CSMA/CA rule. In Japan domain, IEEE 802.11g supports 13 channels defined in the 2400–2483 MHz, and the channel width is 20 MHz.

This thesis uses an IEEE 802.11g WLAN device instead of an IEEE 802.11ah WLAN device, and transmits microwaves in the 2.4 GHz band to the IEEE 802.11g WLAN device. IEEE 802.11ah is another IEEE WLAN standard that was developed in the task group ah of the 802.11 working group and that was published in 2017 [13]. IEEE 802.11ah aims to WSN systems and supports a PHY data rate of more than 100 kbit/s and a maximum transmission range of 1 km [13]. IEEE 802.11ah operates in the 900 MHz band.

2.2.2 Access Point

An AP is a networking device that creates WLAN and allows WLAN stations to wirelessly connect to a wired network, e.g., Internet [4]. The AP is assumed to operates in infrastructure mode, i.e., the wireless network consists of a single AP and multiple stations.

The AP in infrastructure mode periodically broadcasts beacon frames to inform the surrounding WLAN devices about the existence of the AP. The beacon frames have the information that is required to maintain the network connectivity such as AP identifier, security information, and beacon interval. Receiving a beacon frame, WLAN stations can estimate when the next beacon frame is broadcasted.

2.2.3 CSMA/CA

The CSMA/CA is a MAC protocol in usual WLAN [4]. The CSMA/CA realizes that multiple wireless devices use in the same channel while avoiding frame collision. The frame collision occurs when multiple wireless devices transmits frames simultaneously in the same channel. In this case, it is difficult to receive the transmitted frames correctly.

In the CSMA/CA protocol, each wireless device operates following a simple listen-before-talk (LBT) scheme. Each wireless device employing this protocol senses the channel before frame transmission. If the channel is idle, i.e, the channel is not used, the device transmits the frame. Otherwise, if the channel is busy, i.e., the channel is used by anyone, the device defers the frame transmission.

2.2.4 Data Transmission Flow

A transmitter is assumed to transmit data to a receiver. The flow is as follows. First, the transmitter transmits a data frame to the receiver with the CSMA/CA protocol. Next, the receiver receives the data frame and then transmits the responding ACK frame to the transmitter, where the transmission of an ACK frame has a higher priority than the transmission of other data frames [4]. Finally, when the transmitter receives the ACK frame, the flow ends.

Note that the term "success of data transmission" is defined as the situation in which a transmitter transmits a data frame and then receives the responding ACK frame. When the transmitter can not receive the responding ACK frame, it detects a data frame loss and then transmits the same data frame to the receiver again, i.e., retransmits the data frame.

2.2.5 Data Rate on Physical Layer

IEEE 802.11-based WLAN supports multiple PHY data rates for frame transmission [4]. For example, Table 2.1 shows the supported PHY data rates in IEEE 802.11g, and especially PHY data rates of 6, 12, and 24 Mbit/s are mandatory.

Table 2.1: Supported PHY data rates in IEEE 802.11g [4].

PHY data rate (Mbit/s)	Modulation scheme	Coding rate
6	BPSK	1/2
9	BPSK	3/4
12	QPSK	1/2
18	QPSK	3/4
24	16QAM	1/2
36	16QAM	3/4
48	64QAM	2/3
54	64QAM	3/4

Each PHY data rate depends on two factors. One is a digital modulation scheme on each OFDM subcarrier, i.e., binary phase shift keying (BPSK), quadrature phase shift keying (QPSK), 16 quadrature amplitude modulation (QAM), and 64QAM. The other is a coding rate for error correction, i.e., 1/2, 2/3, and 3/4.

Using a higher PHY data rate leads to a higher throughput. However, the higher PHY data rate is used to transmit a frame, the higher SINR at a reception device is needed to successfully receive the frame. When the SINR is below the desired level, the frame cannot be received by the reception device, i.e., a frame loss occurs. The frame loss should be avoided because it wastes time and channel resource in the frame transmission.

2.2.6 Rate Adaptation Schemes

A RAS automatically selects a PHY data rate in a data frame transmission [30]. The RAS aims to improve the throughput performance by achieving both a high PHY data rate and low data frame loss ratio, where the throughput is defined as the amount of data transmitted successfully in a given time period. These schemes determine a data frame loss ratio at fixed intervals on the basis of the several-second time series information, and select a next PHY data rate.

The RAS is not supported by wireless communication standards and depends on the implementation. For example, a WLAN hardware supported by Linux uses a RAS implemented on a mac80211 device driver [49]. The mac80211 device driver controls by software a WLAN hardware on a Linux kernel, i.e., analyzes and generates IEEE 802.11 WLAN frames. Because this device driver is an open-source software, any RAS is realized by modifying the source code.

2.2.7 Conventional RAS of mac80211 Device Driver

This section presents a description of the two conventional RASs of the mac80211 device driver, i.e., PID and Minstrel. Note that the performances of these algorithms have been investigated in [50] and [51].

PID [52]

A station based on PID selects an appropriate PHY data rate based on the general proportional integral derivative controller such that the data frame loss ratio converges to a predetermined target value, $R_{\mathrm{L,target}}$. The station selects the PHY data rate every sampling period T_{PID}.

The kth rate selection operates as follows. First, the station calculates the data frame loss ratio between the $(k-1)$th and kth rate selections, $r_{\mathrm{L}}[k]$. Second, the station calculates the kth error between $R_{\mathrm{L,target}}$ and $r_{\mathrm{L}}[k]$ (denoted by $e[k]$) as

$$e[k] = R_{\mathrm{L,target}} - r_{\mathrm{L}}[k]. \tag{2.2}$$

Third, the station calculates the difference between $e[k]$ and $e[k-1]$ (denoted by $\Delta e[k]$) as

$$\Delta e[k] = e[k] - e[k-1]. \tag{2.3}$$

Moreover, the station computes an exponential moving average of $e[k]$ (denoted by $\hat{e}[k]$) by using $e[k]$ and $\hat{e}[k-1]$ computed at the $(k-1)$th rate selection as

$$\hat{e}[k] = \frac{(\alpha_{\mathrm{smooth}} - 1)\hat{e}[k-1] + e[k]}{\alpha_{\mathrm{smooth}}}, \tag{2.4}$$

where α_{smooth} is a smoothing factor ($\alpha_{\mathrm{smooth}} > 1$). Fourth, the station computes an adjustment value, $v_{\mathrm{adj}}[k]$, as

$$v_{\mathrm{adj}}[k] = C_{\mathrm{P}} e[k] + C_{\mathrm{I}} \hat{e}[k] + C_{\mathrm{D}} \Delta e[k](1 + \alpha_{\mathrm{sharp}}), \tag{2.5}$$

Table 2.2: Minstrel rate table created at the kth update.

Retransmission count	Normal rate	Lookaround rate (generating $i_{\text{rand}}[k] \in \mathcal{N}$)
0	$R(i_{\text{best\_tp}}[k])$	$\max(R(i_{\text{best\_tp}}[k]), R(i_{\text{rand}}[k]))$
1	$R(i_{\text{next\_best\_tp}}[k])$	$\min(R(i_{\text{best\_tp}}[k]), R(i_{\text{rand}}[k]))$
2	$R(i_{\text{best\_prob}}[k])$	$R(i_{\text{best\_prob}}[k])$
3	$R(i_{\text{baserate}}[k])$	$R(i_{\text{baserate}}[k])$

where α_{sharp} is a sharpening factor (if $\alpha_{\text{sharp}} \neq 0$, a fast response is achieved), and C_{P}, C_{I}, and C_{D} are proportional, integral, and derivative coefficients, respectively. Finally, if $v_{\text{adj}}[k] \leq -1$, the station decreases the PHY data rate. If $v_{\text{adj}}[k] \geq 1$, the station increases the PHY data rate, and if $-1 < v_{\text{adj}}[k] < 1$, the station maintains the current PHY data rate.

Minstrel [53]

A station based on Minstrel selects an appropriate PHY data rate by using the previous data frame transmission performance such that the highest throughput performance is achieved. The station updates a rate table every sampling period T_{Minstrel}. The rate table indicates the PHY data rate based on the retransmission count.

The station updates the kth rate table as follows. First, $\mathcal{N}$ is a set of rate indexes that indicate the supported rates, and i is an element of $\mathcal{N}$, i.e., $i \in \mathcal{N}$. Let the PHY data rate corresponding to i be denoted by $R(i)$. Second, the station calculates $p_{\text{s}}(i)[k]$ for every i, which represents the estimated success probability of data frame transmission at $R(i)$ as follows. Let $\Delta n_{\text{transmit}}(i)[k]$ denote the increased number of data frames transmitted at $R(i)$ between the $(k-1)$th and kth updates. Similarly, let $\Delta n_{\text{success}}(i)[k]$ denote the increased number of data frames transmitted successfully at $R(i)$ between the $(k-1)$th and kth updates. Using

$\Delta n_{\text{transmit}}(i)[k]$ and $\Delta n_{\text{success}}(i)[k]$, $p_{\text{s}}(i)[k]$ is calculated as

$$p_{\text{s}}(i)[k] = (1 - \alpha_{\text{scale}})\frac{\Delta n_{\text{success}}(i)[k]}{\Delta n_{\text{transmit}}(i)[k]} + \alpha_{\text{scale}} p_{\text{s}}(i)[k-1], \tag{2.6}$$

where α_{scale} is a scaling value ($0 < \alpha_{\text{scale}} < 1$). Third, the station computes the throughput at $R(i)$ (denoted by $tp(i)[k]$) using the estimated maximum number of data frames transmitted successfully at $R(i)$ per unit time. Note that the symbol "tp" represents "throughput." Fourth, the station determines the following three rate indexes.

- $i_{\text{best\_tp}}[k]$: the rate index of the PHY data rate that will achieve the highest throughput performance
- $i_{\text{next\_best\_tp}}[k]$: the rate index of the PHY data rate that will achieve the second highest throughput performance
- $i_{\text{best\_prob}}[k]$: the rate index of the PHY data rate that will achieve the highest success probability of data frame transmission

These rate indexes are defined as

$$i_{\text{best\_tp}}[k] = \underset{i \in \mathcal{N}}{\arg\max}\; tp(i)[k], \tag{2.7}$$

$$i_{\text{next\_best\_tp}}[k] = \underset{i \in \mathcal{N}, i \neq i_{\text{best\_tp}}[k]}{\arg\max}\; tp(i)[k], \tag{2.8}$$

$$i_{\text{best\_prob}}[k] = \underset{i \in \mathcal{N}}{\arg\max}\; p_{\text{s}}(i)[k], \tag{2.9}$$

respectively. Finally, the station updates the rate table in Table 2.2, where i_{baserate} represents the rate index of the lowest supported PHY data rate.

Using Table 2.2, the station selects an appropriate PHY data rate as follows. The "Normal rate" is used to transmit 90% of data frames and the remaining 10% are transmitted at the "Lookaround rate," for which the station generates a random rate index, $i_{\text{rand}}[k] \in \mathcal{N}$. The station then determines the PHY data rate for the current retransmission count as shown in Table 2.2.

2.3 Stochastic Geometry

Stochastic geometry is a powerful mathematical tool that enables the analysis of the aggregate interference in wireless networks with random topologies [23–25].

Referring to [23], this section explains point processes and theories only in two-dimensional space.

2.3.1 Homogeneous or Inhomogeneous Poisson Point Process

A Poisson point process (PPP) is numerous random spatial points, which are uniformly distributed in $\mathbb{R}^2$. The PPP is characterized only by an intensity parameter.

The homogeneous PPP in $\mathbb{R}^2$ with density $\lambda \in \mathbb{R}$ is defined as a point process in $\mathbb{R}^2$ satisfying the following two conditions. First, for a compact set $B \subset \mathbb{R}^2$, $N(B)$ is a random variable following a Poisson distribution with mean $\lambda|B|$, and the points in B are uniformly distributed. Second, $B_1, B_2, \dots \subset \mathbb{R}^2$ are assumed to be disjoint compact sets, and then random variables $N(B_1), N(B_2), \dots$ are mutually independent.

The inhomogeneous PPP in $\mathbb{R}^2$ with intensity function $\Lambda : \mathbb{R}^2 \to \mathbb{R}$ is defined as a point process in $\mathbb{R}^2$ satisfying the following two conditions. First, for a compact set $B \subset \mathbb{R}^2$, $N(B)$ is a random variable following a Poisson distribution with mean $\int_B \Lambda(x)\,\mathrm{d}x$. Second, $B_1, B_2, \dots \subset \mathbb{R}^2$ are assumed to be disjoint compact sets, and then random variables $N(B_1), N(B_2), \dots$ are mutually independent.

2.3.2 Campbell's Theorem and Probability Generating Functional for PPP

This subsection explains Campbell's theorem and probability generating functional (PGFL) for the PPP. Let a function of a point location be denoted by $f : \mathbb{R}^2 \to \mathbb{R}$, and a $[0,1]$-valued function of a point location be denoted by $v : \mathbb{R}^2 \to [0,1]$. Let a homogeneous PPP in $\mathbb{R}^2$ with density $\lambda \in \mathbb{R}$ be denoted by Φ_{HPPP}, and an inhomogeneous PPP in $\mathbb{R}^2$ with intensity function $\Lambda : \mathbb{R}^2 \to \mathbb{R}$ be denoted by Φ_{IPPP}.

Campbell's theorem contributes to analyzing the sum of the random variables, which depends on random spatial locations. In a wireless network, this theorem enables to derive the mean and variance of the aggregate interference from wireless devices distributed randomly. Referring to Campbell's theorem, the means of the summations $\sum_{x\in\Phi_{\text{HPPP}}} f(x)$ and $\sum_{x\in\Phi_{\text{IPPP}}} f(x)$ are expressed as

$$\mathbb{E}_{\Phi_{\text{HPPP}}}\left(\sum_{x\in\Phi_{\text{HPPP}}} f(x)\right) = \lambda \int_{\mathbb{R}^2} f(x)\,\mathrm{d}x \text{ and} \tag{2.10}$$

$$\mathbb{E}_{\Phi_{\text{IPPP}}}\left(\sum_{x\in\Phi_{\text{IPPP}}} f(x)\right) = \int_{\mathbb{R}^2} f(x)\Lambda(x)\,\mathrm{d}x, \tag{2.11}$$

respectively.

PGFL for the PPP contributes to analyzing the product of the random variables, which depends on random spatial locations. In a wireless network, this theorem enables to derive the moment generating function (MGF), Laplace transform (LT), or characteristic function (CF) of the aggregate interference from wireless devices distributed randomly. Referring to PGFL for the PPP, the means of the products $\prod_{x\in\Phi_{\text{HPPP}}} v(x)$ and $\prod_{x\in\Phi_{\text{IPPP}}} v(x)$ are expressed as

$$\mathbb{E}_{\Phi_{\text{HPPP}}}\left(\prod_{x\in\Phi_{\text{HPPP}}} v(x)\right) = \exp\left(-\lambda \int_{\mathbb{R}^2} [1 - v(x)]\,\mathrm{d}x\right) \text{ and} \tag{2.12}$$

$$\mathbb{E}_{\Phi_{\text{IPPP}}}\left(\prod_{x\in\Phi_{\text{IPPP}}} v(x)\right) = \exp\left(-\int_{\mathbb{R}^2} [1 - v(x)]\Lambda(x)\,\mathrm{d}x\right), \tag{2.13}$$

respectively.

Chapter 3

Time Scheduling for Microwave Power and IEEE 802.11 Data Transmissions

3.1 Overview

This chapter sets two goals to avoid the influence of MPT on WLAN data communications. The first goal is to design a scheduling scheme to solve throughput degradation and disassociation problems caused by the WLAN protocol. The second goal is to confirm the feasibility of the scheduling scheme.

To accomplish these goals, this chapter performs the following steps. First, on the premise of co-channel operation of MPT and IEEE 802.11g-based communications, this chapter proposes a scheduling scheme that allocates time for MPT and IEEE 802.11g-based WLAN communications. By performing co-channel operation of MPT and WLAN communications, the high spectral efficiency can be achieved, i.e., a dedicated frequency band for MPT is not required. In addition, considering that the supplied power to the sensor station (SS) for MPT is very small (on the order of milliwatts) in general, this chapter attempts a method that lets the energy source (ES) transmit microwave power as long as possible, whereas the SS uses power-save operation to reduce its consumed power; thus, the duration of each MPT is set to be longer than that of each data transmission. Then, on the basis of this proposed scheme, this chapter implements a system and conduct experiments to confirm the expected performance. For the feasibility study, this work assumes that the remaining energy of the SS certainly increases when the ES transmits microwave power. In addition, radio radiation protection guidelines related to microwave effects on humans accordingly limit the equivalent isotropically radiated power (EIRP) of MPT [54]. Thus, in the experiments, this work uses a large horn antenna for MPT because antenna size is irrelevant to accomplish the goals of this chapter. Finally, this chapter discusses the feasibility of the system using the proposed scheduling scheme. Specifically, this chapter estimates the maximum allowable distance at which the SS obtains sufficient power to perform wireless communication such that the radio radiation protection guidelines are satisfied. In addition, this chapter also discusses the feasibility of the case where microwave power is transmitted to an IEEE 802.11ah-based wireless sensor using the proposed scheme in co-channel operation. From these results, this chapter can determine what application the proposed scheme can be utilized for in terms of the distance at which the SS obtains sufficient power.

This work would like to emphasize that the motivation of this thesis is to solve throughput degradation and disassociation problems caused by the WLAN protocol. To solve these problems, this chapter designs a scheduling scheme only for a single SS because these problems can happen even when microwave power is transmitted to a single SS. Thus, MPT for multiple stations and directivity control for a transmission antenna are out of the scope of this chapter. Note that in [7, 29], the authors discussed how to transmit microwave power toward multiple stations.

This chapter is organized as follows. Sect. 3.2 shows the setup of the experiment. Sect. 3.3 describes the power-saving operation of a WLAN module. Sect. 3.4 proposes the scheduling scheme. Sect. 3.5 describes the experiments and the results. Then, Sect. 3.6 discusses the feasibility of the proposed scheduling scheme using a link budget. Finally, this chapter is concluded in Sect. 3.7.

3.2 Setup of Experiment

Figure 3.1 shows the setup of the experiment. In this experiment, there are three devices: an ES, AP, and SS.

This work explains the whole process of operation. First, the SS measures its remaining energy and then calculates the timing of the next data transmission

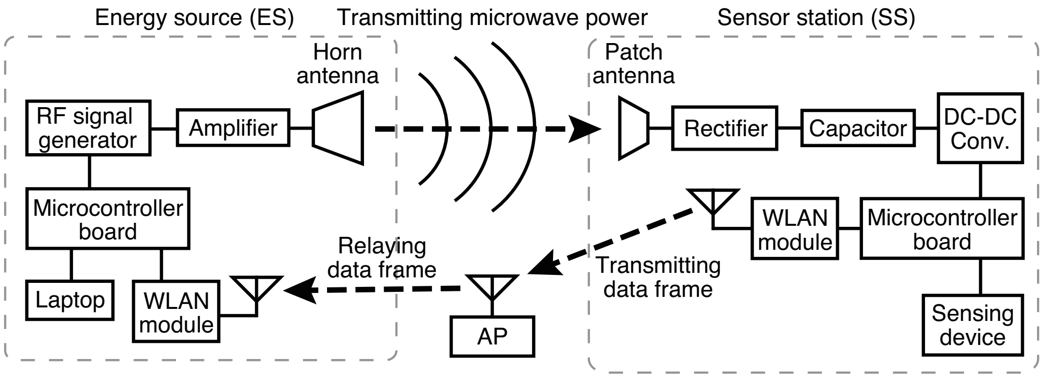

Figure 3.1: Experimental setup. ©2014 IEICE

using the history of the remaining energy. Next, the SS transmits a data frame including the timing of the next data transmission to the ES through the AP. On the basis of the timing of the next data transmission of the SS, the ES transmits microwave power toward the SS, and the remaining energy of the SS increases.

This work explains the details of each device. The ES consists of a horn antenna, an amplifier, a radio frequency signal generator, a microcontroller board, a laptop, and a WLAN module. The microcontroller board determines whether microwave power is transmitted. The microcontroller board also forwards data frames to the laptop, and then the laptop displays the transmission data from the SS. Note that the laptop only displays these data for analysis, not for control of the MPT.

The SS consists of a rectenna (a patch antenna and a rectifier), a capacitor, a DC-DC converter, a microcontroller board, a sensing device, and a WLAN module. The SS is powered by microwave power transmitted from the ES, obtains sensing data, and transmits data frames to the ES. The microcontroller board and the WLAN module of the SS are powered by the capacitor. The microcontroller board determines the power-save operation of the WLAN module and then makes the WLAN module operate in sleep mode except when the SS transmits data frames. Before the SS transmits data frames, the microcontroller board measures a physical quantity with the use of the sensing device and calculates the remaining energy stored in the capacitor by measuring the capacitor voltage. Note that the specific contents of the sensing data are out of the scope of this chapter, and this chapter treats the remaining energy stored in the capacitor of the SS as sensing data. From the history of the remaining energy, the SS estimates the supplied power when the ES transmits microwave power. Note that in this experiment the supplied power is almost constant when the ES transmits microwave power. Then, the microcontroller board determines the timing of the next data transmission. The microcontroller board generates a data frame containing both the sensing data and the information of the timing of the next data transmission, and the SS transmits the data frame to the ES through the AP. When the ES transmits microwaves, the rectenna receives and rectifies the microwaves, charging the capacitor.

The AP periodically broadcasts beacon frames to manage the network. When the AP receives a data frame from the SS, it forwards the data frame to the ES.

3.3 Power-Save Operation of WLAN Module

The primary component of the total power consumption of the SS is the power consumption of the WLAN module. Thus, to save energy, the SS is required to use a power-save operation of the WLAN module, except when the SS communicates. Note that if this work does not use the power-save operation, the energy that the SS consumes increases and would be significantly more than the supplied energy from MPT. This section introduces the power-save operation of the WLAN module.

Figure 3.2 shows the relationship among the timing when the AP broadcasts beacon frames, the state of the power consumption of the SS, and the mode of the power-save operation of the WLAN module. Note that the pattern of power consumption was obtained from a preliminary experiment, and the details are discussed in Sect. 3.5.

As shown in Fig. 3.2, the AP periodically broadcasts beacon frames. In addition, beacon frames that contain delivery traffic indication map (DTIM) information are broadcasted every predetermined number of beacon frames. Hereafter, the beacon frames that contain DTIM information are simply referred to as "DTIM beacons."

There are two modes related to the power-save operation of the WLAN module: active and sleep modes. The microcontroller board switches these two modes of the WLAN module depending on the demand for transmission. As shown in Fig. 3.2, the power consumption of the SS is large when the SS transmits data frames or receives DTIM beacons because the WLAN module is completely powered to

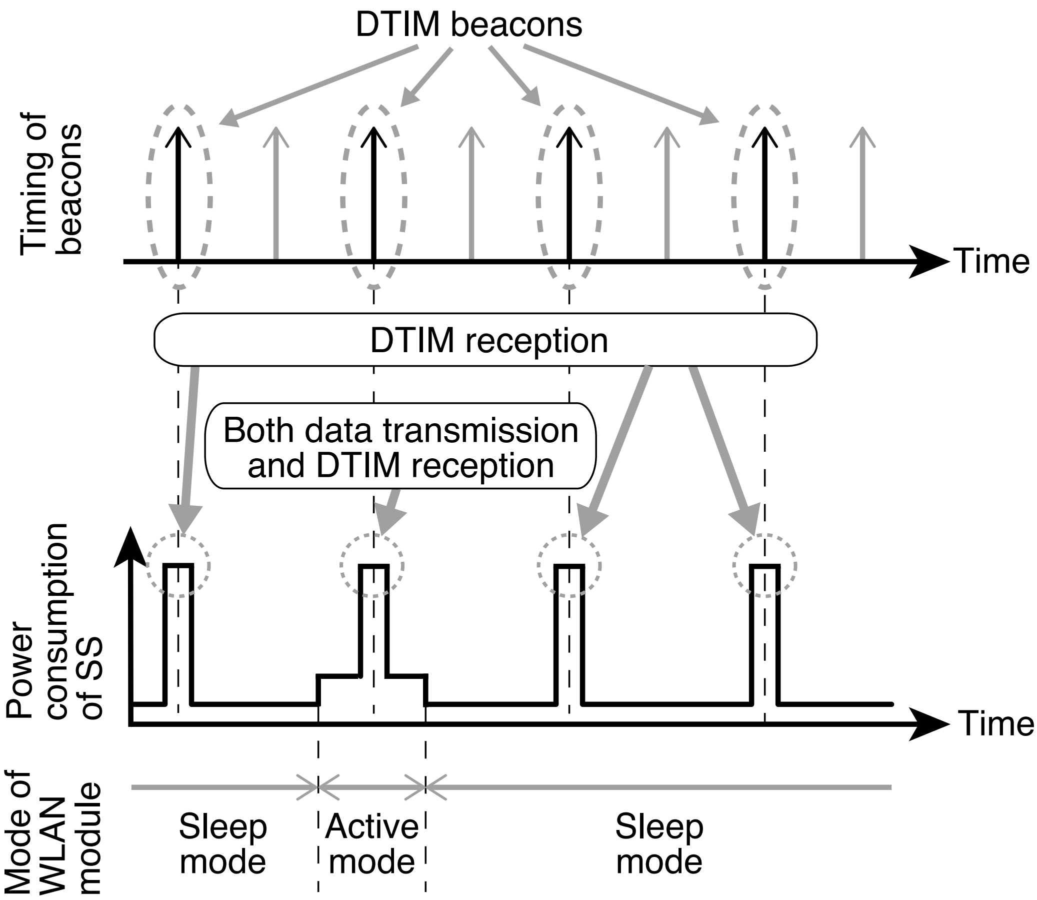

Figure 3.2: Power consumption of SS during communication. ©2014 IEICE

perform wireless communication.

For the SS to transmit data frames, before the DTIM beacon is broadcasted, the microcontroller board switches the mode of the WLAN module from sleep mode to active mode. In this case, the SS attempts to transmit data frames just before it receives the DTIM beacon. When a certain time has elapsed since the WLAN module is switched to active mode, the microcontroller board switches the mode of WLAN module from active mode to sleep mode. In sleep mode, the SS only receives DTIM beacons to maintain the association with the AP and does not transmit data frames.

3.4 Proposed Microwave Power and Data Transmission Scheduling

This section explains the proposed scheduling scheme. In this scheduling scheme, an SS that has little remaining energy refrains from data transmission to save energy, i.e., the SS does not transmit data frames periodically.

3.4.1 Requirements for Microwave Power and Data Transmission

To reduce the power consumption of the SS, it is desirable that the voltage of the capacitor of the SS is as large as the withstand voltage of the capacitor. The reason is as follows. Regarding the efficiency of the DC-DC converter connected after the capacitor, an input voltage that is close to the output constant voltage is desirable. In addition, in this experiment, the withstand voltage of the capacitor is lower than the constant output voltage of the DC-DC converter. Thus, this work sets the target energy of the capacitor at the energy stored in the capacitor charged up to the withstand voltage. Hereinafter, this energy is referred to as E_{max}.

As clarified in [11], the SS should share the information on the timing of MPT such that the SS transmits data frames when the ES does not transmit microwave power. In addition, as also clarified in [11], the ES should stop MPT around the timing of DTIM beacons because if the ES transmits microwave power around the timing of DTIM beacons, the SS is disassociated from the AP.

3.4.2 Operational Flow

Figure 3.3 shows the operational flow of the proposed scheduling scheme. This figure shows the relationship among the timing when the AP broadcasts DTIM beacons, the state of the power consumption of the SS, and the state of MPT.

The parameters and constants used in Fig. 3.3 are summarized in Tables 3.1 and 3.2, respectively. Note that the constants shown in Table 3.2 are predetermined from measurements of the power consumption of the SS using a DC power source.

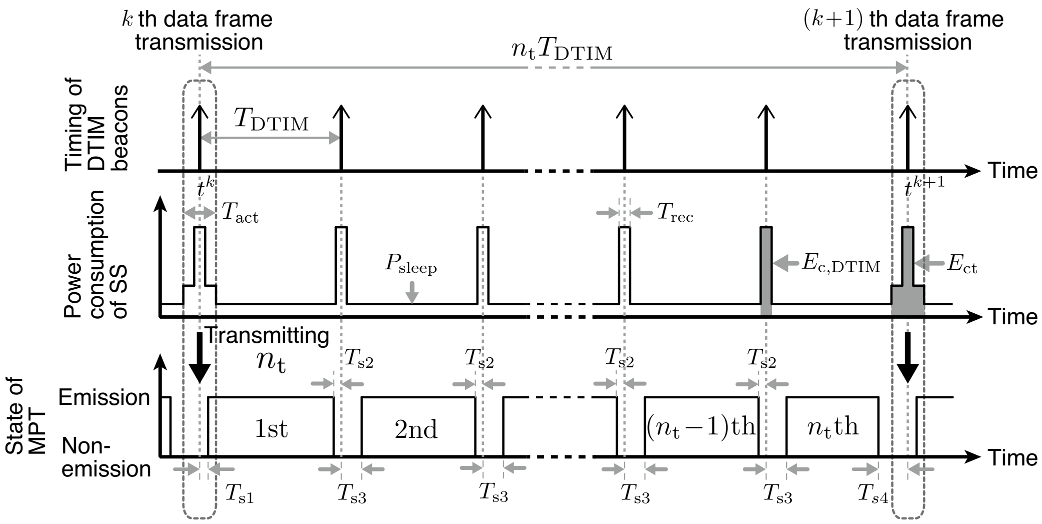

Figure 3.3: Operational flow of proposed scheduling system. ©2014 IEICE

Table 3.1: Definitions of parameters.

Symbols	Definitions
E_{max}	Maximum allowable energy that capacitor stores
T_{DTIM}	DTIM interval
T_{s1}	Guard time between DTIM beacon and MPT when transmitting data
T_{s2}	Guard time between MPT and DTIM beacon when in sleep mode
T_{s3}	Guard time between DTIM beacon and MPT when in sleep mode
T_{s4}	Guard time between MPT and DTIM beacon when transmitting data

Table 3.2: Definitions of predetermined constants.

Symbols	Definitions
E_{ct}	Energy consumption of SS for data frame transmission
$E_{c,DTIM}$	Energy consumption of SS for DTIM reception
P_{sleep}	Power consumption of SS in sleep mode
T_{act}	Duration of active mode of SS
T_{rec}	Duration of SS energy consumption to receive DTIM beacon

3.4.3 Sharing Information on Timing of Next Data Transmission

The SS, just before a data transmission, determines the timing of the next data transmission on the basis of the remaining energy of the SS so as to maintain its energy close to E_{max}. Then, the SS informs the ES of the timing of the next data transmission, i.e., the timing of the active mode. In addition, the SS also informs the ES whether the SS requires MPT.

This work explains the details of sharing the information below. Let t_k denote the timing of the kth data frame transmission of the SS. As explained in Sect. 3.3, because the SS transmits data frames immediately before the SS receives DTIM beacons, t_{k+1} is given by $t_{k+1} = t_k + n_t T_{DTIM}$ ($n_t = 1, 2, \ldots$), where T_{DTIM} represents the DTIM interval. The data frame consists of sensing data and n_t. On the basis of the informed n_t from the SS, the ES calculates t_{k+1}. Then, the ES transmits microwave power in $[t_k, t_{k+1}]$, except during the transmission of the DTIM beacons, as shown in Fig. 3.3 such that the microwave power does not prevent the SS from the reception of DTIM beacons.

To inform not only the timing of the next active mode but also the information regarding whether the SS requires MPT, this work introduces an optional value where$n_t = 0$, whereas the ES always transmits microwave power when $n_t = 1, 2, \ldots$. When $n_t = 0$, t_{k+1} is set as $t_{k+1} = t_k + T_{DTIM}$, and the ES does not transmit microwave power during $[t_k, t_{k+1}]$.

To summarize, when the SS informs n_t (= $0, 1, 2, \ldots$) to the ES at t_k, t_{k+1} is given by

$$t_{k+1} = \begin{cases} t_k + T_{DTIM} & \text{if } n_t = 0 \\ t_k + n_t T_{DTIM} & \text{if } n_t = 1, 2, \ldots . \end{cases} \tag{3.1}$$

Recall that by informing n_t, the ES calculates t_{k+1} and determines whether the ES transmits microwave power.

3.4.4 Method to Determine Appropriate n_t

This work explains the method to determine the appropriate value for n_t such that the energy stored in the capacitor of the SS converges to E_{max} as explained in

Sect. 3.4.1. Let $n_{t,k}^{\star}$ denote n_t transmitted with the kth data transmission. The value of $n_{t,k}^{\star}$ impacts the energy stored in the capacitor in the $(k+1)$th data transmission.

When the SS is switched from sleep mode to active mode, the SS estimates both the energy consumption of the SS and the supplied energy to the SS. Let the "estimated energy consumption of the SS during $[t_k, t_{k+1}]$" and the "estimated supplied energy to the SS during $[t_k, t_{k+1}]$" to a certain n_t be denoted by $\hat{e}_c(n_t)$ and $\hat{e}_t(n_t)$, respectively. The SS calculates $\hat{e}_c(n_t)$ as

$$\begin{aligned}\hat{e}_c(n_t) &= E_{ct} + P_{sleep}(T_{DTIM} - T_{act}) \\ &\quad + (n_t - 1)[E_{c,DTIM} + P_{sleep}(T_{DTIM} - T_{rec})]. \end{aligned} \tag{3.2}$$

Then, this work explains how to calculate $\hat{e}_t(n_t)$. First, the SS calculates the aggregated duration during which the ES transmits microwave power in the time interval $[t_k, t_{k+1}]$. Let $t_{tr}(n_t)$ denote the aggregated duration to a certain n_t, and $t_{tr}(n_t)$ is evaluated as

$$t_{tr}(n_t) = \begin{cases} 0 & \text{if } n_t = 0 \\ n_t T_{DTIM} - (T_{s1} + T_{s4}) & \\ \quad -(n_t - 1)(T_{s2} + T_{s3}) & \text{if } n_t = 1, 2, \ldots. \end{cases} \tag{3.3}$$

Second, the SS estimates the supplied power to the SS when the ES transmits microwave power. Let $\hat{p}_r$ denote the estimated supplied power when the ES transmits microwave power. Note that the SS measures the energy stored in the capacitor before every data transmission, and let e_k denote the measured energy before the kth data transmission. On the basis of e_{k-1}, e_k, and $n_{t,k-1}^{\star}$, the SS updates $\hat{p}_r$ as

$$\hat{p}_r = \begin{cases} \hat{p}_r & \text{if } n_{t,k-1}^{\star} = 0 \\ \dfrac{e_k - e_{k-1} + \hat{e}_c(n_{t,k-1}^{\star})}{t_{tr}(n_{t,k-1}^{\star})} & \text{if } n_{t,k-1}^{\star} = 1, 2, \ldots. \end{cases} \tag{3.4}$$

Last, using $t_{tr}(n_t)$ and $\hat{p}_r$, $\hat{e}_t(n_t)$ is evaluated by

$$\hat{e}_t(n_t) = \hat{p}_r t_{tr}(n_t). \tag{3.5}$$

Using e_k, $\hat{e}_c(n_t)$, and $\hat{e}_t(n_t)$, the SS determines $n_{t,k}^{\star}$. Specifically, the SS determines $n_{t,k}^{\star}$ such that the estimated energy stored in the capacitor of the SS in the

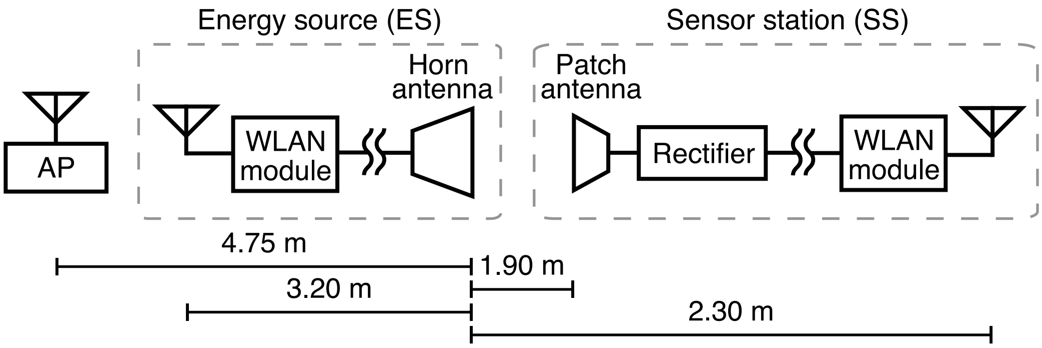

Figure 3.4: Position of each device in experimental setup. ©2014 IEICE

$(k+1)$th data transmission is nearest to $E_{\max}$. Let $\hat{e}_{k+1}(n_t)$ denote the estimated energy in the $(k+1)$th data transmission to a certain n_t, and $\hat{e}_{k+1}(n_t)$ is estimated by

$$\hat{e}_{k+1}(n_t) = e_k + \hat{e}_t(n_t) - \hat{e}_c(n_t). \tag{3.6}$$

Using $\hat{e}_{k+1}(n_t)$, the SS determines $n^\star_{t,k}$ as

$$n^\star_{t,k} = \begin{cases} 0 & \text{if } \hat{e}_{k+1}(n_t) \geq E_{\max}, \forall n_t, \\ \arg\min_{n_t \in \mathcal{N}} E_{\max} - \hat{e}_{k+1}(n_t) & \text{otherwise,} \end{cases} \tag{3.7}$$

where $\mathcal{N} = \{n | \hat{e}_{k+1}(n) < E_{\max}, n = 1, \ldots, N\}$, and N represents the maximum value for $n^\star_{t,k}$. In addition, in (3.7), $n^\star_{t,k}$ has a unique value because $E_{\max} - \hat{e}_{k+1}(n_t)$ has different values for n_t.

3.5 Experiment

3.5.1 Parameters

Figure 3.4 shows the position of each device and the distances between antennas. The SS is set in front of the horn antenna of the ES, and both the WLAN module of the ES and the AP are set behind the horn antenna to prevent serious interference. Figure 3.5 shows the SS and the horn antenna of the ES.

This work uses “Arduino Fio” [55] as the microcontroller board of the ES and the SS. Moreover, this work uses “XBee Wi-Fi” [56] as the WLAN modules of

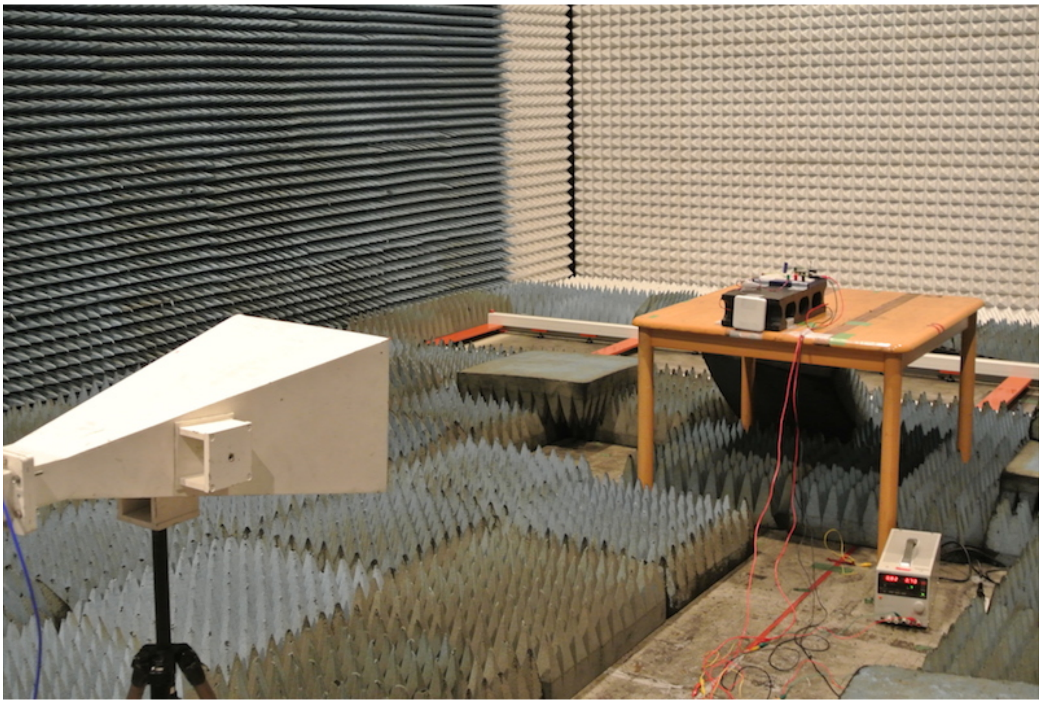

Figure 3.5: Experimental setup of horn antenna and SS. ©2014 IEICE

the ES and the SS. The SS, ES, and AP transmit or receive user datagram protocol (UDP) data using 2.446–2.468 GHz bands. On the other hand, the ES transmits microwave power on the frequency of 2.457 GHz. The input power of the horn antenna is 12.8 W when the ES transmits microwave power. The antenna gain of the horn antenna is 19 dBi, and that of the patch antenna is 7.7 dBi. The capacitor of the SS has a capacitance of 10 F and a dielectric strength of 2.7 V. The DC-DC converter of the SS converts the capacitor voltage to 3.3 V, which is required for the input voltage for both the microcontroller board and the WLAN module.

Tables 3.3 and 3.4 show the parameters and the constants, respectively. The constants shown in Table 3.4 are predetermined from the measurement of the consumed power when the SS is powered by using a DC power source.

3.5.2 Experimental Results

Figure 3.6 shows the power consumption of the SS and the state of MPT when this work operates the implemented system. In Fig. 3.6, the SS receives DTIM beacons

Table 3.3: Values of parameters.

Parameters	Values
E_{max}	36.45 J
T_{DTIM}	10.24 s
T_{s1}	100 ms
T_{s2}	200 ms
T_{s3}	800 ms
T_{s4}	1000 ms

Table 3.4: Values of predetermined constants.

Constants	Values
E_{ct}	21.51 mJ
$E_{\mathrm{c,DTIM}}$	17.4 mJ
P_{sleep}	6.6 mW
T_{act}	90 ms
T_{rec}	40 ms

when the power consumption of the SS is high, and the SS operates in sleep mode when the power consumption of the SS is low. As shown in Fig. 3.6, the SS receives DTIM beacons when the ES does not transmit microwave power, and the SS operates in sleep mode when the ES transmits microwave power. Thus, this work confirmed the successful implementation of the scheduling scheme shown in Fig. 3.3.

Figure 3.7(a) shows both the timings of data frame transmissions of the SS and the values of the transmitted $n^{\star}_{\mathrm{t},k}$, and Fig. 3.7(b) shows the transition of the energy stored in the capacitor of the SS. As shown in Fig. 3.7(b), the energy stored in the capacitor increased and successfully converged to E_{max}. This occurs because the ES transmits microwave power in response to the data frames from the SS

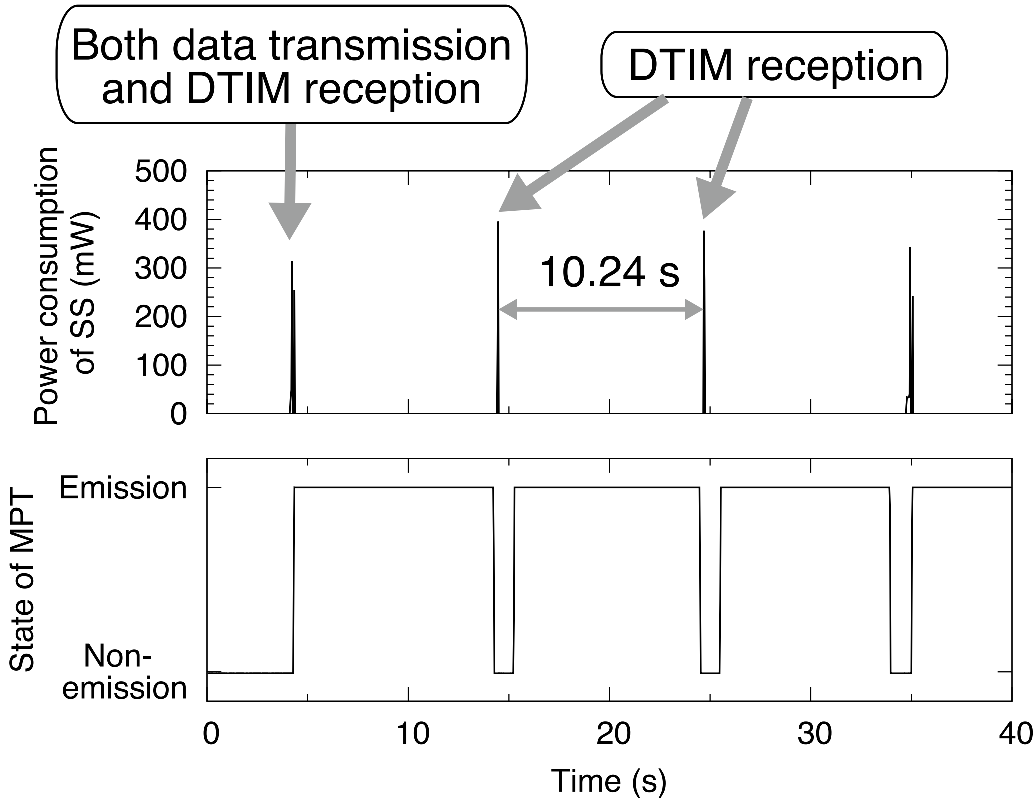

Figure 3.6: Operation of the implemented system. ©2014 IEICE

in the implemented system. In other words, the ES does not transmit microwave power if the SS fails to transmit data frames. In addition, if the SS fails to receive DTIM beacons because of microwaves for MPT, the power consumption of the SS exceeds the supplied power for MPT, and then the energy stored in the capacitor decreases.

In Fig. 3.7(b), the average increment of the energy stored in the capacitor is 22.9 mW when the energy increases. When both the power consumption of the SS and the duration over which the ES does not transmit microwave power are taken into account, the obtained power of the SS when the ES transmits microwave power is estimated as

$$\begin{aligned} &\frac{22.9\,\mathrm{mW} \cdot T_{\mathrm{DTIM}} + E_{\mathrm{c,DTIM}} + P_{\mathrm{sleep}}(T_{\mathrm{DTIM}} - T_{\mathrm{rec}})}{T_{\mathrm{DTIM}} - (T_{\mathrm{s2}} + T_{\mathrm{s3}})} \\ &\approx 34.5\,\mathrm{mW}. \end{aligned} \tag{3.8}$$

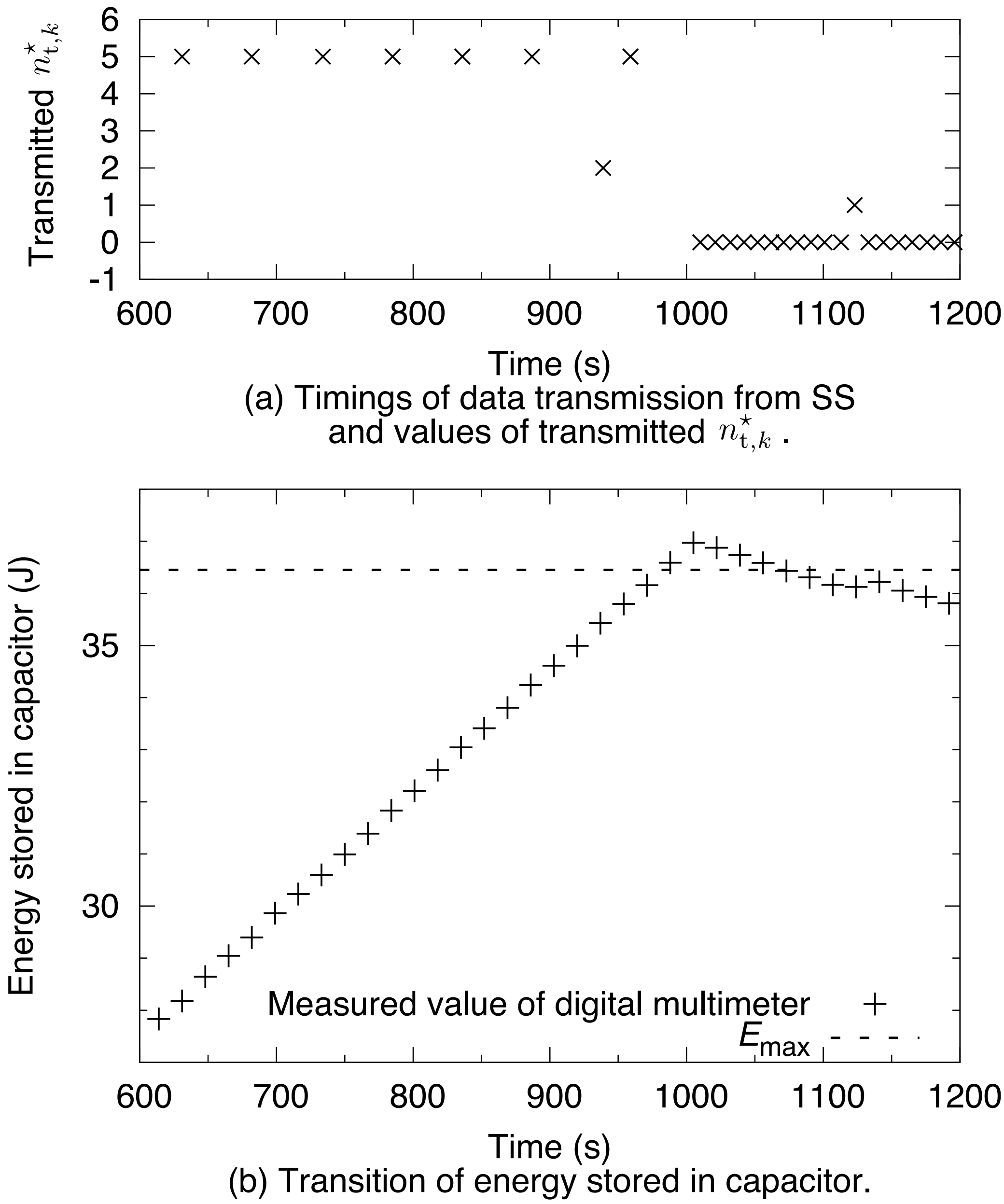

Figure 3.7: Energy stored in the capacitor and timing of data transmission. ©2014 IEICE

Table 3.5 shows the power density at each antenna when the ES transmits microwave power. Table 3.6 shows the link budget related to the experimental results. Using the power density at the patch antenna, the gain of the patch

Table 3.5: Power density at each antenna when input power of horn antenna is 12.8 W.

Position of antenna	Power density
Patch antenna of SS	19.44 W/m^2
WLAN module antenna of SS	11.72 W/m^2
Antenna of AP	1.67 mW/m^2
WLAN module antenna of SS	26.6 $\mu W/m^2$

Table 3.6: Link budget using experimental results.

	Values
Input power of horn antenna	41.07 dBm
Gain of horn antenna	19 dBi
Free space propagation loss	45.83 dB
Gain of patch antenna	7.7 dBi
Power efficiency of rectifier	−6.01 dB
Estimated output power of rectifier	15.93 dBm
Measured output power of rectifier	15.31 dBm

antenna, and the measured output power from the rectifier, the power efficiency of the rectifier is calculated.

3.6 Feasibility of Proposed System

This section discusses the feasibility of the proposed system by examining the maximum distance between the ES and the SS.

Regarding that microwaves affect human bodies, there are radio radiation protection guidelines that limit the power density at a certain distance from the power transmitter antenna in Japan [54]. According to these guidelines, the limited

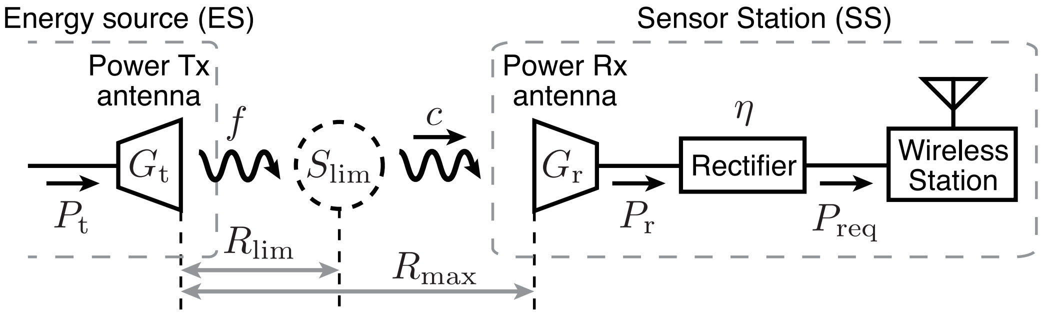

Figure 3.8: Positions of devices for analysis. ©2014 IEICE

Table 3.7: Definitions of symbols used in Fig. 3.8.

Symbols	Definitions	Units
c	Speed of light	m/s
f	Frequency for MPT	Hz
P_t	Input power of power transmitter antenna	W
G_t	Gain of power transmitter antenna	
R_{lim}	Maximum allowable distance satisfying guidelines	W
S_{lim}	Power density limit of guidelines	W/m^2
G_r	Gain of power receiver antenna	
P_r	Output power of power receiver antenna	W
η	Power efficiency of rectifier	
P_{req}	Required supplied power to SS	W
R_{max}	Maximum distance at which system is realized	m

maximum power density is 10 W/m^2 if this work uses 2.4 GHz or 6 W/m^2 if this work uses 900 MHz. In addition, this work regards radio wave propagation as free space propagation.

Figure 3.8 shows the positions of devices for this analysis, and the definitions of the symbols used in Fig. 3.8 are summarized in Table 3.7, where

$$S_{lim} = \frac{G_t P_t}{4\pi {R_{lim}}^2} \Leftrightarrow G_t P_t = 4\pi S_{lim} {R_{lim}}^2. \tag{3.9}$$

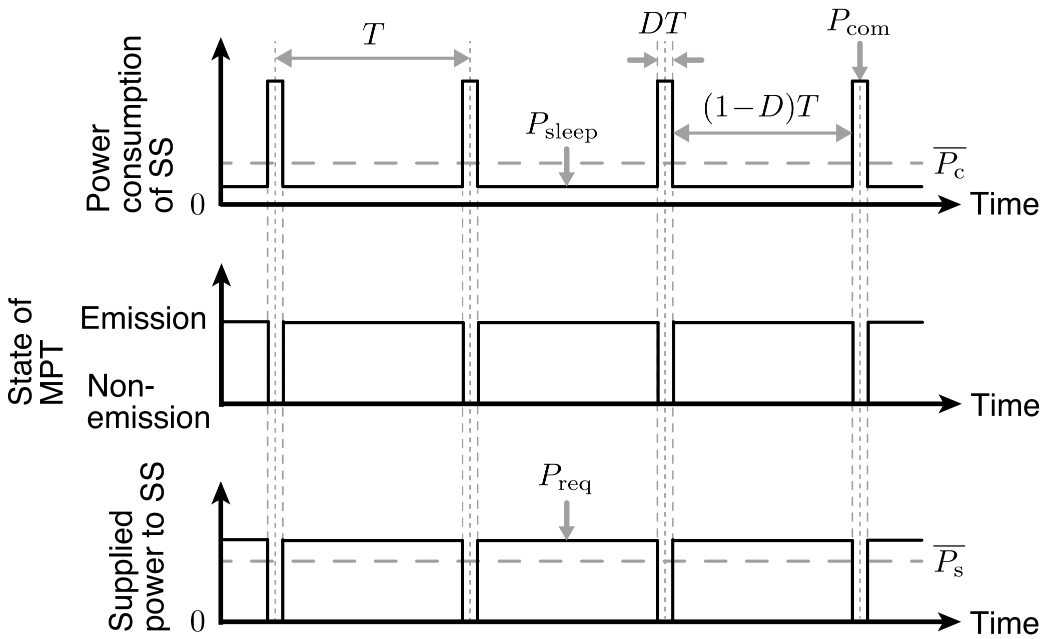

Figure 3.9: Assumed operational flow for analysis. ©2014 IEICE

Referring to the Friis transmission formula and using (3.9), P_{r} is written as

$$P_{\mathrm{r}} = G_{\mathrm{r}} G_{\mathrm{t}} P_{\mathrm{t}} \left(\frac{c}{4\pi R_{\mathrm{max}} f} \right)^2 = \frac{G_{\mathrm{r}} S_{\mathrm{lim}}}{4\pi} \left(\frac{R_{\mathrm{lim}} c}{R_{\mathrm{max}} f} \right)^2 . \tag{3.10}$$

Hence, P_{req} is written as

$$\begin{aligned} P_{\mathrm{req}} &= \eta P_{\mathrm{r}} = \eta G_{\mathrm{r}} G_{\mathrm{t}} P_{\mathrm{t}} \left(\frac{c}{4\pi R_{\mathrm{max}} f} \right)^2 \\ &= \frac{\eta G_{\mathrm{r}} S_{\mathrm{lim}}}{4\pi} \left(\frac{R_{\mathrm{lim}} c}{R_{\mathrm{max}} f} \right)^2 . \end{aligned} \tag{3.11}$$

As shown in (3.11), P_{req} is independent of G_{t} and P_{t}.

On the basis of the proposed scheduling system described in Sect. 3.4, this work assumes that the operational flows related to the SS and the ES are followed in Fig. 3.9. The definitions of the symbols used in Fig. 3.9 are summarized in Table 3.8. Note that duty ratio D is defined as the ratio of the active time of the SS to the cycle time T. This work provides equations related to the symbols used

Table 3.8: Definitions of symbols used in Fig. 3.9.

Symbols	Definitions	Units
T	Period with which SS communicates	s
D	Duty ratio	
P_{com}	Power consumption of SS to communicate	W
P_{req}	Required supplied power to SS	W
P_{sleep}	Power consumption of SS in sleep mode	W
$\overline{P_{\mathrm{c}}}$	Average power consumption of SS	W
$\overline{P_{\mathrm{s}}}$	Average supplied power to SS	W

in Fig. 3.9. $\overline{P_{\mathrm{c}}}$ and $\overline{P_{\mathrm{s}}}$ are defined as

$$\begin{aligned}\overline{P_{\mathrm{c}}} &:= [DTP_{\mathrm{com}} + (1-D)TP_{\mathrm{sleep}}]/T \\ &= DP_{\mathrm{com}} + (1-D)P_{\mathrm{sleep}}\end{aligned} \tag{3.12}$$

and

$$\overline{P_{\mathrm{s}}} := (1-D)TP_{\mathrm{req}}/T = (1-D)P_{\mathrm{req}}, \tag{3.13}$$

respectively. As shown in (3.12) and (3.13), both $\overline{P_{\mathrm{c}}}$ and $\overline{P_{\mathrm{s}}}$ are independent of T. Because the SS receives the minimum power necessary to perform wireless communication, this work assumes that the power consumption of the SS is equal to the supplied power to the SS, i.e., $\overline{P_{\mathrm{c}}} = \overline{P_{\mathrm{s}}}$. Hence, using (3.12) and (3.13), P_{req} is written as

$$P_{\mathrm{req}} = \frac{DP_{\mathrm{com}} + (1-D)P_{\mathrm{sleep}}}{1-D}. \tag{3.14}$$

Using (3.11) and (3.14), this work eliminates P_{req} and solves for R_{max}, and then R_{max} is written as

$$R_{\mathrm{max}} = \frac{R_{\mathrm{lim}}c}{2f}\sqrt{\frac{\eta(1-D)G_{\mathrm{r}}S_{\mathrm{lim}}}{\pi[DP_{\mathrm{com}} + (1-D)P_{\mathrm{sleep}}]}}. \tag{3.15}$$

Using (3.15), this work calculates R_{max} versus D. Table 3.9 shows the values of the parameters. In this analysis, there are two cases, i.e., frequency used for

Table 3.9: Parameters for analysis.

Parameters	Values	
	Case 1	Case 2
f	2.4 GHz	900 MHz
R_{lim}	1 m	1 m
S_{lim}	10 W/m^2	6 W/m^2
G_{r}	7.7 dBi	7.7 dBi
η	95%	95%
P_{com}	100 mW	100 mW
P_{sleep}	1 μW	1 μW

MPT is either 2.4 GHz or 900 MHz. Figure 3.10 shows the maximum distance R_{max} for each case. In Fig. 3.10, the horizontal axis indicates the duty ratio D. In addition, the vertical dashed line in Fig. 3.10 indicates the duty ratio in the experiment described in Sect. 3.5 ($D = 40\,\text{ms}/10.24\,\text{s} \approx 3.9 \times 10^{-1}\%$).

As shown in Fig. 3.10, the maximum distance realized by the system is longer using 900 MHz than using 2.4 GHz for MPT. In addition, even if the ES transmits microwave power using 2.4-GHz bands, the SS can receive sufficient power from the ES when $D \approx 3.9 \times 10^{-1}\%$, and the distance between the power transmitter and receive antennas is 10 m.

3.7 Conclusion

This chapter has studied the implementation and feasibility of using MPT to operate an SS that communicates with ES on a WLAN, where the center frequency of the microwave frequency used for MPT is set to be the same as that of WLAN to achieve high spectral efficiency. To avoid the influence of MPT on WLAN data communications, the CSMA/CA protocol of WLAN could be a solution; however, throughput degradation due to data rate control and disassociation from the AP due to the association algorithm could happen.

In order to solve these problems and realize the largest possible coverage of

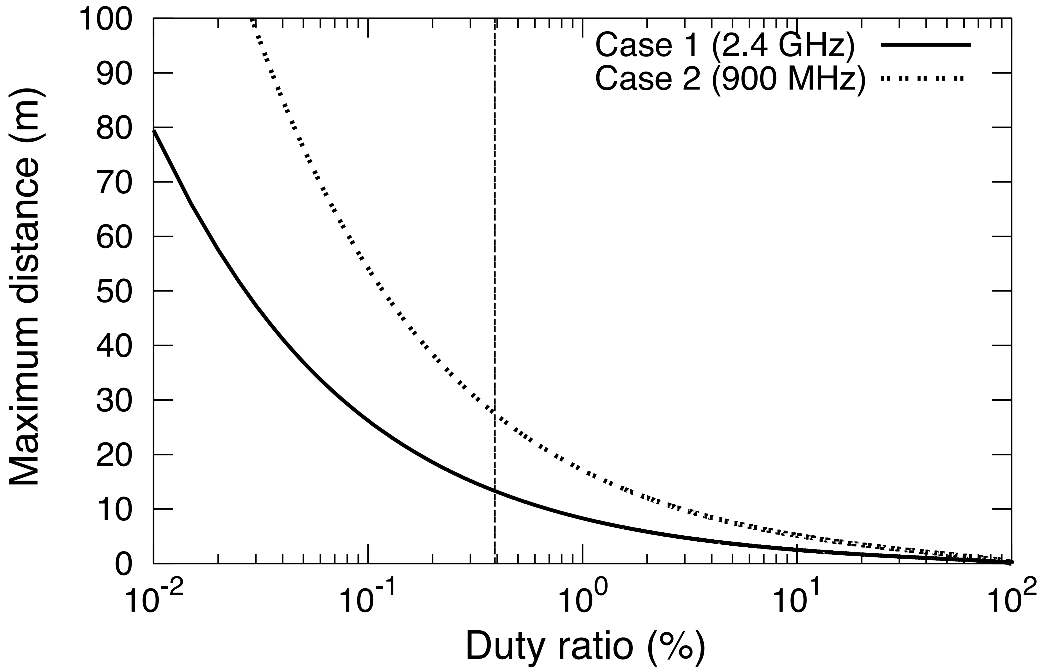

Figure 3.10: Maximum distance realized by system. ©2014 IEICE

MPT, this work has proposed a scheduling scheme in which MPT and wireless communications operate in different periods of time, and the MPT supplies a maximal amount of energy to the SS. Thus, the SS needs to inform the ES about the timings of data frame transmissions. Recall that the purpose of this work is to develop a scheduling scheme such that throughput degradation and disassociation problems due to the WLAN protocol are solved.

Then, this work implemented the proposed scheduling system. From the results of experiments, this work confirmed that the time sharing between MPT and WLAN data communications is successfully implemented. In addition, it is also confirmed that the remaining energy of the SS converges to the predetermined target value, i.e., the WLAN-based SS continuously works well.

Finally, on the basis of link budget analysis, this work clarified the maximum allowable distance between the power transmitter and receiver antennas when the proposed scheduling scheme is utilized. As a result, this work showed that the scheduling scheme can be applied to a room or a closed space.

Chapter 4

Rate Adaptation for WLAN Station Powered with Microwave Power Transmission

4.1 Overview

This chapter proposes an RAS based on exposure assessment using rectenna output for a WLAN station exposed to microwave radiation for MPT, and then carries out experiments to evaluate the performance of the system on which the proposed scheme is implemented. The rectenna was installed in the device powered with MPT, and converts the microwave power it receives into direct current power. The rectenna output enables a station based on the proposed scheme to assess whether it is exposed to microwave radiation for MPT. The historical data corresponding to the assessment result are used by the station to select an appropriate PHY data rate, where two independent memories, each of which contains a different set of historical data for rate adaptation, are prepared in advance.

The proposed scheme was implemented on a WLAN station by modifying a mac80211 device driver [49] that is widely used as a WLAN driver in Linux systems. This device driver uses two conventional RASs by default, i.e., PID [52] and Minstrel [53]. By modifying either PID or Minstrel, this chapter implemented PID-based or Minstrel-based proposed schemes on a WLAN station.

This chapter is organized as follows. Sect. 4.2 contains the proposal for an RAS with rectenna output. The experiments conducted to evaluate the performance are described in Sect. 4.3. Sect. 4.4 discusses the advantages of the proposed scheme. Finally, this chapter is concluded in Sect. 4.5.

4.2 Rate Adaptation Scheme Based on Exposure Assessment Using Rectenna Output

This section proposes an RAS based on exposure assessment using rectenna output. The design of this proposed scheme focuses on the use of historical data in both of the conventional RASs, i.e., PID and Minstrel. Recall that historical data are obtained from previous transmissions, e.g., historical data of the data frame loss ratio. This proposed scheme has the following two features: (i) the station assesses whether it is exposed to microwave radiation for MPT by using rectenna output power; (ii) the station selects an appropriate PHY data rate using historical data corresponding to the assessment result. The reason for using rectenna output power is twofold. First, a rectenna has been installed in a station powered with MPT and thus there is no need to install other devices to perform the exposure assessment. Second, the use of rectenna output power enables a station equipped with the rectenna to directly assess whether it is exposed to microwave radiation for MPT.

Fig. 4.1 illustrates the flowchart of the proposed scheme. This work explains kth rate adaptation at the time t_k as follows. Immediately before rate adaptation, the station measures the rectenna output power, $p_{\mathrm{o}}[k]$. Then, by using $p_{\mathrm{o}}[k]$, the station assesses whether it is exposed to microwave radiation for MPT. Let the power threshold be denoted by P_{th}. P_{th} should be determined from the power the station receives from microwaves for MPT. The reasons are as follows. The output power of the rectenna that receives microwaves for communication is less than 1 μW. The reason is that the rectenna output power is not more than the maximum transmission power that limited to 10 mW/MHz in Japan, and that at 2.4 GHz, the free space propagation loss at 1 m distance is equal to 40 dB in theory. On the other hand, the output power of the rectenna that receives microwaves for MPT is more than that of the rectenna that receives microwaves for communication, where, this work assumes that the supplied power to the station is of the order of milliwatt.

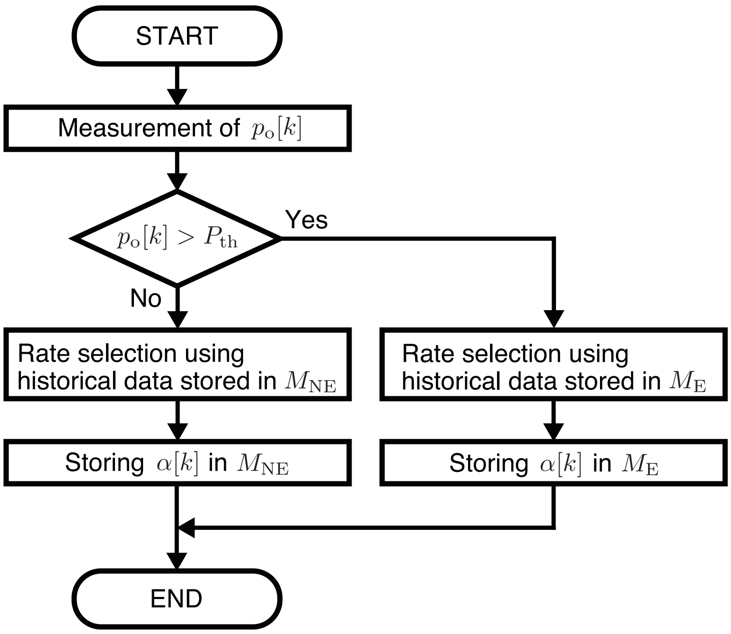

Figure 4.1: Flowchart of kth rate adaptation in the proposed scheme, where $\alpha[k]$ is the historical data obtained during $[t_{k-1}, t_k]$. ©2015 IEICE

Then, by using the historical data in the memory corresponding to the assessment result, the station selects an appropriate PHY data rate. The two independent memories in which the historical data for rate adaptation purposes are stored are denoted by M_E and M_{NE}, where the subscripts "E" and "NE" represent "exposure" and "non-exposure," respectively. When $p_o[k] > P_{th}$, the station determines that it is exposed to microwave radiation for MPT, after which it selects an appropriate PHY data rate using the historical data stored in M_E, which contains the corresponding historical exposure data. At the same time, the historical data obtained during $[t_{k-1}, t_k]$ is stored in M_E. On the other hand, when $p_o[k] \leq P_{th}$, the station determines that it is not exposed to microwave radiation for MPT and then selects an appropriate PHY data rate using the historical data stored in M_{NE}, which contains the historical data corresponding to non-exposure to microwave radiation for MPT. At the same time, historical data obtained during $[t_{k-1}, t_k]$ are stored in M_{NE}.

The scheme proposed in this work does not define a concrete RAS; instead, it uses historical data corresponding to the state of exposure to microwave radiation for MPT. Hence, a station based on the proposed scheme is able to use RASs corresponding to the exposure assessment result. In the experiments described in

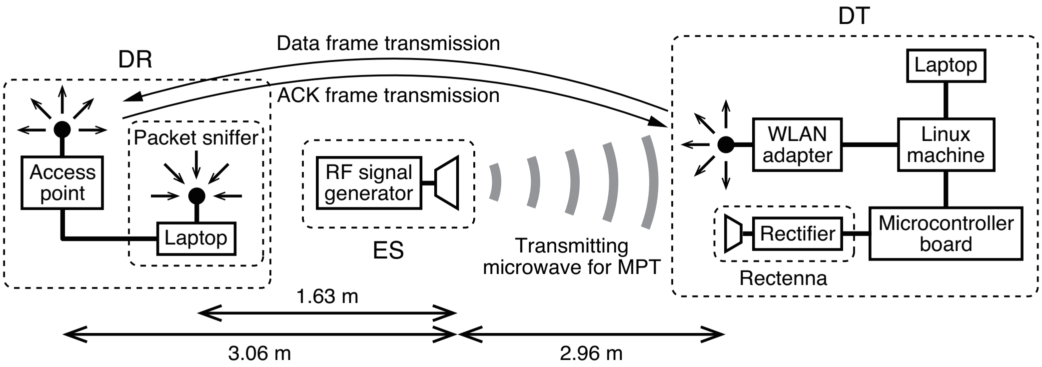

Figure 4.2: Experimental setup. ©2015 IEICE

Sect. 4.3, this work implemented the proposed scheme on a station such that the PHY data rate is selected on the basis of a single conventional RAS regardless of the magnitude of $p_o[k]$. This has the purpose of enabling a comparison with the conventional RAS. For example, in the "PID-based proposed scheme," $p_o[k]$ is measured immediately before the kth rate selection is measured, following which the PHY data rate is selected much in the same way as described in Sect. 2.2.7. Unlike in conventional PID, in the PID-based proposed scheme, historical data corresponding to the magnitude of $p_o[k]$ is used to select the PHY data rate. When $p_o[k] > P_{th}$, the PHY data rate is selected by using both $\hat{e}[k_{last,E}]$ and $e[k_{last,E}]$ that satisfy

$$k_{last,E} = \max_{k' \in \mathcal{N}_E} k', \tag{4.1}$$

where $\mathcal{N}_E = \{ n \mid p_o[n] > P_{th}, n = 1, \ldots, k-1 \}$. When $p_o[k] \leq P_{th}$, the PHY data rate is selected by using both $\hat{e}[k_{last,NE}]$ and $e[k_{last,NE}]$ that satisfy

$$k_{last,NE} = \max_{k' \in \mathcal{N}_{NE}} k', \tag{4.2}$$

where $\mathcal{N}_{NE} = \{ n \mid p_o[n] \leq P_{th}, n = 1, \ldots, k-1 \}$.

4.3 Experiments

This section presents an explanation of the experiments in this chapter. All measurements were performed in a radio frequency (RF) anechoic chamber to ensure the absence of any sources of wireless transmissions except for the system described in Sect. 4.3.1.

4.3.1 Experimental Setup

Fig. 4.2 illustrates the experimental setup for the performance evaluation of the proposed scheme. The experimental system consists of the following three devices, an ES, a data transmitter (DT), and a data receiver (DR).

The details of each of these devices are as follows. The ES intermittently transmits continuous microwaves for MPT to the DT and consists of a transmission antenna, an amplifier, and an RF signal generator. The microwaves generated by the RF signal generator are amplified via the amplifier, and are then transmitted from the transmission antenna to the DT.

The DT continuously transmits data frames to the DR. It consists of a commercial WLAN adapter (Logitec LAN-W150NU2AB, rt2800usb device driver), a Linux machine (Raspberry Pi Model B+ [57], Linux kernel 3.12.23+), a laptop (Apple MacBook Air, OS X 10.9.5), a microcontroller board (Arduino Uno board [58]), and a rectenna. The microcontroller board measures the rectenna output power and assesses whether the DT is exposed to microwave radiation for MPT, and then shares the information of the exposure assessment with the Linux machine. The Linux machine, which is remotely operated by the laptop, generates the data that are transmitted from the WLAN adapter.

The DR manages the network, receives the data frames transmitted from the DT, and captures the frames transmitted by the network as a packet sniffer. The DR consists of an access point (AP, Allied Telesis AT-TQ2403) and a laptop (Apple MacBook Pro, OS X 10.8.4). The AP generates and manages an IEEE 802.11g-based WLAN. The laptop receives the data frames transmitted from the DT via the AP and captures the frames transmitted from both the DT and the DR using its internal WLAN device. Note that the frame capture at the DR laptop is for the purpose of evaluating the throughput performance of the proposed scheme and is independent of the rate selection at the DT.

In this chapter, the experiments were conducted only in the environment consisting of one DT and one DR, whereas the performance evaluation of the proposed scheme in an environment consisting of multiple DTs and DRs is beyond the scope

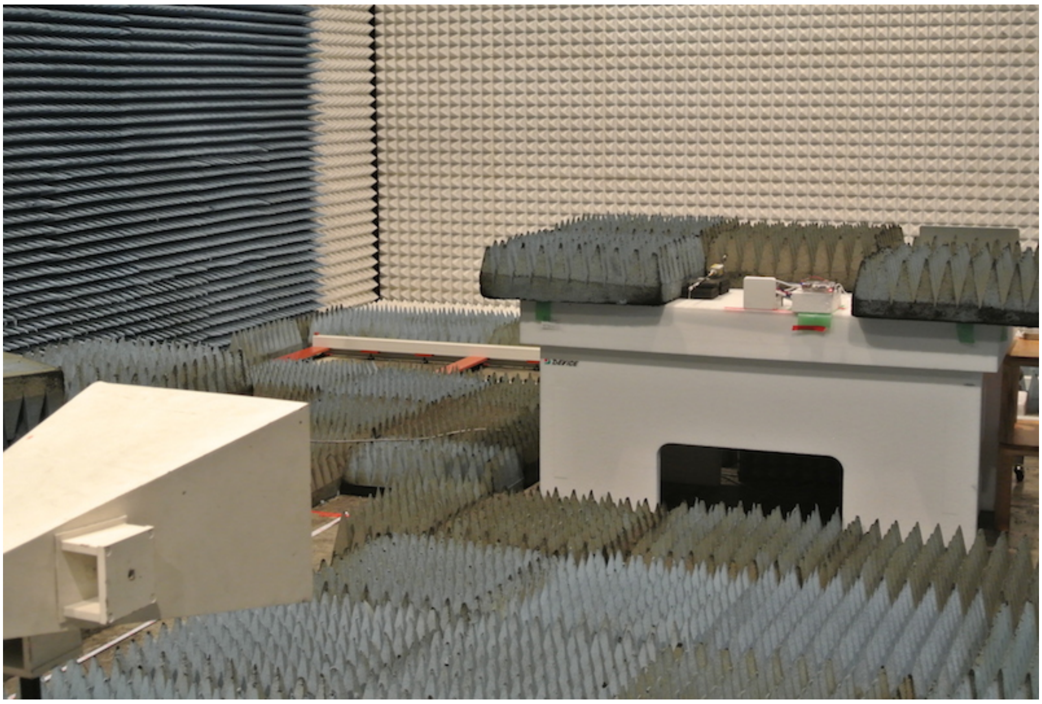

Figure 4.3: DT and power transmission antenna. ©2015 IEICE

of this chapter. The reason is that the performance in the environment consisting of multiple nodes depends not only on the RAS but also on other factors, e.g., contention between the multiple nodes and the method of transmitting microwave power to the multiple nodes. In addition, this work can verify the performance of the proposed scheme either in the environment consisting of multiple DTs and DRs or in the environment consisting of one DT and one DR. There are two reasons for this. One is that, in RASs, the PHY data rate for each pair of DT and DR is selected independently. The other one is that the two features of the proposed scheme, i.e., the exposure assessment using rectenna output and the use of historical data corresponding to the assessment result, are also performed independently on each DT.

4.3.2 Parameters

Fig. 4.2 shows the position of each of the devices, and Fig. 4.3 shows the entire DT and the power transmission antenna of the ES. Figs. 4.2 and 4.3 also show that

Table 4.1: Power density at each antenna when the ES transmits microwaves for MPT.

Antenna position	Power density
DT rectenna	0.86 mW/cm^2
DT WLAN adapter	0.92 mW/cm^2
DR laptop	1.33 μW/cm^2
DR AP	0.97 μW/cm^2

the DT is placed in front of the transmission antenna, whereas the DR is placed behind the transmission antenna such that the microwave power transmitted from the ES only affects the DT. The DR AP, transmission antenna, and DT are placed in a straight line. The distances from the transmission antenna to the DR AP, DR laptop, and DT are 3.06 m, 1.63 m, and 2.96 m, respectively.

The ES repeatedly transmits continuous microwaves for MPT to the DT for 1.4 s and then pauses for 5.0 s. Note that the duration of the microwave transmission, 1.4 s, satisfies the following two conditions. It ensures that the DT does not become disassociated from the DR AP because of the consecutive non-reception of beacon frames, and, additionally, it ensures that the PHY data rate is reduced during this period. The central frequency of the microwaves is set to be 2.457 GHz, and the bandwidth is less than 2 kHz. The gain of the power transmission antenna is 16.4 dBi. When the ES transmits the microwaves, the transmission power of the ES is set to be 17.9 W. In this case, the power density at each antenna position has the value listed in Table 4.1. Moreover, the DT rectenna output power when the ES transmited microwaves for MPT is 31 mW, whereas the DT rectenna output power when the ES did not transmit microwaves for MPT is 0 mW.

The DT transmits data frames at eight different PHY data rates: 6, 9, 12, 18, 24, 36, 48, and 54 Mbit/s. The central frequency for data transmission is set to be 2.457 GHz. Recall that MPT interferes with data transmission even when an adjacent channel is used for the purpose. The DT uses Iperf 2.0.5 [59] and generates UDP data traffic with an offered load of 54 Mbit/s, i.e., the network is saturated by traffic. The UDP datagram size is set to be 1,470 B and this size has no effect on the advantage of the proposed scheme because the throughput degradation discussed in this work is caused by the ACK frame loss.

The proposed scheme was implemented on the DT Linux machine by modifying the mac80211 device driver. Now, P_{th} was set to be 6 mW taking both that the DT rectenna output power of 0 mW when the ES did not transmit microwaves for MPT and that the DT rectenna output power of 31 mW when the ES transmited microwaves for MPT into account. This work emphasizes that this value is for assessing that the rectenna output power is either 0 mW or 31 mW and does not sensitively affect the performance of the proposed scheme. In addition, to compare the role of the exposure assessment by using the rectenna output in the proposed scheme, this work investigated the RAS without rectenna output for comparison as described in Sect. 4.3.3. As described in Sect. 4.2, regardless of the use of the rectenna output, the proposed scheme is implemented such that the PHY data rate is selected on the basis of either PID or Minstrel. The proposed scheme was modified as follows when implemented. As shown in Fig. 4.4, when the station determined that it was not exposed to microwave radiation for MPT in the $(k-1)$th rate adaptation, but instead determines that it is exposed to microwave radiation for MPT in kth rate adaptation, the station copies over the contents of M_{NE} to M_{E} immediately before the rate selection using M_{E}. Even when this work adds these modifications to the proposed scheme, this work are able to confirm its effectiveness because the content of M_{NE} shows the same behavior regardless of these modifications.

Based on the above discussion, this work investigated the performance of each of the three PID-based and each of the three Minstrel-based RASs, i.e., the PID, PID-based proposed scheme with and PID-based scheme without rectenna output for comparison, Minstrel, and Minstrel-based proposed scheme with and Minstrel-based scheme without rectenna output for comparison. The parameters used in both the PID-based and Minstrel-based RASs were initialized with the values in Tables 4.2 and 4.3, respectively, and were constant.

The experiments enabled to evaluate the UDP throughput, PHY data rate used in the data frame transmission, and data frame loss ratio for each RAS. Firstly, the UDP throughput was estimated based on the number of ACK frames the DR laptop captured with Wireshark [60]. Recall that the frame capture at the DR laptop is for the purpose of evaluating the throughput performance of the proposed scheme and is independent of the rate selection at the DT. Even though the use of

Table 4.2: PID default parameters.

T_{PID}	$R_{\mathrm{L,target}}$	α_{smooth}	α_{sharp}	C_{P}	C_{I}	C_{D}
125 ms	14%	8	0	15	9	15

Table 4.3: Minstrel default parameters.

T_{Minstrel}	α_{scale}
100 ms	0.25

Iperf would enable us to calculate the UDP throughput, this work estimated the UDP throughput with the captured frames. The reason is that the period of the UDP throughput estimation with the captured frames can be set shorter than that of the UDP throughput calculation with Iperf. Secondly, the PHY data rate in the PID-based RASs was measured on the DT Linux machine by using the debug function. On the other hand, the PHY data rate in the Minstrel-based RASs was estimated on the DR laptop by using captured data frames. In the Minstrel-based RASs, the reason for using captured data frames is that the PHY data rate used in each data transmission is unknown even when the debug function is used [53]. Lastly, the data frame loss ratio was measured on the DT Linux machine by using the debug function. This work emphasizes that the DT Linux machine was not able to completely obtain the data frame loss ratio because it did not have the required performance.

4.3.3 Rate Adaptation Scheme Based on Exposure Assessment Not Using Rectenna Output for Comparison

The performance of the proposed scheme was evaluated depending on whether the station uses rectenna output. For this reason, this work now explains the operation of an RAS without rectenna output for comparison. The station based

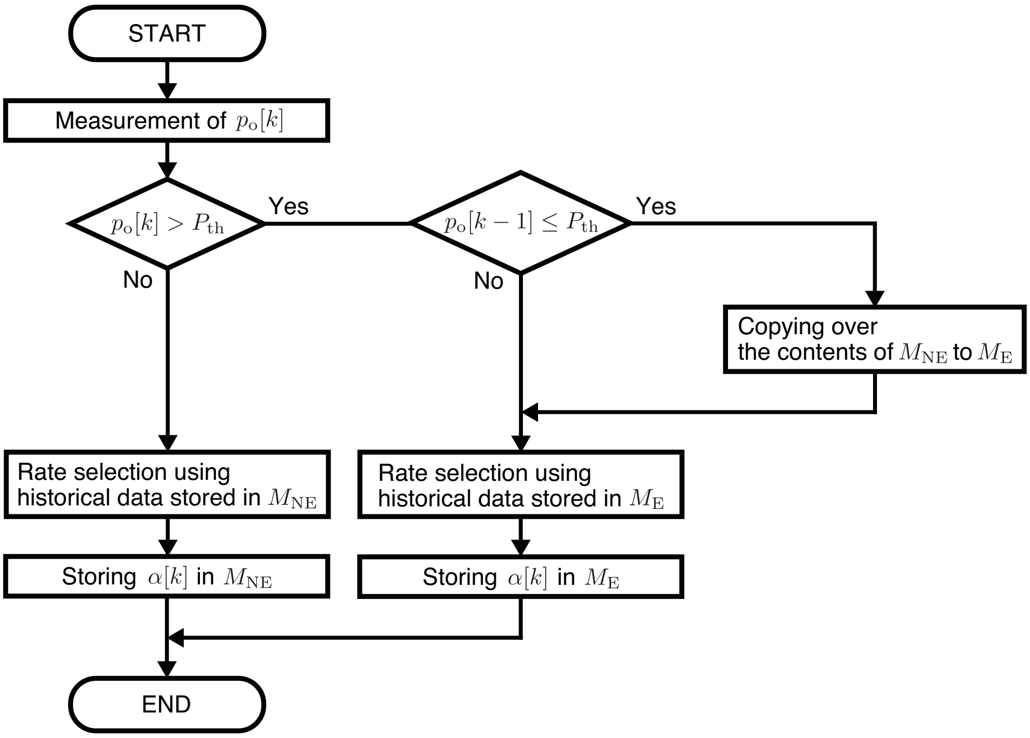

Figure 4.4: Flowchart of kth rate adaptation in the proposed scheme implemented for the experiments, where $\alpha[k]$ is the historical data obtained during $[t_{k-1}, t_k]$. ©2015 IEICE

on the scheme without rectenna output uses the results of previous data frame transmissions to assess whether the station is exposed to microwave radiation for MPT.

This work explains the operation in the kth rate adaptation at the time t_k using the value of $r_L[k]$ described in Sect. 2.2.7. Recall that $r_L[k]$ denotes the data frame loss ratio during $[t_{k-1}, t_k]$. Note that, even in the Minstrel-based scheme without rectenna output for comparison, $r_L[k]$ is calculated. Let the number of data frames transmitted during $[t_{k-1}, t_k]$ be denoted by $\Delta n_{\text{transmit}}[k]$. In the same way as the proposed scheme, two memories M_E and M_{NE} are prepared. Using these memories, the kth rate adaptation is performed as follows. When $r_L[k-1] < 50\%$, if $r_L[k] \geq 50\%$, the station determines that it is exposed to microwave radiation for MPT, and then selects an appropriate PHY data rate using the historical data stored in M_E and then stores in M_E the historical data obtained during $[t_{k-1}, t_k]$. Then, the station continues to use historical data stored in M_E until $\Delta n_{transmit}[m] \geq 3\Delta n_{transmit}[m-1]$ in the mth rate adaptation for any $m > k$. On the other hand, when the station uses the historical data stored in M_E in the $(k-1)$th rate adaptation, if $\Delta n_{transmit}[k] \geq 3\Delta n_{transmit}[k-1]$, it determines that it is not exposed to microwave radiation for MPT, and then selects an appropriate PHY data rate using historical data stored in M_{NE} and stores in M_{NE} the historical data obtained during $[t_{k-1}, t_k]$. Then, the station continues to use the historical data stored in M_{NE} until both $r_L[m-1] < 50\%$ and $r_L[m] \geq 50\%$ in the mth rate adaptation for any $m > k$.

4.3.4 Experimental Results

Fig. 4.5 shows both the UDP throughput and PHY data rate for each of the PID-based RASs. In addition, Fig. 4.6 shows both the data frame loss ratio and PHY data rate for each of the PID-based RASs. The red lines in Fig. 4.5 confirm that the PHY data rate is reduced when the DT is exposed to microwave radiation for MPT. Comparing both the UDP throughput and the PHY data rate in Fig. 4.5a with those in both Figs. 4.5b and 4.5c, it is clear that there has been an improvement. Note that, in Figs. 4.5b and 4.5c, there is a period during which the DT uses the lowest PHY data rate immediately after the MPT is discontinued. This is because the rate selection interval in the PID scheme is set to be 125 ms.

Fig. 4.7 shows both the UDP throughput and PHY data rate for each of the Minstrel-based RASs. In addition, Fig. 4.8 shows both the data frame loss ratio and PHY data rate for each of the Minstrel-based RASs. Except for the change in the link quality, the UDP throughput in Fig. 4.7a can be considered the same as that in Figs. 4.7b and 4.7c. On the other hand, after the MPT is discontinued, a PHY data rate of less than 48 Mbit/s is sometimes used in Fig. 4.7a, while that of 54 Mbit/s is always used in Figs. 4.7b and 4.7c.

4.4 Discussion

Taking the observations in Sect. 4.3 into account, this section discusses the advantages of the proposed scheme.

Exposure assessment based on the rectenna output allows a device equipped

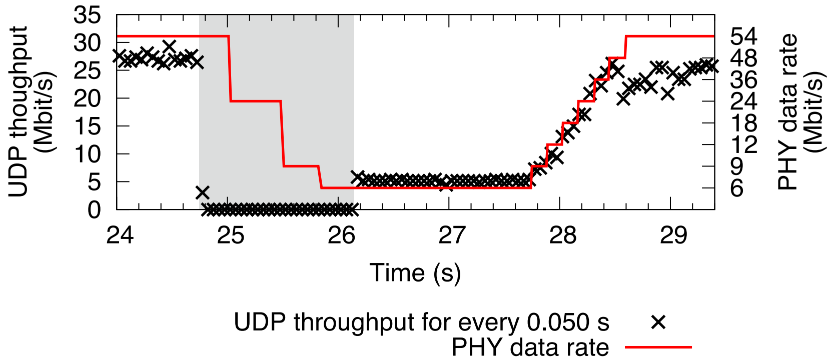

(a) PID

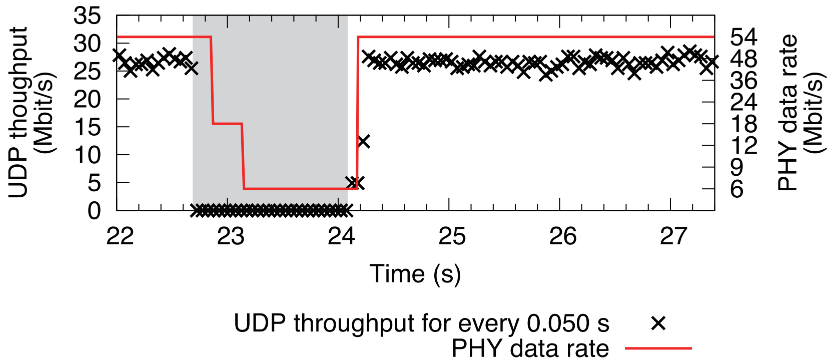

(b) PID-based proposed scheme

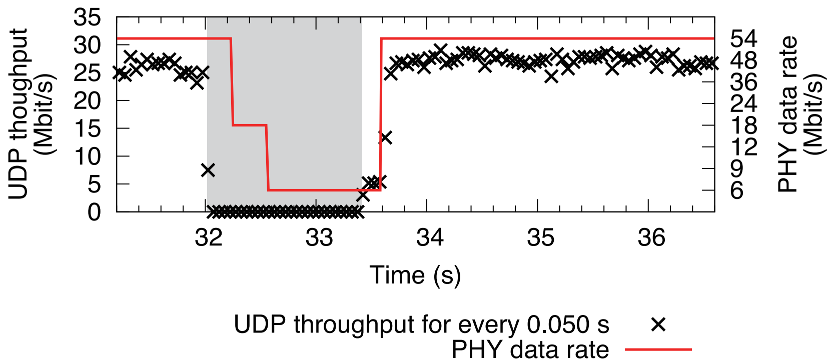

(c) PID-based scheme without rectenna output for comparison

Figure 4.5: UDP throughput and PHY data rate for each of the three PID-based RASs, where the grey area indicates the time during which the DT is exposed to microwave radiation for MPT. ©2015 IEICE

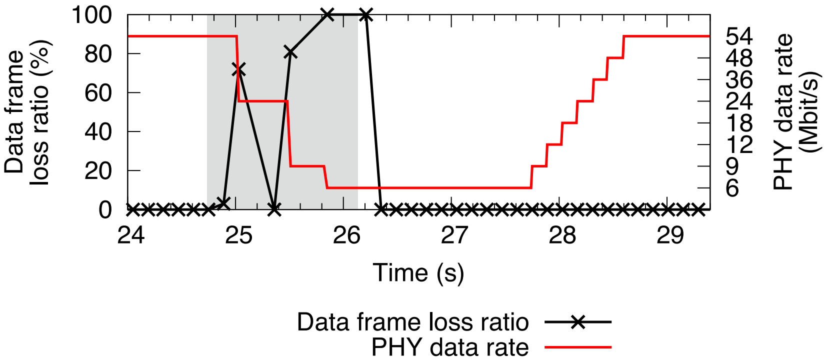

(a) PID

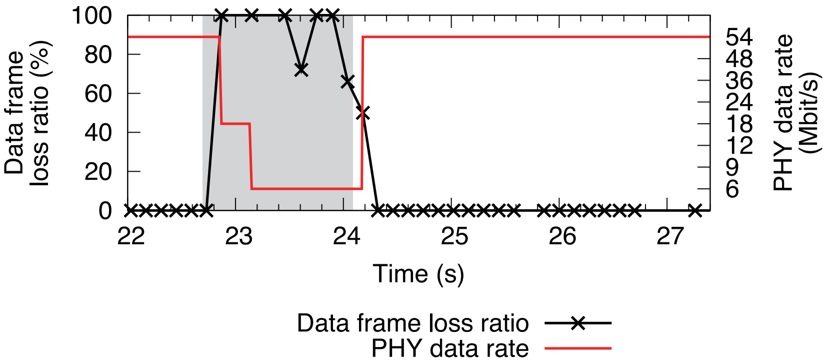

(b) PID-based proposed scheme

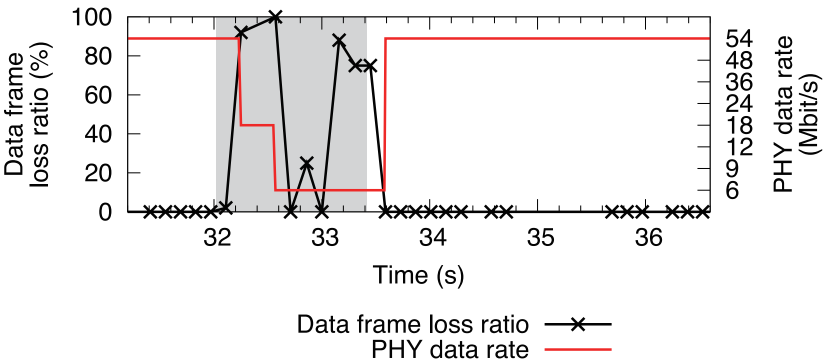

(c) PID-based scheme without rectenna output for comparison

Figure 4.6: Data frame loss ratio and PHY data rate for each of the three PID-based RASs, where the grey area indicates the time during which the DT is exposed to microwave radiation for MPT. ©2015 IEICE

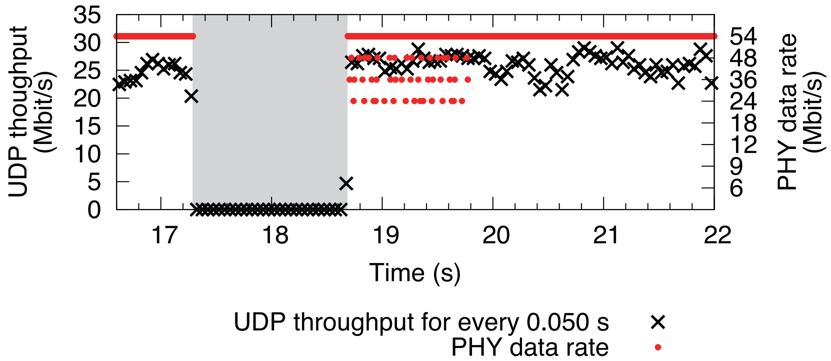

(a) Minstrel

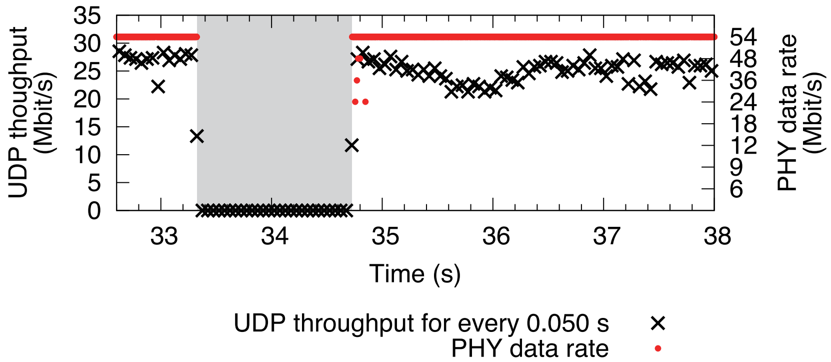

(b) Minstrel-based proposed scheme

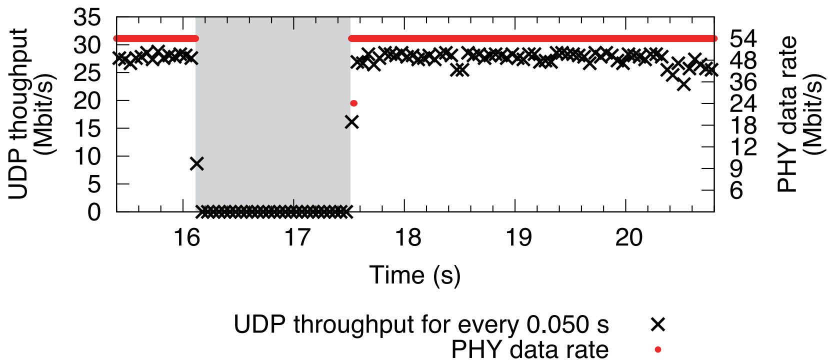

(c) Minstrel-based scheme without rectenna output for comparison

Figure 4.7: UDP throughput and PHY data rate for each of the three Minstrel-based RASs, where the grey area indicates the time during which the DT is exposed to microwave radiation for MPT. ©2015 IEICE

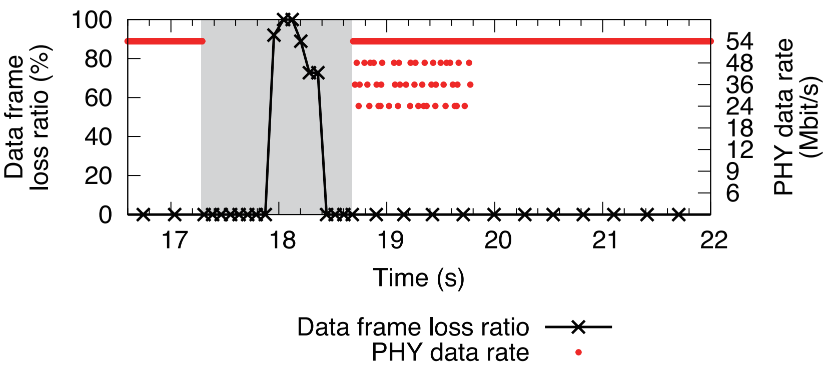

(a) Minstrel

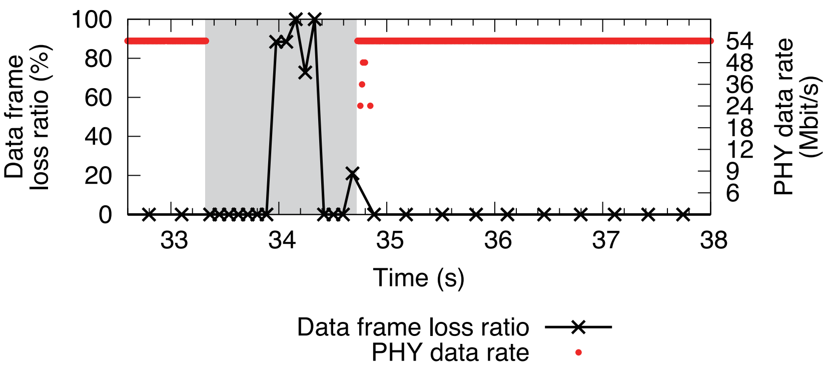

(b) Minstrel-based proposed scheme

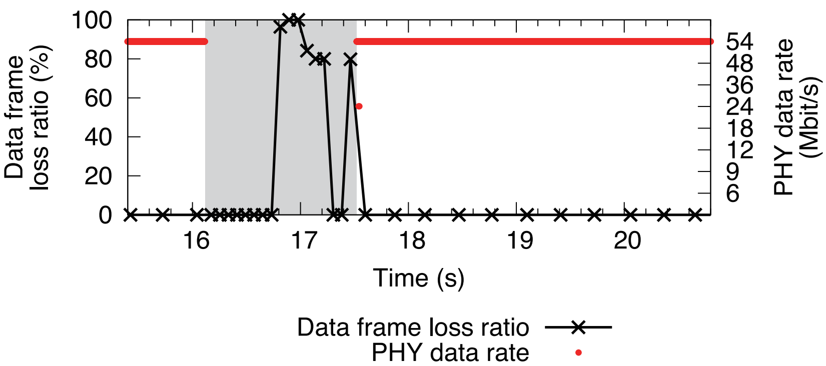

(c) Minstrel-based scheme without rectenna output for comparison

Figure 4.8: Data frame loss ratio and PHY data rate for each of the three Minstrel-based RASs, where the grey area indicates the time during which the DT is exposed to microwave radiation for MPT. ©2015 IEICE

with the rectenna to precisely recognize in real-time that the device is exposed to microwave radiation for MPT. Here it should be noted that if a device is powered with MPT, the device has a rectenna installed. According to either Figs. 4.5b and 4.5c or Figs. 4.7b and 4.7c, the UDP throughput of the proposed scheme can be regarded as the same as that of the RAS without rectenna output for comparison, except for the change in the quality of the link. However, the use of the scheme without rectenna output for comparison has the following two disadvantages. Firstly, as described in Sect. 1, because of the exposure assessment based on the data frame loss ratio, when severe SNR degradation occurs at the receiver, the station based on the scheme erroneously determines that it is exposed to microwave radiation for MPT even when it is not. Secondly, because of the exposure assessment based on the number of transmitted data frames, when the station transmits data frames under unsaturated traffic conditions or when there are other nodes that operate in the same band as the station, the station can erroneously determine that it is exposed to microwave radiation for MPT even when this is not the case. The cause of this is that the number of transmitted data frames fluctuates depending both on the traffic conditions and on the contention level.

Using historical data corresponding to the state of exposure to microwave radiation for MPT has the following advantages in comparison with using continuously historical data stored in a single memory.

- After discontinuation of the MPT, the high PHY data rate is maintained, and thus throughput degradation does not occur. Compared with Fig. 4.5b, Fig. 4.5a shows that the PHY data rate was reduced over the period from 24.8 to 26.2 s temporarily, after which a PHY data rate below 48 Mbit/s was used over the period from 26.2 to 28.6 s. On the other hand, Fig. 4.5b shows that a PHY data rate below 48 Mbit/s was not used over the period from 24.2 to 26.6 s.
- Using historical data corresponding to the exposure assessment result prevents the content of historical data from being corrupted. Compared with Fig. 4.7b, Fig. 4.7a shows that a PHY data rate below 48 Mbit/s was sometimes used over the period from 18.7 to 19.8 s. On the other hand, Fig. 4.7b shows that a PHY data rate below 48 Mbit/s was not used over the period from 34.9 to 35.8 s. The reason for this is that in Fig. 4.7a, the contents stored in M_{NE} were corrupted due to a data frame loss when the DT is exposed to

microwave radiation for MPT.

4.5 Conclusion

This section proposed an RAS based on exposure assessment using rectenna output for a WLAN station powered with MPT. The objective of the proposed scheme was to prevent the throughput degradation that occurs when the station is exposed to microwave radiation for MPT. This objective was achieved by utilizing the rectenna output to assess whether the station is exposed to microwave radiation for MPT. Note that a device powered with MPT has a rectenna. The proposed scheme is based on the use of two independent memories in which historical data for rate adaptation were stored with the aim of mitigating the PHY data rate degradation when the station is exposed to microwave radiation for MPT. The historical data stored in the two memories were used to determine when the station was either exposed or not exposed to microwave radiation for MPT. This work implemented the proposed scheme on a station using a commercial WLAN device and a widely used device driver. The results confirmed the effectiveness of the proposed scheme.

Chapter 5

Knowledge-based Design of Primary Exclusive Region for Spectrum Database

5.1 Overview

This chapter presents a framework for updating the PER. In the proposed framework, when the PU's interference constraint is not satisfied, the PU sends a message to the database indicating that the PU is experiencing harmful interference. When the database receives the message, it updates the PER satisfying the PU's interference constraint. The database utilizes its available knowledge such as the locations and power levels of STs to perform the PER update. After the update, this chapter evaluates the PER radius by deriving it for each type of database knowledge by using stochastic geometry. Stochastic geometry is a tractable mathematical tool for the analysis of wireless networks with random spatial models [24,61]. Specifically, the effect is significant in the analysis of the probability of rare events and in the performance evaluation for various parameters. In this chapter, an analysis with stochastic geometry enables to calculate the PER size satisfying the PU's interference constraint without Monte Carlo simulations, i.e., without many simulation runs.

The purpose of the work is to evaluate the spectrum reuse efficiency depending on whether the knowledge about the secondary user is available or unavailable.

Specifically, this chapter verifies that more detailed database knowledge about the SU density and transmission power leads to a smaller PER size.

The contributions of this chapter are twofold. The first contribution is the proposal of a new update framework for the database, which is required to dynamically adjust the SU's strategy in consideration of the incumbent PU. The second contribution is a qualitative discussion of the multiple types of database knowledge in several scenarios. The database can determine an appropriate PER if it has a complete awareness of the locations and power levels of all the STs. However, it is difficult for the database to always have information about all the STs because they may move and use power control.

The remainder of this chapter is organized as follows. Sect. 5.2 presents the system model. Sect. 5.3 derives the radius of the PER by using stochastic geometry. Sect. 5.4 describes the proposed framework. Sect. 5.5 explains the database knowledge for determining the PER. Sect. 5.6 evaluates the performance of the proposed framework in several scenarios, i.e., Nakagami-m fading superimposed on log-normal shadowing and log-normal shadowing scenarios. Finally, the conclusions and future work are presented in Sect. 5.7.

5.2 System Models

5.2.1 Locations of PU and SU

Fig. 5.1 illustrates an example of a system. This work assumes, without loss of generality, that a PR has an antenna for transmission and reception, and is located at the origin o on $\mathbb{R}^2$. STs are assumed to be distributed with a uniform Poisson point process with intensity λ_{ST}, i.e., λ_{ST} denotes the density of an ST. This work assumes that STs attempt to operate in a single radio channel allocated to the PU.

The database responds to an ST by transmitting its available spectrum band when the ST queries the database with its location. The database is assumed to associate with all STs and to know the PR location. The database determines the PER radius r_{e}, where the PER is a closed disk of radius r_{e} centered at o. Let the circular region be denoted by $b(o, r_{\mathrm{e}})$. On the basis of the PER, the database responds by either transmitting its transmission permission or prohibition to the ST. That is, the database allows the STs outside the PER (i.e., on $\mathbb{R}^2 \setminus b(o, r_{\mathrm{e}})$)

to transmit data, and forbids the STs inside the PER (i.e., on $b(o, r_e)$) to transmit data. In addition, when the database allows an ST to transmit data, the database transmits information of the available power level set to the ST. The knowledge of the STs, i.e., locations of the querying STs and the available power level sets of the STs, is stored in the database. Let a set of locations of STs on $\mathbb{R}^2 \setminus b(o, r_e)$ be denoted by $\Phi_{ST} \setminus b(o, r_e)$.

For an ST at $x \in \Phi_{ST} \setminus b(o, r_e)$, let the transmission power level of the ST and the fading coefficient (with unit mean) between the ST and the PR be denoted by p_x and h_x, respectively. This work assumes that $\{p_x\}$ are independent and identically distributed (i.i.d.) discrete random variables with a probability mass function $f_p(p)$. This work assumes that the transmission power levels of STs are discrete random variables, considering that the STs transmit at various power levels. This is because current standards, such as WLAN [4] and long-term evolution advanced (LTEA) [62], support the use of multiple discrete transmission power levels and a power control mechanism. This work emphasizes that it does not matter when the transmission power levels of STs are continuous random variables. $\{h_x\}$ are i.i.d. random variables with a probability density function $f_h(h)$. Let random variables distributed with $f_p(p)$ and $f_h(h)$ be denoted by p and h, respectively. Let a set of the available power levels for the data transmissions of the STs be denoted by $\mathcal{P}$.

5.2.2 Definition of primary outage

This section defines a PU's outage as follows: A PU's outage occurs when the level of aggregate interference power that the PR receives from all STs outside the PER exceeds a maximum tolerable interference threshold of the PU. Let the aggregate interference power level be denoted by I_{agg}; then, I_{agg} can be written as follows:

$$I_{agg} = \sum_{x \in \Phi_{ST} \setminus b(o, r_e)} h_x p_x \|x\|^{-\alpha}, \tag{5.1}$$

where α represents the path loss exponent, and $\|x\|$ denotes the Euclidean distance between x and the origin. Note that I_{agg} is a random variable depending on $f_p(p)$, $f_h(h)$, and the locations of the STs. PU outage, as defined in this paragraph, can be rewritten as $I_{agg} > I_{th}$, where I_{th} represents the maximum tolerable interference threshold of the PU. This work defines the outage probability of a PU as $\mathbb{P}(I_{agg} >$

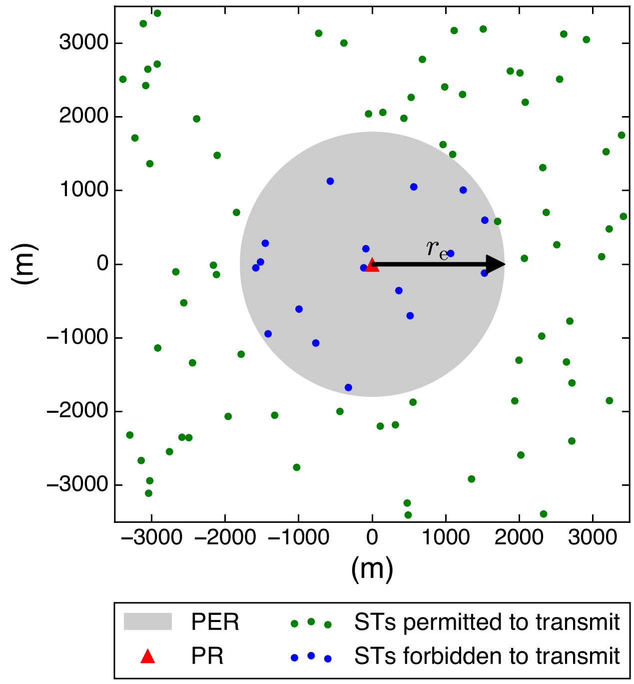

Figure 5.1: Example of system ($\lambda_{\mathrm{ST}} = 2 \times 10^{-6}\,\mathrm{m}^{-2}$). ©2016 IEICE

I_{th}) and consider this outage probability as a function of r_{e}, $P_{\mathrm{out}}(r_{\mathrm{e}})$, i.e., $P_{\mathrm{out}}(r_{\mathrm{e}}) = \mathbb{P}(I_{\mathrm{agg}} > I_{\mathrm{th}})$.

This work assumes that the spectrum usage is improved if this work can reduce the PER radius r_{e}. The validity of this assumption is derived from an increase in the size of the area $\mathbb{R}^2 \setminus b(o, r_{\mathrm{e}})$ with a reduction in r_{e}, where the STs in $\mathbb{R}^2 \setminus b(o, r_{\mathrm{e}})$ receive messages from the database with permission to transmit. However, overall I_{agg} increases with a reduction in r_{e} due to an increase in the number of transmitting STs, and thus, the outage probability $\mathbb{P}(I_{\mathrm{agg}} > I_{\mathrm{th}})$ also increases.

This work assumes that the database determines r_{e} such that

$$P_{\mathrm{out}}(r_{\mathrm{e}}) \leq \beta_{\mathrm{target}}, \tag{5.2}$$

where β_{target} denotes the outage probability value of the target PU. Considering that $P_{\mathrm{out}}(r_{\mathrm{e}})$ increases with a decrease in r_{e}, this work finds that there is a minimum r_{e} satisfying $P_{\mathrm{out}}(r_{\mathrm{e}}) \leq \beta_{\mathrm{target}}$. Let the minimum r_{e} be denoted by $r_{\mathrm{e,min}}$; then, the following condition is satisfied:

$$P_{\mathrm{out}}(r_{\mathrm{e,min}}) = \beta_{\mathrm{target}}. \tag{5.3}$$

5.3 Derivation of PER Radius Using Stochastic Geometry

Based on the system model described in Sect. 5.2.2, this section presents a derivation of $r_{\mathrm{e,min}}$ for β_{target} by using stochastic geometry. This work achieves this by using an approach known as "cumulant matching approach [63]," which enables to approximately express an unknown distribution as a well-known distribution by matching the cumulants of the unknown distribution to those of the well-known distribution.

This work calculates the nth cumulant of I_{agg}, κ_n, using the moment generating function of I_{agg}, $M_{I_{\mathrm{agg}}}(s)$. κ_n for $n = 1, 2, \ldots$ uniquely determine the distribution of I_{agg}. In particular, the first cumulant κ_1 and second cumulant κ_2 are the mean and variance of I_{agg}, respectively, i.e., $\mathbb{E}_{I_{\mathrm{agg}}}(I_{\mathrm{agg}}) = \kappa_1$ and $\mathrm{Var}_{I_{\mathrm{agg}}}(I_{\mathrm{agg}}) = \kappa_2$, where $\mathrm{Var}_X(X)$ denotes the variance of a random variable X. By using Campbell's theorem [23], $M_{I_{\mathrm{agg}}}(s)$ can be rewritten as follows:

$$\begin{aligned}
M_{I_{\mathrm{agg}}}(s) &= \mathbb{E}_{I_{\mathrm{agg}}}(\mathrm{e}^{sI_{\mathrm{agg}}}) \\
&= \mathbb{E}_{\Phi_{\mathrm{ST}}}\left(\prod_{x \in \Phi_{\mathrm{ST}} \setminus b(o, r_{\mathrm{e}})} \exp(s p_x h_x \|x\|^{-\alpha}) \right) \\
&= \exp\left\{ 2\pi\lambda_{\mathrm{ST}} \sum_{p \in \mathcal{P}} \int_0^\infty \int_{r_{\mathrm{e}}}^\infty \Big[\exp(sphr^{-\alpha}) - 1 \Big] r f_h(h) f_p(p) \,\mathrm{d}r \mathrm{d}h \right\}. \quad (5.4)
\end{aligned}$$

Using (5.4), κ_n can be written as follows:

$$\begin{aligned}
\kappa_n &= \left. \frac{\mathrm{d}^n \ln M_{I_{\mathrm{agg}}}(s)}{\mathrm{d}s^n} \right|_{s=0} \\
&= 2\pi\lambda_{\mathrm{ST}} \sum_{p \in \mathcal{P}} \int_0^\infty \int_{r_{\mathrm{e}}}^\infty (phr^{-\alpha})^n r f_h(h) f_p(p) \,\mathrm{d}r \mathrm{d}h \\
&= \frac{2\pi\lambda_{\mathrm{ST}}}{(n\alpha - 2) {r_{\mathrm{e}}}^{n\alpha - 2}} \mathbb{E}_h(h^n) \mathbb{E}_p(p^n), \quad (5.5)
\end{aligned}$$

where $\mathbb{E}_h(h^n)$ and $\mathbb{E}_p(p^n)$ represent the nth moments of h and p, respectively, and can be expressed as follows:

$$\mathbb{E}_h(h^n) = \int_0^\infty h^n f_h(h)\,\mathrm{d}h, \tag{5.6}$$

$$\mathbb{E}_p(p^n) = \sum_{p\in\mathcal{P}} p^n f_p(p). \tag{5.7}$$

Using the cumulant matching approach with κ_n, this work can express $P_{\text{out}}(r_\text{e})$ for r_e analytically, and evaluate $r_{\text{e,min}}$ for β_{target} numerically by describing r_e and $P_{\text{out}}(r_\text{e})$ with $r_{\text{e,min}}$ and β_{target}, respectively. This work considers two well-known distributions for the approximation of the aggregate interference distribution: the gamma distribution (GD) approximation and the shifted log-normal distribution (SLND) approximation.

5.3.1 Gamma distribution approximation

When this work approximates the aggregate interference distribution with the GD, referring to [64–66], the probability density function (PDF) of the aggregate interference I_{agg}, f_G, can be expressed as follows:

$$f_\text{G}(I_{\text{agg}}) \simeq \frac{1}{\Gamma(k_\text{G})\theta_\text{G}^{k_\text{G}}} I_{\text{agg}}^{k_\text{G}-1} \mathrm{e}^{-I_{\text{agg}}/\theta_\text{G}}, \tag{5.8}$$

$$k_\text{G} = \kappa_1^2/\kappa_2 \tag{5.9}$$

$$\theta_\text{G} = \kappa_2/\kappa_1, \tag{5.10}$$

where $\Gamma(\cdot)$ denotes the gamma function defined as $\Gamma(s) = \int_0^\infty t^{s-1}\mathrm{e}^{-t}\,\mathrm{d}t$. In addition, $P_{\text{out}}(r_\text{e})$ can be expressed as follows:

$$P_{\text{out}}(r_\text{e}) = \mathbb{P}(I_{\text{agg}} > I_{\text{th}}) \simeq 1 - \frac{\gamma(k_\text{G}, I_{\text{th}}/\theta_\text{G})}{\Gamma(k_\text{G})}, \tag{5.11}$$

where $\gamma(\cdot,\cdot)$ denotes the lower incomplete gamma function defined as $\gamma(s,x) = \int_0^x t^{s-1}\mathrm{e}^{-t}\,\mathrm{d}t$. (5.9) and (5.10) are derived by considering that the GD with a shape parameter k_G and scale parameter θ_G has the first cumulant (mean) of $k_\text{G}\theta_\text{G}$ and second cumulant (variance) of $k_\text{G}\theta_\text{G}^2$.

5.3.2 Shifted log-normal distribution approximation

When this work approximates the aggregate interference distribution with the SLND, referring to [67–69], the PDF of the aggregate interference I_{agg}, f_{SLN}, can be expressed as follows:

$$f_{\mathrm{SLN}}(I_{\mathrm{agg}}) \simeq \frac{1}{\sqrt{2\pi}\sigma_{\mathrm{SLN}}(I_{\mathrm{agg}} - c_{\mathrm{SLN}})} \exp\left\{\frac{[\ln(I_{\mathrm{agg}} - c_{\mathrm{SLN}}) - \mu_{\mathrm{SLN}}]^2}{2{\sigma_{\mathrm{SLN}}}^2}\right\} \tag{5.12}$$

$$c_{\mathrm{SLN}} = \kappa_1 - \exp\left(\mu_{\mathrm{SLN}} + \frac{{\sigma_{\mathrm{SLN}}}^2}{2}\right) \tag{5.13}$$

$$\mu_{\mathrm{SLN}} = \frac{1}{2}\left[\ln\left(\frac{\kappa_2}{\exp({\sigma_{\mathrm{SLN}}}^2) - 1}\right) - {\sigma_{\mathrm{SLN}}}^2\right] \tag{5.14}$$

$${\sigma_{\mathrm{SLN}}}^2 = \ln\left(\sqrt[3]{W + \sqrt{W^2 - 1}} + \sqrt[3]{W - \sqrt{W^2 - 1}} - 1\right) \tag{5.15}$$

$$W = 1 + {\kappa_3}^2/(2{\kappa_2}^3). \tag{5.16}$$

In addition, $P_{\mathrm{out}}(r_{\mathrm{e}})$ can be expressed as follows:

$$P_{\mathrm{out}}(r_{\mathrm{e}}) = \mathbb{P}(I_{\mathrm{agg}} > I_{\mathrm{th}}) \simeq Q\left(\frac{\ln(I_{\mathrm{th}} - c_{\mathrm{SLN}}) - \mu_{\mathrm{SLN}}}{\sigma_{\mathrm{SLN}}}\right), \tag{5.17}$$

where $Q(\cdot)$ denotes the Q-function defined as $Q(x) = (1/\sqrt{2\pi}) \int_x^{\infty} \exp(-t^2/2)\,\mathrm{d}t$.

5.4 Proposed Framework for Updating PER

This section explains the principle of the proposed framework. Fig. 5.2 shows the proposed framework for updating the PER. The proposed framework assumes that the database is connected both with the PR and with the STs through wired networks, and that messages from each entity are instantly transmitted. When the PU experiences outage, the PU transmits a message to the database indicating that the interference constraint of the PU is not met. Receiving the message, the database updates the PER. On the basis of the updated PER, the database either transmits transmission permission or transmission prohibition to the querying STs.

It is necessary to point out that the study of the impact of the database update delay on performance is beyond the scope of this chapter; instead, the purpose of this work is to evaluate the spectrum reuse efficiency depending on whether knowledge about the SU is available. Specifically, this work focuses on the unusual situation that a PU experiences harmful interference when an SU operates in the licensed spectrum sent from the database, and a message from the PU indicating

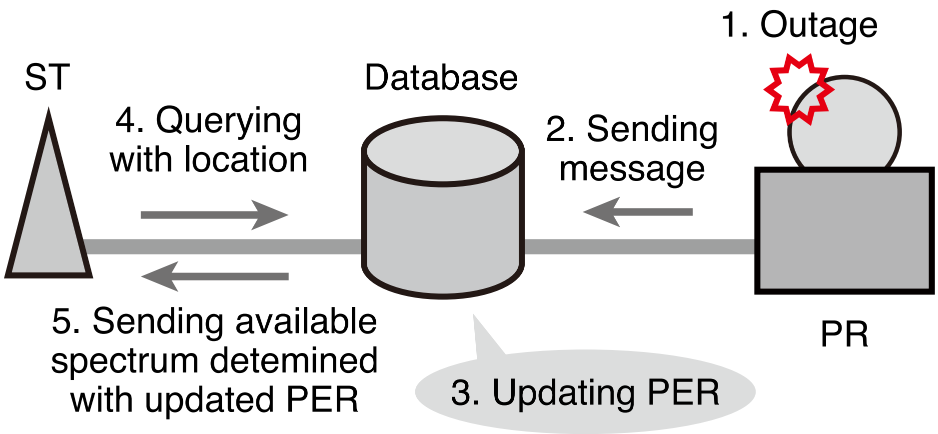

Figure 5.2: Proposed framework for updating PER size. ©2016 IEICE

that the PU is experiencing harmful interference arrives at the database within a very short time.

The proposed scheme is not directly applicable to TV systems. This is because, although the database establishes a PER centered at the location of a PR in the proposed scheme, the location of a PR is unknown to the database of a TV system [70]. On the other hand, in a radar system, the number of the primary receivers is very small and their locations are well known to the database [70].

5.5 Database Knowledge for Numerical Evaluation

Here this section provides particulars of the knowledge, which is stored in the database, and which is used to update the PER. Depending on these particulars, the size of the PER after the update varies. Let the database knowledge set be denoted by $\mathcal{K}_{\mathrm{DB}}$. This work assumes that $\mathcal{K}_{\mathrm{DB}}$ consists of two knowledge sets, namely $\mathcal{K}_{p_{\mathrm{ST}}}$ and $\mathcal{K}_{\lambda_{\mathrm{ST}}}$, i.e., $\mathcal{K}_{\mathrm{DB}} = \{\mathcal{K}_{p_{\mathrm{ST}}}, \mathcal{K}_{\lambda_{\mathrm{ST}}}\}$.

This work explains each knowledge set separately. The knowledge set $\mathcal{K}_{p_{\mathrm{ST}}}$ indicates whether the database knows the distribution of the power levels of the STs. $\mathcal{K}_{p_{\mathrm{ST}}}$ affects the value of $\mathbb{E}_p(p^n)$ in (5.5). Now, this work considers the following two cases.

1. One case is $\mathcal{K}_{p_{\mathrm{ST}}} = \{f_p\}$, i.e., the database knows the power levels of all STs and their distribution f_p. This case assumes that the power levels of all STs

are distributed with f_p, i.e., $\mathbb{E}_p(p^n)$ is given by (5.7).

2. The other case is $\mathcal{K}_{p_{\mathrm{ST}}} = \emptyset$, i.e., the database does not know the power levels of all STs and does not know the distribution of these power levels. This case considers the worst case in which all STs use the maximum power level $p_{\max} = \max_{p' \in \mathcal{P}} p'$, i.e., $\mathbb{E}_p(p^n)$ is given by $\mathbb{E}_p(p^n) = {p_{\max}}^n$. Of course, STs are assumed to transmit with power $p_{\max}$ as a worst case. By overestimating the ST transmission power, a large PER is established even when the database does not know ST power levels during an early stage.

The knowledge set $\mathcal{K}_{\lambda_{\mathrm{ST}}}$ indicates whether the database knows the actual density of the STs. $\mathcal{K}_{\lambda_{\mathrm{ST}}}$ affects the value of λ_{ST} in (5.5). This work considers the following two cases.

1. One case is $\mathcal{K}_{\lambda_{\mathrm{ST}}} = \{\widetilde{\lambda}_{\mathrm{ST}}\}$, i.e., the database knows that the actual density of the STs is $\widetilde{\lambda}_{\mathrm{ST}}$. This case assumes that STs are distributed with a density of $\widetilde{\lambda}_{\mathrm{ST}}$, i.e., $\lambda_{\mathrm{ST}} = \widetilde{\lambda}_{\mathrm{ST}}$.

2. The other case is $\mathcal{K}_{\lambda_{\mathrm{ST}}} = \emptyset$, i.e., the database does not know the actual density of the STs. This case considers the worst case in which the STs occur in a very high-density distribution $\lambda_{\mathrm{ST,worst}}$, i.e., $\lambda_{\mathrm{ST}} = \lambda_{\mathrm{ST,worst}}$

The purpose of this work is to evaluate the spectrum reuse efficiency depending on whether the knowledge about the secondary user is available; thus, a discussion of cases in which the knowledge is imperfect is beyond the scope of this chapter. However, in general, when the information is imperfect, this work has to provide a sufficient margin for the PER so that the PER radius satisfies (5.2).

5.6 Numerical Evaluation

This section evaluates the performance of the proposed framework. Let $r_{\mathrm{e,min}}(\beta_{\mathrm{target}}; \mathcal{K}_{p_{\mathrm{ST}}}, \mathcal{K}_{\lambda_{\mathrm{ST}}})$ denote $r_{\mathrm{e,min}}$ for β_{target} in database knowledge $\mathcal{K}_{\mathrm{DB}} = \{\mathcal{K}_{p_{\mathrm{ST}}}, \mathcal{K}_{\lambda_{\mathrm{ST}}}\}$. This work obtains $r_{\mathrm{e,min}}$ for β_{target} in the case $\mathcal{K}_{\mathrm{DB}}$, by evaluating $P_{\mathrm{out}}(r_{\mathrm{e}})$ for r_{e} in the case $\mathcal{K}_{\mathrm{DB}}$ and then by describing r_{e} and $P_{\mathrm{out}}(r_{\mathrm{e}})$ with $r_{\mathrm{e,min}}$ and β_{target}, respectively.

Table 5.1: ST power levels and their probabilities.

Power level p	Probability $f_p(p)$
0.001 W	0.4
0.01 W	0.3
0.1 W	0.2
1 W	0.1

5.6.1 Parameters

This work assumes two fading scenarios. The first scenario uses Nakagami-m fading superimposed on log-normal shadowing. Recalling that the fading random variable h is distributed with unit mean, $\mathbb{E}_h(h^n)$ can be written as

$$\mathbb{E}_h(h^n) = \frac{\Gamma(m+n)}{\Gamma(m)m^n} \exp\left[\frac{n(n-1)\sigma_{\mathrm{dB}}{}^2}{2\xi^2}\right], \tag{5.18}$$

where m and σ_{dB} denote the Nakagami-m fading parameter and the log-normal shadowing parameter with the dB-spread, respectively, and $\xi = 10/\ln(10)$ [71]. The second scenario is with log-normal shadowing. Similarly, $\mathbb{E}_h(h^n)$ can be written as

$$\mathbb{E}_h(h^n) = \exp\left[\frac{n(n-1)\sigma_{\mathrm{dB}}{}^2}{2\xi^2}\right]. \tag{5.19}$$

Table 5.1 shows the power levels of STs and their probabilities, i.e., $\mathcal{P} = \{0.001, 0.01, 0.1, 1\}$ and $p_{\max} = 1$.

This work simply uses $\widetilde{\lambda}_{\mathrm{ST}} = 10^{-3}\,\mathrm{m}^{-2}$ and $\lambda_{\mathrm{ST,worst}} = 10^{-6}\,\mathrm{m}^{-2}$ such that $\lambda_{\mathrm{ST,worst}} \geq \widetilde{\lambda}_{\mathrm{ST}}$ is satisfied, as an example analysis. In general, with an increase in $\lambda_{\mathrm{ST,worst}}$, this work has to enlarge the radius of the primary exclusive region in the case $\mathcal{K}_{\lambda_{\mathrm{ST}}} = \emptyset$ because of an increase in the number of transmitting STs.

Finally, Table 5.2 lists the parameters and their values.

5.6.2 Trivial scheme for determining the PER radius

This work uses the following system model to determine r_{e} by using a trivial scheme, which this work then compares with the results obtained by the proposed

Table 5.2: Parameters.

Parameter	Value
α	4
$\widetilde{\lambda}_{\mathrm{ST}}$	$10^{-6}\,\mathrm{m}^{-2}$
$\lambda_{\mathrm{ST,worst}}$	$10^{-3}\,\mathrm{m}^{-2}$
m	1
σ_{dB}	6
I_{th}	10^{-8} W

scheme. Note that this system model differs from that shown in Fig. 1. Fig. 5.3 shows the system model for the trivial scheme with a PR at its origin. The database establishes a circular PER centered at the PR with a radius of r_{e}. The PER radius is determined such that the aggregate interference at the PR from N_{ST} transmitting STs at the edge of the PER, I_{agg}, is less than a threshold I_{th}. The transmission power levels of the STs are assumed to be $p_{\max}$, where this work recalls that $p_{\max} = \max_{p' \in \mathcal{P}} p'$. In addition, this work assumes that there is no fading.

Using this system model, this work derives $r_{\mathrm{e,min}}$ for β_{target}, i.e, $r_{\mathrm{e,min}}$ is the minimum r_{e} satisfying (5.2). I_{agg} can be defined as follows:

$$I_{\mathrm{agg}} = N_{\mathrm{ST}} p_{\max} {r_{\mathrm{e}}}^{-\alpha}. \tag{5.20}$$

I_{agg} is not a random variable, and $\mathbb{P}(I_{\mathrm{agg}} > I_{\mathrm{th}}) \leq \beta_{\mathrm{target}}$ is satisfied whenever $I_{\mathrm{agg}} \leq I_{\mathrm{th}}$. Thus, $r_{\mathrm{e,min}}$ is obtained from $I_{\mathrm{agg}} = I_{\mathrm{th}}$, and can be expressed as follows:

$$r_{\mathrm{e,min}} = \sqrt[\alpha]{\frac{N_{\mathrm{ST}} p_{\max}}{I_{\mathrm{th}}}}. \tag{5.21}$$

5.6.3 Numerical results

Fig. 5.4 shows $\mathbb{P}(I_{\mathrm{agg}} > I_{\mathrm{th}})$ for I_{th} in the case $\mathcal{K}_{\mathrm{DB}} = \{\{f_p\}, \{\widetilde{\lambda}_{\mathrm{ST}}\}\}$. Figs. 5.4a and 5.4b show the results for the first scenario in which Nakagami-m fading is superimposed on log-normal shadowing and for the second scenario of log-normal shadowing, respectively. The blue and red lines are obtained from the approximations with the GD and with the SLND, respectively. The black line was obtained by performing a Monte Carlo simulation, where the number of

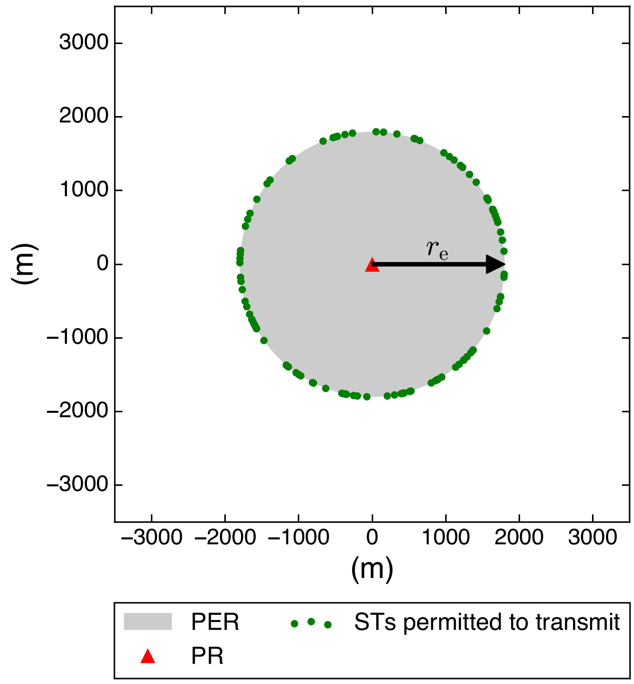

Figure 5.3: Example of system model of the trivial scheme (N_{ST} = 100). ©2016 IEICE

simulation runs is 5×10^6. This figure shows that the performance for both of these approximations is almost the same as for the black line when $\mathbb{P}(I_{agg} > I_{th})$ is lower than 10^{-3}. In addition, it shows that the use of the SLND provides more accurate approximation than that of the GD when $\mathbb{P}(I_{agg} > I_{th})$ is lower than 10^{-3}.

Fig. 5.5 shows $P_{out}(r_e)$ for r_e in the case $\mathcal{K}_{DB} = \{\{f_p\}, \{\widetilde{\lambda}_{ST}\}\}$, where the points indicated by crosses are obtained by performing a Monte Carlo simulation, where the number of simulation runs is 5×10^6 for each cross point. In addition, Figs. 5.5a and 5.5b show the results for the first scenario of Nakagami-m fading superimposed on log-normal shadowing and for the second scenario of log-normal shadowing, respectively, where the blue and red lines are directly obtained from (5.11) and (5.17), respectively. This figure confirms that this work can quantitatively compare the simulation and approximate analysis results for $P_{out}(r_e)$.

Fig. 5.6 shows the minimum PER radius $r_{e,min}$ satisfying the probability β_{target} of the PU experiencing outage with respect to database knowledge $\mathcal{K}_{DB}$ in the first scenario, where Nakagami-m fading superimposed on log-normal shadowing is as-

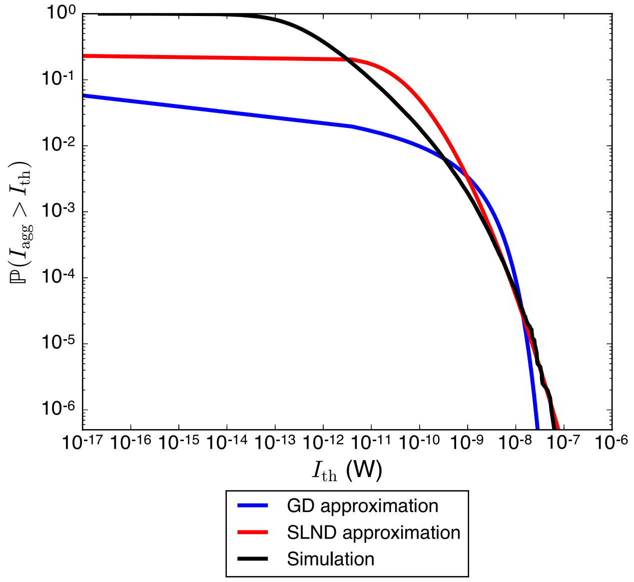

(a) First scenario of Nakagami-m fading superimposed on log-normal shadowing ($r_{\mathrm{e}} = 172\,\mathrm{m}$).

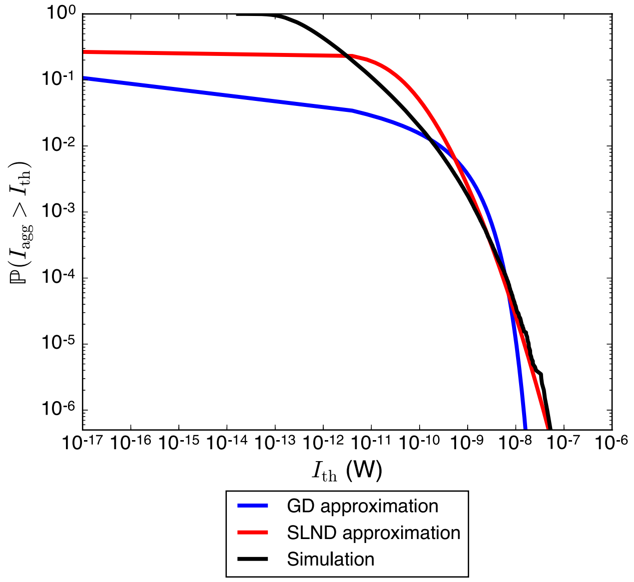

(b) Second scenario of log-normal shadowing ($r_{\mathrm{e}} = 171\,\mathrm{m}$).

Figure 5.4: $\mathbb{P}(I_{\mathrm{agg}} > I_{\mathrm{th}})$ for I_{th} in the case $\mathcal{K}_{\mathrm{DB}} = \{\{f_p\}, \{\widetilde{\lambda}_{\mathrm{ST}}\}\}$. ©2016 IEICE

sumed. This figure confirms that $r_{\mathrm{e,min}}(\beta_{\mathrm{target}}; \mathcal{K}_{p_{\mathrm{ST}}}, \mathcal{K}_{\lambda_{\mathrm{ST}}})$ monotonically increases

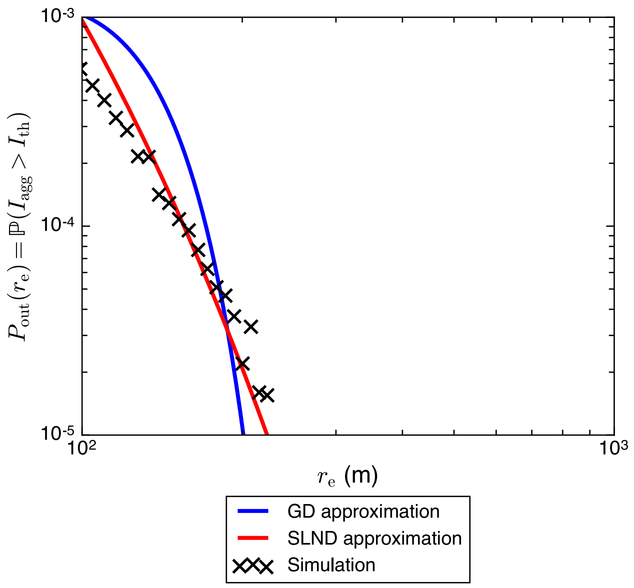

(a) First scenario of Nakagami-m fading superimposed on log-normal shadowing.

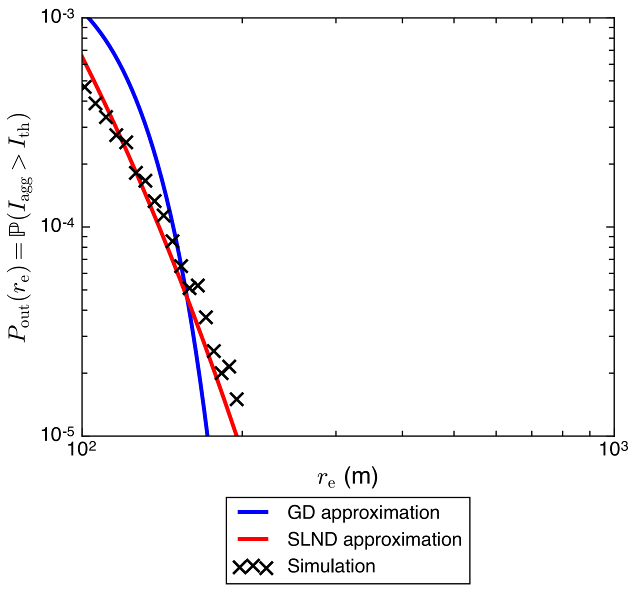

(b) Second scenario of log-normal shadowing.

Figure 5.5: $r_{\rm e}$ vs. $P_{\rm out}(r_{\rm e})$ in case $\mathcal{K}_{\rm DB} = \{\{f_p\}, \{\widetilde{\lambda}_{\rm ST}\}\}$ (cross points indicate Monte Carlo simulation results). ©2016 IEICE

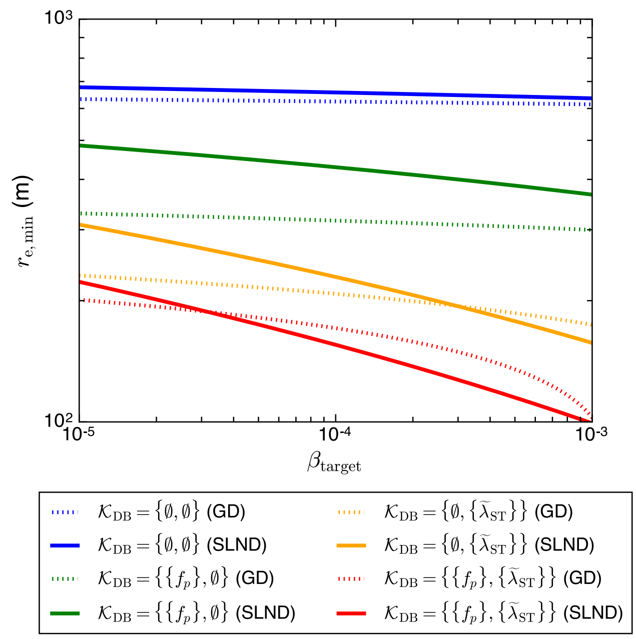

Figure 5.6: $r_{\mathrm{e,min}}$ vs. β_{target} with respect to $\mathcal{K}_{\mathrm{DB}}$ in the first scenario of Nakagami-m fading superimposed on log-normal shadowing. ©2016 IEICE

with decreasing β_{target}, i.e., the stricter the interference constraint imposed upon the PU, the larger the PER radius must be determined to ensure that (5.2) is satisfied. In addition, for all β_{target}, both $r_{\mathrm{e,min}}(\beta_{\mathrm{target}}; \{f_p\}, \mathcal{K}_{\lambda_{\mathrm{ST}}}) < r_{\mathrm{e,min}}(\beta_{\mathrm{target}}; \emptyset, \mathcal{K}_{\lambda_{\mathrm{ST}}})$ and $r_{\mathrm{e,min}}(\beta_{\mathrm{target}}; \mathcal{K}_{p_{\mathrm{ST}}}, \{\tilde{\lambda}_{\mathrm{ST}}\}) < r_{\mathrm{e,min}}(\beta_{\mathrm{target}}; \mathcal{K}_{p_{\mathrm{ST}}}, \emptyset)$. That is, more detailed knowledge of the SU density and transmission power levels leads to a smaller PER radius satisfying (2) and to a more efficient spatial reuse of the licensed spectrum as described in Sect 3.2.

Fig. 5.7 shows $r_{\mathrm{e,min}}$ for satisfying β_{target} with respect to $\mathcal{K}_{\mathrm{DB}}$ in the second scenario, where log-normal shadowing is assumed. Each curve in Fig. 5.7 is below the corresponding curve in Fig. 5.6. This is because the elimination of the effect of Nakagami-m fading reduces the variance of h, and then $\mathbb{P}(I_{\mathrm{agg}} > I_{\mathrm{th}})$ decreases.

Fig. 5.8 shows $r_{\mathrm{e,min}}$ for satisfying β_{target} with respect to $\mathcal{K}_{\mathrm{DB}}$ in the first scenario, where Nakagami-m fading superimposed on log-normal shadowing is assumed. Note that, only in this evaluation, this work assumes that $\mathcal{P} = \{1\,\mathrm{W}\}$ and $p_{\max} = 1\,\mathrm{W}$, i.e., the variance of p is zero. This figure explains that $r_{\mathrm{e,min}}(\beta_{\mathrm{target}}; \emptyset, \mathcal{K}_{\lambda_{\mathrm{ST}}}) = r_{\mathrm{e,min}}(\beta_{\mathrm{target}}; \{f_p\}, \mathcal{K}_{\lambda_{\mathrm{ST}}})$ for all β_{target} in the same $\mathcal{K}_{\lambda_{\mathrm{ST}}}$. This is because in the worst

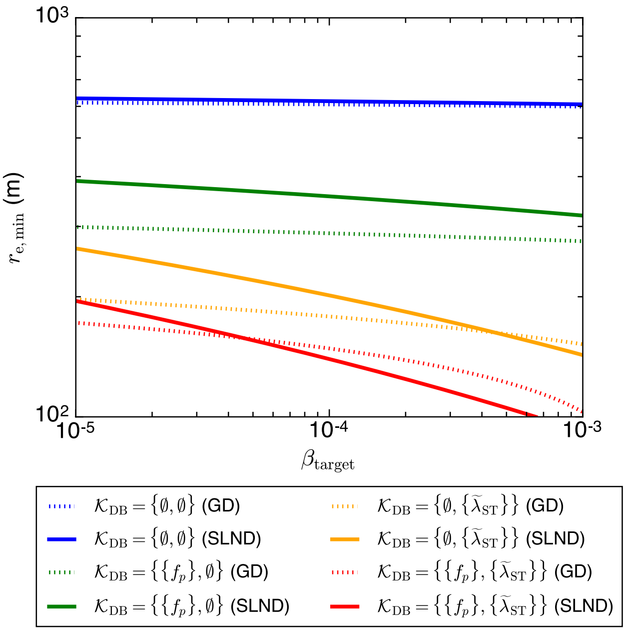

Figure 5.7: $r_{\mathrm{e,min}}$ vs. β_{target} with respect to $\mathcal{K}_{\mathrm{DB}}$ in the second scenario of log-normal shadowing. ©2016 IEICE

case $\mathcal{K}_{p_{\mathrm{ST}}} = \emptyset$, STs are assumed to be using the maximum power level.

Fig. 5.9 shows $r_{\mathrm{e,min}}$ for β_{target} with respect to $\mathcal{K}_{\mathrm{DB}} = \{\mathcal{K}_{p_{\mathrm{ST}}}, \emptyset\}$ in the first scenario, where Nakagami-m fading superimposed on log-normal shadowing is assumed. In addition, this figure is obtained from the SLND approximation. This figure confirms that this work has to enlarge the radius of the primary exclusive region in the case $\mathcal{K}_{\lambda_{\mathrm{ST}}} = \emptyset$ with an increase in $\lambda_{\mathrm{ST,worst}}$.

Fig. 5.10 shows $r_{\mathrm{e,min}}$ for β_{target} in the trivial scheme obtained by using (5.21). This figure also shows $r_{\mathrm{e,min}}$ for β_{target} with respect to database knowledge $\mathcal{K}_{\mathrm{DB}}$ in the proposed scheme, where this work assumes Nakagami-m fading superimposed on log-normal shadowing and use the SLND approximation. This work emphasizes that the distribution of the power levels of the ST is the same as that in Table 1. This figure confirms that the proposed scheme enables to determine the PER size for β_{target}, whereas the trivial scheme requires an appropriate N_{ST} such that $P_{\mathrm{out}}(r_{\mathrm{e}})$ is less than β_{target}.

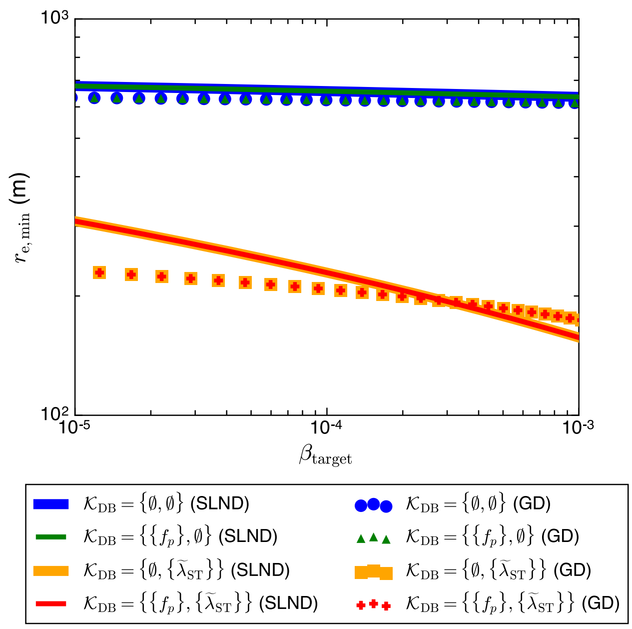

Figure 5.8: $r_{\mathrm{e,min}}$ vs. β_{target} with respect to $\mathcal{K}_{\mathrm{DB}}$ in the first scenario of Nakagami-m fading superimposed on log-normal shadowing ($\mathcal{P} = \{1\ \mathrm{W}\}$). ©2016 IEICE

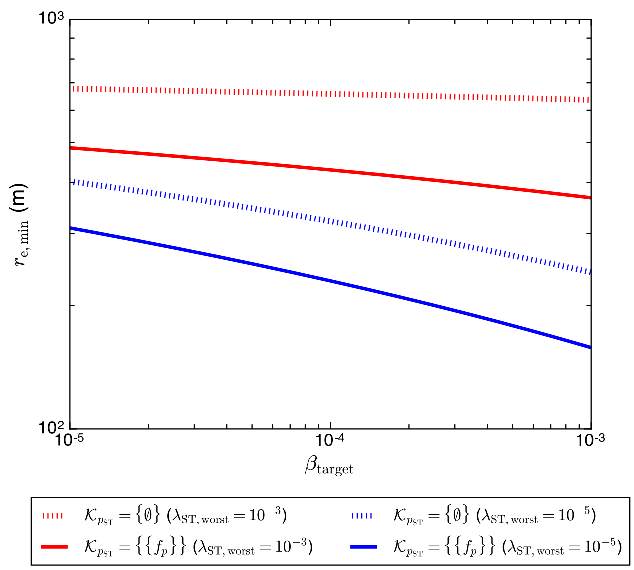

Figure 5.9: $r_{\mathrm{e,min}}$ vs. β_{target} with respect to $\mathcal{K}_{\mathrm{DB}} = \{\mathcal{K}_{p_{\mathrm{ST}}}, \emptyset\}$ in the first scenario of Nakagami-m fading superimposed on log-normal shadowing, obtained from SLND approximation. ©2016 IEICE

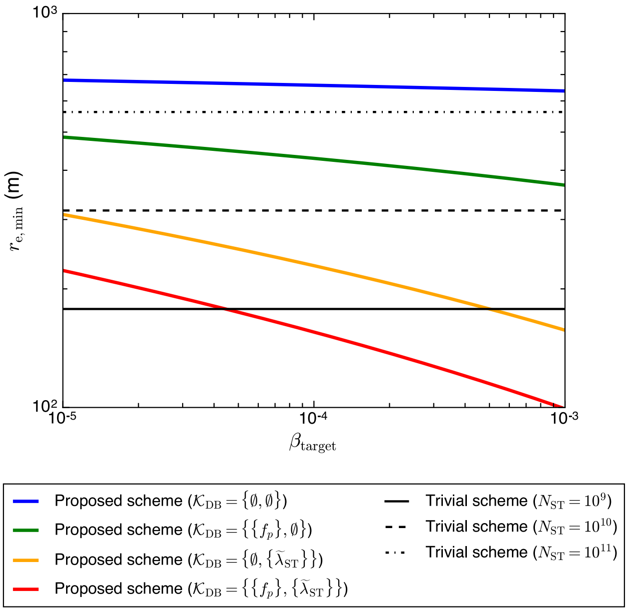

Figure 5.10: $r_{\mathrm{e,min}}$ vs. β_{target} in trivial scheme, and $r_{\mathrm{e,min}}$ vs. β_{target} in proposed scheme, where the first scenario of Nakagami-m fading superimposed on log-normal shadowing is assumed and the SLND approximation is used. ©2016 IEICE

5.7 Conclusion

A PU could experience harmful interference due to random channel gain and aggregate interference from STs even when an SU uses licensed spectrum on the basis of a PER created with a database. This work solved this problem by proposing a PER update framework for protecting a PU. In the proposed framework, the PU informs the database that it is experiencing harmful interference, and then, receiving the information, the database updates the PER by using knowledge it has stored about the SU. On the basis of the proposed framework, this work assumed a circular PER and applied stochastic geometry to derive an optimal PER radius. Finally, this work employed various scenarios to evaluate the PER radius that satisfies the outage probability of the target PU for each set of database knowledge and confirmed that the more detailed the stored knowledge of the density and transmission powers of the SU, the smaller the PER radius that needs to be determined after the update.

The purpose of this work is to evaluate the spectrum reuse efficiency depending on whether the knowledge about the secondary user is available or unavailable, where all messages are assumed to be instantly transmitted. In this work, two issues are beyond the scope of this chapter. One issue is to design a scheme for updating the PER when the database knowledge is imperfect and to evaluate the impact of the imperfectness on the performance as mentioned in Sect. 5.5. The other issue is to evaluate the impact of the delay among entities, i.e., the delay between the database and the PU and between the database and the SU, respectively, on the performance as described in Sect. 5.4.

Chapter 6

Exclusive Region Design for Spatial Grid-Based Spectrum Database

6.1 Overview

This chapter presents a stochastic geometry analysis for a spatial grid-based spectrum database system. In this system, by dividing a two-dimensional space into multiple regions, the local information, which includes the PR antenna pattern, and the ST density and transmission power, in each divided region can be considered. As spatial grids, this chapter introduces the polar and square grids. The polar grid divides the space into annular sectors and realizes a simple stochastic geometry analysis. On the other hand, the square grid divides the space into square regions and is assumed to be used in an actual spectrum database system. For both the spatial grids, this chapter introduces the allowable transmission probability (ATP) of an ST in each divided region for describing the PER and derives the cumulants of the aggregate interference at a PR from all the transmitting STs with stochastic geometry. Additionally, this chapter discusses the moments of the interference power at a PR from a single ST, which is distributed uniformly in a divided region. Further, this chapter formulates a continuous optimization problem for determining the ST ATP in each divided region, for designing the PER. This work imposes a constraint related to the PU OP on the optimization problem, where the PU OP is defined as the probability that the PR aggregate interference exceeds the maximum tolerable interference threshold at the PR. Finally, this chapter solves the problem for certain scenarios and verify that the complex-shaped PER, corresponding to the local information, is designed.

The contributions of this chapter are twofold: The first contribution is the analysis of the aggregate interference with the PGFL for the PPP, assuming that the distribution of the STs in each divided region follows an inhomogeneous PPP. This work can generate mutually independent inhomogeneous PPPs and analyze the aggregate interference at a PR from all the transmitting STs. The second contribution is the design of the PER as the solution of a continuous optimization problem by introducing an ST APT in each divided region. Conventional PER design is a combinatorial optimization problem because a region either permits or prohibits the STs to transmit. By introducing an ST APT to describe the PER, this work relaxes the problem to a continuous optimization problem and solve this problem with a non-linear solver.

The remainder of this chapter is organized as follows: Sect. 6.2 presents the system model in a spatial grid-based spectrum database. Sect. 6.3 derives the statistics of the aggregate interference at a PR. Sect. 6.4 explains the optimization problem for designing a PER. Sect. 6.5 describes the numerical evaluation in various scenarios. Finally, Sect. 6.6 presents the conclusions.

6.2 System Model

6.2.1 System Outline

In a two-dimensional space, a PR is located at the origin, the STs are distributed randomly, and there is a database. The space is divided into multiple regions. The PR is assumed to be at a fixed location, for example, a radar receiver. The database and STs are assumed to exchange information; the means of communication is beyond the scope of this chapter. The database is assumed to collect the ST locations and the transmission power levels.

This work considers a case, where an ST operates in a single radio channel allocated to the PR. This work can then extend the discussion to a case, where an ST operates in multiple radio channels allocated to the PR.

When an ST attempts to operate in a channel, it transmits a query to the database with its location information. On receiving the ST's query, the database replies to the ST permitting or prohibiting transmission. The ST receives permission and operates in the channel.

6.2.2 Spatial Grid

This work introduces two types of spatial grids, polar and square, and present their mathematical expressions.

Polar Grid

Fig. 6.1 shows the outline of the polar grid. This grid divides the space into $N_r N_\varphi$ annular sectors, where N_r and N_φ are the number of radial and angular divisions, respectively. In polar coordinates ((r, θ)), each annular sector shown in Fig. 6.2, $U_{i_r j_\varphi}$ for $i_r \in \mathcal{I}_r = \{0, \ldots, N_r - 1\}$ and $j_\varphi \in \mathcal{J}_\varphi = \{0, \ldots, N_\varphi - 1\}$, can be expressed as

$$U_{i_r j_\varphi} = \{ (r, \varphi) \mid R_1\sqrt{i_r} \le r < R_1\sqrt{i_r + 1}, 2\pi j_\varphi / N_\varphi \le \varphi < 2\pi(j_\varphi + 1)/N_\varphi \}, \tag{6.1}$$

where R_1 represents the radius of the divided sector, $U_{0 j_\varphi}$; all the divided annular sectors have the same area size, $\pi {R_1}^2 / N_\varphi$. Obviously, $\{U_{i_r j_\varphi}\}_{i_r \in \mathcal{I}_r,\, j_\varphi \in \mathcal{J}_\varphi}$ are disjoint with each other. Note that this work ignores an ST outside $\bigcup_{i_r \in \mathcal{I}_r} \bigcup_{j_\varphi \in \mathcal{J}_\varphi} U_{i_r j_\varphi}$ because the interference from it at the PR is negligible.

Square Grid

Fig. 6.3 shows the outline of the square grid. This grid divides the space into ${N_{xy}}^2$ square regions with a side length, W, where N_{xy} represents the number of horizontal and vertical divisions and is an even number. In Cartesian coordinates ((x, y)), each square region shown in Fig. 6.4, $V_{i_x j_y}$, for i_x, $j_y \in \mathcal{I}_{xy} = \{-N_{xy}/2, \ldots, 0, \ldots, N_{xy}/2 - 1\}$ can be expressed as

$$V_{i_x j_y} = \{ (x, y) \mid i_x W \le x < (i_x + 1)W, j_y W \le y < (j_y + 1)W \}, \tag{6.2}$$

where all the divided square regions have the same area size, W^2. Obviously, $\{V_{i_x j_y}\}_{i_x \in \mathcal{I}_{xy},\, j_y \in \mathcal{I}_{xy}}$ are disjoint with each other. Note that this work ignores an ST outside $\bigcup_{i_x \in \mathcal{I}_{xy}} \bigcup_{j_y \in \mathcal{I}_{xy}} V_{i_x j_y}$ because the interference from it at the PR is negligible.

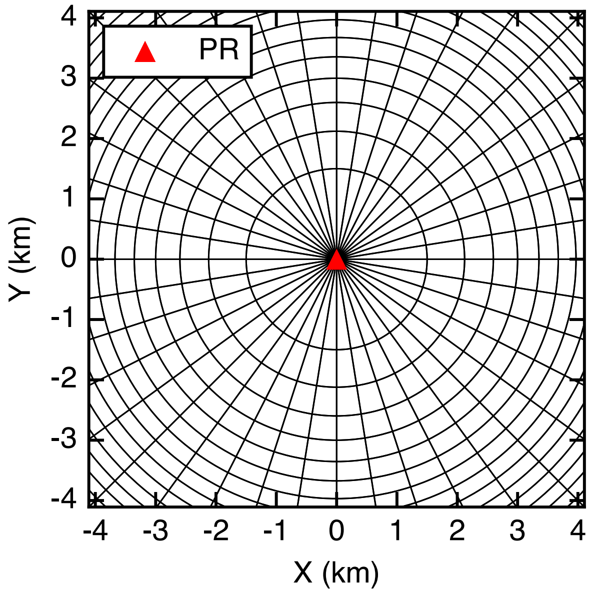

Figure 6.1: Outline of polar grid.

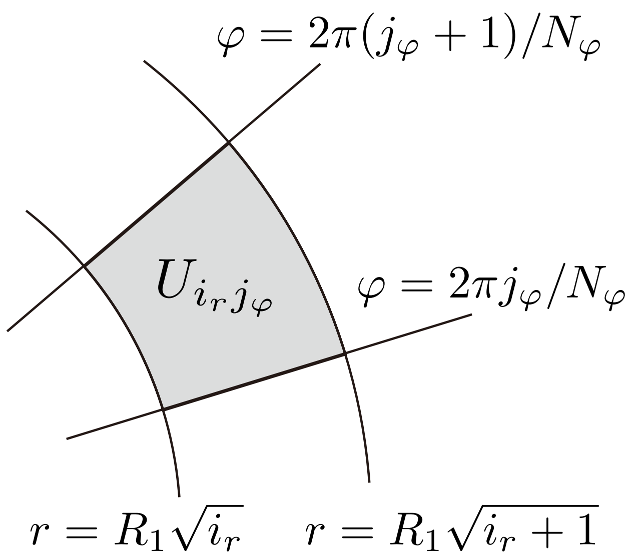

Figure 6.2: Single divided region of polar grid.

6.2.3 Single Divided Region

This work models a single divided region, S, i.e., $S = U_{i_r j_\varphi}$ in the polar grid case or $S = V_{i_x j_y}$ in the square grid case. Let the area size of S be denoted by $|S|$.

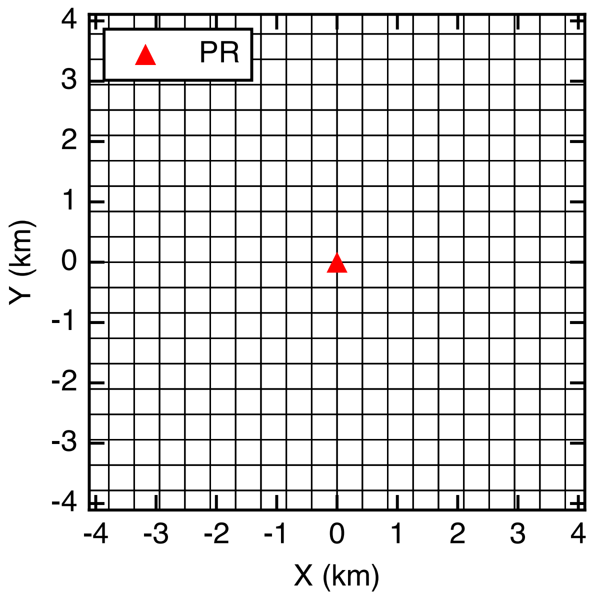

Figure 6.3: Outline of square grid.

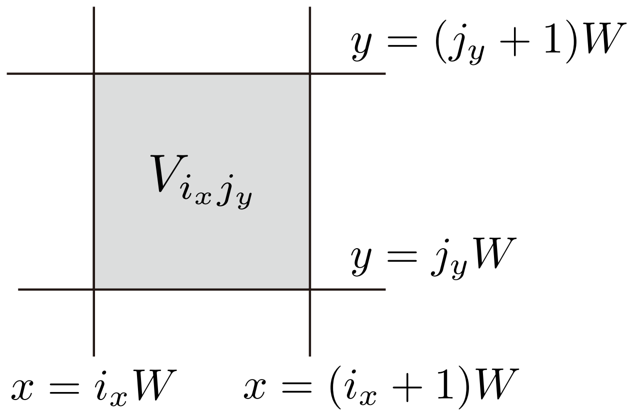

Figure 6.4: Single divided region of square grid.

The database stores three types of information related to the region, S. The first information is the ST density in S, denoted by λ_S. λ_S can be generated from the information on the number of STs in S. The distribution of the STs in S is assumed follow an inhomogeneous PPP with an intensity function, Λ_S. Λ_S is expressed as

$$\Lambda_S(z) = \begin{cases} \lambda_S & \text{if } z \in S, \\ 0 & \text{otherwise.} \end{cases} \tag{6.3}$$

The second information is the ST transmitting power in S, denoted by p_S. p_S can be generated from the available transmission power levels of the STs in S. The third information is the constant gain between the PR at the origin and the STs in S, denoted by g_S. g_S can be generated from the antenna patterns of the PR and STs in S.

This work introduces the ST ATP in S, denoted by a_S with $0 \leq a_S \leq 1$. When the database replies to the queried ST in S, it transmits the transmission permission and prohibition with probabilities of a_S and $(1 - a_S)$, respectively. The transmitting STs on S also follow an inhomogeneous PPP and their intensity function can be expressed as $a_S \Lambda_S$. Let the inhomogeneous PPP be denoted by $\Phi_{S,\text{TX}}$.

6.3 Aggregate Interference

This section derives the statistics of the aggregate interference at the PR from all the transmitting STs. Let the aggregate interference power be denoted by I_{total}. I_{total} is obtained as the summation of the aggregate interference power at the PR from the transmitting STs in each divided region.

6.3.1 Interference

This work defines the aggregate interference power from the transmitting STs in a single divided region, S, denoted by I_S. I_S is defined as

$$I_S = \sum_{z \in \Phi_{S,\text{TX}}} h_z g_S p_S \|z\|^{-\alpha}, \tag{6.4}$$

where h_z denotes the fading coefficient (with unit mean) between $z \in \mathbb{R}^2$ and the origin, $\|z\|$ denotes the Euclidean distance between $z \in \mathbb{R}^2$ and the origin, and α is the path-loss exponent with $\alpha > 2$. This work assumes that the fading coefficient, h_z, is an independent and identically distributed (i.i.d.) random variable, h, with unit mean and a probability density function (pdf), f_h.

6.3.2 Interference Cumulant

This work derives the nth cumulant of I_S and then, derive the nth cumulant of I_{total}. Let the nth cumulant of a random variable, X, for $n = 1, 2, \ldots$ be denoted by $\kappa_n(X)$. $\kappa_n(X)$ for $n = 1, 2, \ldots$ uniquely determine the distribution of X; for example, $\kappa_1(X)$ and $\kappa_2(X)$ are the mean and variance of X, respectively [72].

From the PGFL for the PPP (Theorem 4.9 in [23]), the MGF of I_S, denoted by $M_{I_S}(s)$, is expressed as follows:

$$\begin{aligned} M_{I_S}(s) &= \mathbb{E}_{I_S}(\mathrm{e}^{sI_S}) \\ &= \mathbb{E}_{\Phi_{S,\text{TX}}}\left(\mathrm{e}^{s\sum_{z\in\Phi_{S,\text{TX}}} h_z g_S p_S \|z\|^{-\alpha}}\right) \\ &= \mathbb{E}_{\Phi_{S,\text{TX}}}\left(\prod_{z\in\Phi_{S,\text{TX}}} \mathbb{E}_h\left(\mathrm{e}^{shg_S p_S\|z\|^{-\alpha}}\right)\right) \\ &= \exp\left[a_S \int_{\mathbb{R}^2} \left(\mathbb{E}_h\left(\mathrm{e}^{shg_S p_S\|z\|^{-\alpha}}\right) - 1\right) \Lambda_S(\mathrm{d}z)\right] \\ &= \exp\left[a_S\lambda_S \int_S \left(\mathbb{E}_h\left(\mathrm{e}^{shg_S p_S\|z\|^{-\alpha}}\right) - 1\right) \mathrm{d}z\right]. \end{aligned} \tag{6.5}$$

The MGF, $M_{I_S}(s)$, corresponds to the Laplace transform of I_S, which is used in several stochastic geometry works. For example, in the special case, $S = \mathbb{R}^2$, referring to [23], $M_{I_S}(s)$ is expressed as follows:

$$M_{I_S}(s) = \exp\left(-\pi a_S \lambda_S {g_S}^{\delta} {p_S}^{\delta} \mathbb{E}_h(h^{\delta}) \Gamma(1-\delta)(-s)^{\delta}\right), \tag{6.6}$$

$$\delta = 2/\alpha, \tag{6.7}$$

where $\Gamma(\cdot)$ denotes the gamma function. In this chapter, the MGF is used because this work focuses on the cumulants of the aggregate interference.

From (6.5), the nth cumulant, $\kappa_n(I_S)$, is expressed as follows:

$$\kappa_n(I_S) = \frac{\mathrm{d}^n}{\mathrm{d}s^n} \ln M_{I_S}(s)\bigg|_{s=0}$$
$$= a_S \lambda_S \int_S \mathbb{E}_h\left(h^n {g_S}^n {p_S}^n \|z\|^{-n\alpha}\right) \mathrm{d}z$$
$$= a_S \lambda_S {g_S}^n {p_S}^n \mathbb{E}_h(h^n) A_n(S), \tag{6.8}$$
$$\mathbb{E}_h(h^n) = \int_0^\infty h^n f_h(h)\,\mathrm{d}h, \tag{6.9}$$
$$A_n(S) = \int_S \|z\|^{-n\alpha}\,\mathrm{d}z. \tag{6.10}$$

$A_n(S)/|S|$ represents the nth moment of the interference power at the PR from a single ST that is distributed uniformly in S and transmits with unit power. (6.10) shows that $A_n(S)$ depends only on the spatial grid and the location of S.

Polar Grid

In the polar grid case ($S = U_{i_r j_\varphi}$), I_{total} can be expressed as

$$I_{\text{total}} = \sum_{i_r \in \mathcal{I}_r} \sum_{j_\varphi \in \mathcal{J}_\varphi} I_{U_{i_r j_\varphi}}. \tag{6.11}$$

$\{I_{U_{i_r j_\varphi}}\}_{i_r \in \mathcal{I}_r,\, j_\varphi \in \mathcal{J}_\varphi}$ are mutually independent random variables because $\{\Phi_{U_{i_r j_\varphi}, \mathrm{TX}}\}_{i_r \in \mathcal{I}_r,\, j_\varphi \in \mathcal{J}_\varphi}$ are mutually independent inhomogeneous PPPs. Thus, from the cumulant additivity property [72], $\kappa_n(I_{\text{total}})$ can be expressed as

$$\kappa_n(I_{\text{total}}) = \sum_{i_r \in \mathcal{I}_r} \sum_{j_\varphi \in \mathcal{J}_\varphi} \kappa_n(I_{U_{i_r j_\varphi}}). \tag{6.12}$$

From (6.1), $A_n(U_{i_r j_\varphi})$ can be modified as

$$A_n(U_{i_r j_\varphi}) = \int_{U_{i_r j_\varphi}} \|z\|^{-n\alpha}\,\mathrm{d}z$$
$$= \int_{2\pi j_\varphi/N_\varphi}^{2\pi(j_\varphi+1)/N_\varphi} \mathrm{d}\varphi \int_{R_1\sqrt{i_r}}^{R_1\sqrt{i_r+1}} r^{1-n\alpha}\,\mathrm{d}r$$
$$= \frac{\pi}{k {R_1}^{2k} N_\varphi}\left[{i_r}^{-k} - (i_r+1)^{-k}\right], \tag{6.13}$$
$$k = n\alpha/2 - 1. \tag{6.14}$$

Thus, from (6.8), (6.12), and (6.13), $\kappa_n(I_{\text{total}})$ in the polar grid can be calculated analytically.

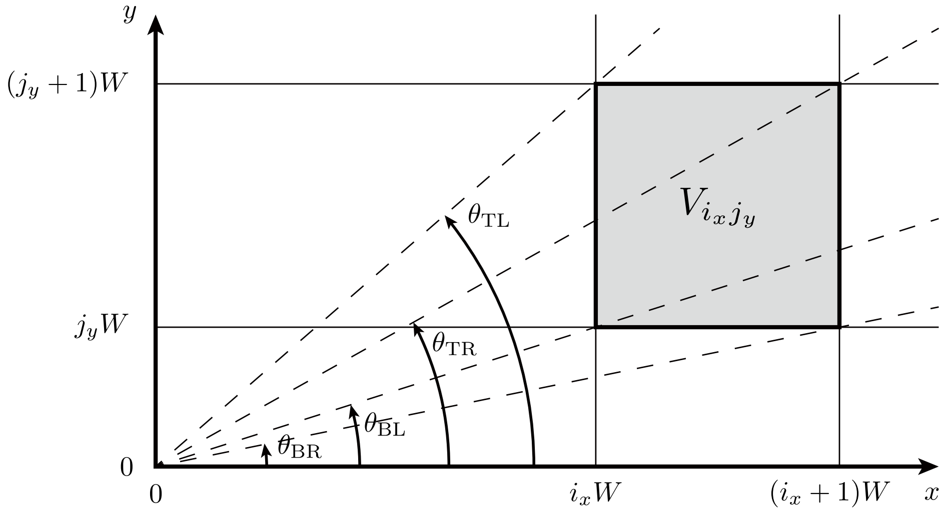

Figure 6.5: Single divided square region for analysis

Square Grid

In the square grid case ($S = V_{i_xj_y}$), I_{total} can be expressed as

$$I_{\text{total}} = \sum_{i_x \in \mathcal{I}_{xy}} \sum_{j_y \in \mathcal{I}_{xy}} I_{V_{i_xj_y}}. \tag{6.15}$$

$\{I_{V_{i_xj_y}}\}_{i_x, j_y \in \mathcal{I}_{xy}}$ are mutually independent random variables because $\{\Phi_{V_{i_xj_y},\mathrm{TX}}\}_{i_x, j_y \in \mathcal{I}_{xy}}$ are mutually independent inhomogeneous PPPs. Thus, from the cumulant additivity property [72], $\kappa_n(I_{\text{total}})$ can be expressed as

$$\kappa_n(I_{\text{total}}) = \sum_{i_x \in \mathcal{I}_{xy}} \sum_{j_y \in \mathcal{I}_{xy}} \kappa_n(I_{V_{i_xj_y}}). \tag{6.16}$$

Using Fig. 6.5, this work simplifies $A_n(V_{i_xj_y})$, where θ_{BR}, θ_{BL}, θ_{TR}, and θ_{TL}, in this figure, are angles and given as follows:

$$\theta_{\mathrm{BR}} = \arctan(j_y/(i_x+1)), \tag{6.17}$$
$$\theta_{\mathrm{BL}} = \arctan(j_y/i_x), \tag{6.18}$$
$$\theta_{\mathrm{TR}} = \arctan((j_y+1)/(i_x+1)), \tag{6.19}$$
$$\theta_{\mathrm{TL}} = \arctan((j_y+1)/i_x). \tag{6.20}$$

Then, $A_n(V_{i_x j_y})$ is modified in polar coordinates as follows:

$$\begin{aligned}
A_n(V_{i_x j_y}) &= \int_{V_{i_x j_y}} \|z\|^{-n\alpha}\, \mathrm{d}z \\
&= \int_{\theta_{\mathrm{BR}}}^{\theta_{\mathrm{BL}}} \int_{j_y W/\sin\varphi}^{(i_x+1)W/\cos\varphi} r^{1-n\alpha}\, \mathrm{d}r \mathrm{d}\varphi \\
&\quad + \int_{\theta_{\mathrm{BL}}}^{\theta_{\mathrm{TR}}} \int_{i_x W/\cos\varphi}^{(i_x+1)W/\cos\varphi} r^{1-n\alpha}\, \mathrm{d}r \mathrm{d}\varphi \\
&\quad + \int_{\theta_{\mathrm{TR}}}^{\theta_{\mathrm{TL}}} \int_{i_x W/\cos\varphi}^{(j_y+1)W/\sin\varphi} r^{1-n\alpha}\, \mathrm{d}r \mathrm{d}\varphi \\
&= \frac{1}{k' W^{k'}} \left[B_n^1 + B_n^2 + B_n^3 + B_n^4 \right]
\end{aligned} \tag{6.21}$$

$$B_n^1 = \begin{cases} 0 & \text{if } i_x = 0, \\ i_x{}^{-k'} \int_{\theta_{\mathrm{BL}}}^{\theta_{\mathrm{TL}}} \cos^{k'} \varphi\, \mathrm{d}\varphi & \text{otherwise,} \end{cases} \tag{6.22}$$

$$B_n^2 = \begin{cases} 0 & \text{if } j_y = -1, \\ (j_y + 1)^{-k'} \int_{\theta_{\mathrm{TL}}}^{\theta_{\mathrm{TR}}} \sin^{k'} \varphi\, \mathrm{d}\varphi & \text{otherwise,} \end{cases} \tag{6.23}$$

$$B_n^3 = \begin{cases} 0 & \text{if } i_x = -1, \\ (i_x + 1)^{-k'} \int_{\theta_{\mathrm{TR}}}^{\theta_{\mathrm{BR}}} \cos^{k'} \varphi\, \mathrm{d}\varphi & \text{otherwise,} \end{cases} \tag{6.24}$$

$$B_n^4 = \begin{cases} 0 & \text{if } j_y = 0, \\ j_y{}^{-k'} \int_{\theta_{\mathrm{BR}}}^{\theta_{\mathrm{BL}}} \sin^{k'} \varphi\, \mathrm{d}\varphi & \text{otherwise,} \end{cases} \tag{6.25}$$

$$k' = n\alpha - 2. \tag{6.26}$$

When α is an integer, the integrations in (6.22), (6.23), (6.24), and (6.25) can be expressed as closed-forms; thus, (6.21) can be also expressed as a closed-form. For example, in the special case, $\alpha = 4$ and $n = 1$ ($k' = 2$), (6.22), (6.23), (6.24), and (6.25) are expressed by the following closed-form expressions:

$$B_1^1 = \begin{cases} 0 & \text{if } i_x = 0, \\ \frac{1}{2{i_x}^2} C(\theta_{\mathrm{TL}}, \theta_{\mathrm{BL}}, 1) & \text{otherwise,} \end{cases} \tag{6.27}$$

$$B_1^2 = \begin{cases} 0 & \text{if } j_y = -1, \\ \frac{1}{2(j_y+1)^2} C(\theta_{\mathrm{TR}}, \theta_{\mathrm{TL}}, -1) & \text{otherwise,} \end{cases} \tag{6.28}$$

$$B_1^3 = \begin{cases} 0 & \text{if } i_x = -1, \\ \frac{1}{2(i_x+1)^2} C(\theta_{\mathrm{BR}}, \theta_{\mathrm{TR}}, 1) & \text{otherwise,} \end{cases} \tag{6.29}$$

$$B_1^4 = \begin{cases} 0 & \text{if } j_y = 0, \\ \frac{1}{2{j_y}^2} C(\theta_{\mathrm{BL}}, \theta_{\mathrm{BR}}, -1) & \text{otherwise,} \end{cases} \tag{6.30}$$

$$\begin{aligned} C(\theta_1, \theta_2, q) = q\{&[\tan\theta_1 + (\tan\theta_1)^{-1}]^{-1} \\ &- [\tan\theta_2 + (\tan\theta_2)^{-1}]^{-1}\} + \theta_1 - \theta_2, \end{aligned} \tag{6.31}$$

$$\theta_1,\ \theta_2 \in \{\theta_{\mathrm{BL}}, \theta_{\mathrm{TL}}, \theta_{\mathrm{TR}}, \theta_{\mathrm{BR}}\}, \tag{6.32}$$

$$q \in \{-1, 1\}. \tag{6.33}$$

Thus, from (6.8), (6.16), and (6.21), $\kappa_n(I_{\mathrm{total}})$ in the square grid can be calculated analytically.

6.3.3 Cumulant Matching

This work treats the distribution of I_{total} as a log-normal distribution, approximately, using the cumulant matching approach [63]. In this approach, by matching the nth cumulant of an unknown distribution to the nth cumulant of a well-known distribution, the unknown distribution can be approximated by the well-known distribution. Let the pdf of I_{total} be denoted by $f_{I_{\mathrm{total}}}$; $f_{I_{\mathrm{total}}}$ is approximately expressed as

$$f_{I_{\text{total}}}(I) \simeq \frac{1}{\sqrt{2\pi}\sigma_{\text{LN}} I} \exp\left[-\frac{(\ln I - \mu_{\text{LN}})^2}{2\sigma_{\text{LN}}{}^2} \right], \tag{6.34}$$

$$\mu_{\text{LN}} = \ln\left(\frac{\kappa_1(I_{\text{total}})^2}{\sqrt{\kappa_2(I_{\text{total}}) + \kappa_1(I_{\text{total}})^2}} \right), \tag{6.35}$$

$$\sigma_{\text{LN}} = \sqrt{\ln\left(\frac{\kappa_2(I_{\text{total}})}{\kappa_1(I_{\text{total}})^2} + 1 \right)}, \tag{6.36}$$

where $(\mu_{\text{LN}}, \sigma_{\text{LN}})$ are the log-normal distribution parameters.

This cumulant matching approach is adopted in several works related to stochastic geometry [24]. These works have treated the distribution of an aggregate interference using various well-known distributions, approximately. In [19,22,73], a log-normal distribution has been used, as in this work. In [19, 67, 69], a shifted log-normal distribution [68] has been used. In [19, 64–66], a gamma distribution has been used. The primary focus of this work is to design a PER based on a spatial grid; hence, this work uses a log-normal distribution to approximate the aggregate interference. Cases, where other well-known distributions are used, are beyond the scope of this work.

6.4 PU OP and PER Design

With the derived expressions, this section designs a PER using an optimization problem. On this problem, this work imposes a constraint related to the PU OP. Recall that the PU OP is defined as the probability that I_{total} exceeds the maximum tolerable interference threshold at the PR, I_{th}; i.e., the PU OP can be expressed as $\mathbb{P}(I_{\text{total}} > I_{\text{th}})$.

6.4.1 PU OP

The PU OP, $\mathbb{P}(I_{\text{total}} > I_{\text{th}})$, can be expressed as the complementary cumulative distribution function (CCDF) of I_{total}. From the discussion in 6.3.3, $\mathbb{P}(I_{\text{total}} > I_{\text{th}})$

can be approximately expressed as follows:

$$\mathbb{P}(I_{\mathrm{total}} > I_{\mathrm{th}}) \simeq Q\left(\frac{\ln I_{\mathrm{th}} - \mu_{\mathrm{LN}}}{\sigma_{\mathrm{LN}}}\right), \tag{6.37}$$

where $Q(\cdot)$ denotes a Q-function defined as $Q(x) = (1/\sqrt{2\pi}) \int_x^{\infty} \exp(-t^2/2)\,\mathrm{d}t$.

6.4.2 Optimization Problem Formulation

This work formulates the optimization problem for designing a PER. The object of the optimization problem is to minimize the area of the PER, defined as the summation of $a_S|S|$. This work uses this object function to enlarge the region, where the STs are permitted to transmit. This work imposes a constraint wherein the PU OP, $\mathbb{P}(I_{\mathrm{total}} > I_{\mathrm{th}})$, is less than a target, β_{target}.

This work formulates the optimization problem in the polar grid case ($S = U_{i_r j_\varphi}$). This optimization problem is expressed as follows:

$$\begin{aligned} \underset{(a_{U_{i_r j_\varphi}})_{i_r \in \mathcal{I}_r,\, j_\varphi \in \mathcal{J}_\varphi}}{\text{minimize}} \quad & \sum_{i_r \in \mathcal{I}_r} \sum_{j_\varphi \in \mathcal{J}_\varphi} (1 - a_{U_{i_r j_\varphi}})|U_{i_r j_\varphi}| \\ \text{subject to} \quad & \mathbb{P}(I_{\mathrm{total}} > I_{\mathrm{th}}) \leq \beta_{\mathrm{target}} \\ & a_{U_{i_r j_\varphi}} \in [0, 1]. \end{aligned} \tag{6.38}$$

Let the best solution, $a_{U_{i_r j_\varphi}}$, of this problem be denoted by $a^{\star}_{U_{i_r j_\varphi}}$.

This work formulates the optimization problem in the square grid case ($S = V_{i_x j_y}$). The optimization problem in the square grid case is expressed as follows:

$$\begin{aligned} \underset{(a_{V_{i_x j_y}})_{i_x,\, j_y \in \mathcal{I}_{xy}}}{\text{minimize}} \quad & \sum_{i_x \in \mathcal{I}_{xy}} \sum_{j_y \in \mathcal{I}_{xy}} (1 - a_{V_{i_x j_y}})|V_{i_x j_y}| \\ \text{subject to} \quad & \mathbb{P}(I_{\mathrm{total}} > I_{\mathrm{th}}) \leq \beta_{\mathrm{target}} \\ & a_{V_{i_x j_y}} \in [0, 1]. \end{aligned} \tag{6.39}$$

Let the best solution, $a_{V_{i_x j_y}}$, of this problem be denoted by $a^{\star}_{V_{i_x j_y}}$.

Optimization problems, (6.38) and (6.39), are constrained non-linear optimization problems.

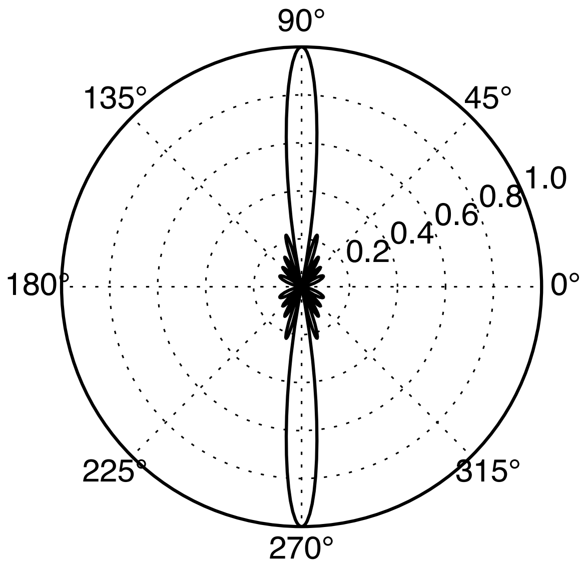

Figure 6.6: PR antenna pattern, $g(\varphi)$.

6.5 Numerical Evaluation

By solving (6.38) and (6.39), this section designs an optimized PER for various cases. In addition, this work quantitatively evaluates the optimized PER size and the simulated PU OP, obtained by Monte Carlo simulation.

6.5.1 Parameters

This work considers two scenarios regarding the ST density, λ_S and the transmission power, p_S, in each divided region, S. In the first scenario, λ_S and p_S for any divided region S are set to $\lambda_S = 10^{-5}\,\mathrm{m}^{-2}$ and $p_S = 1\,\mathrm{W}$, respectively. The purpose of the first scenario is to evaluate the impact of the PR antenna pattern on the optimized PER. In the second scenario, N_φ is set to be a multiple of four and

Table 6.1: Parameters.

Parameter	Value
α	4
N_r	15
R_1	1.5 km
N_{array}	10
m_{N}	2.5
$\sigma_{\text{S,dB}}$	6
I_{th}	10^{-12} W
β_{target}	10^{-2}

the tuple, (λ_S, p_S), for the divided region, S, is given by

$$(\lambda_S, p_S) = \begin{cases} (10^{-5}\,\text{m}^{-2}, 1\,\text{W}) & S \text{ in the first quadrant,} \\ (5 \times 10^{-6}\,\text{m}^{-2}, 1\,\text{W}) & S \text{ in the second quadrant,} \\ (5 \times 10^{-6}\,\text{m}^{-2}, 0.5\,\text{W}) & S \text{ in the third quadrant,} \\ (10^{-5}\,\text{m}^{-2}, 0.5\,\text{W}) & S \text{ in the fourth quadrant.} \end{cases} \tag{6.40}$$

The purpose of the second scenario is to evaluate the impact of not only the PR antenna pattern but also the ST density and the transmission power in the optimized PER.

This work assumes that the divided regions in the polar and square grid cases have the same area size. Then, W, which is the side length of the square grid, can be expressed as

$$W = \sqrt{\pi {R_1}^2 / N_\varphi}. \tag{6.41}$$

In addition, the ATP in the divided region, S, including the origin, is set to be zero; i.e., $a_{U_{i_r j_\varphi}} = 0$ for $i_r = 0$ and any j_φ in the polar grid case, and $a_{V_{i_x j_y}} = 0$ for $i_x \in \{-1, 0\}$ and $j_y \in \{-1, 0\}$ in the square grid case.

This work uses the Nakagami-m fading superimposed on the log-normal shadowing [71]; $\mathbb{E}(h^n)$ can be written as

$$\mathbb{E}(h^n) = \frac{\Gamma(m_\mathrm{N}+n)}{\Gamma(m_\mathrm{N}){m_\mathrm{N}}^n} \exp\left[\frac{n(n-1){\sigma_{\mathrm{S,dB}}}^2}{2\xi^2}\right], \tag{6.42}$$

where m_N and $\sigma_{\mathrm{S,dB}}$ denote the Nakagami-m fading parameter and the log-normal shadowing parameter with a dB-spread, respectively; $\xi = 10/\ln(10)$.

When this work evaluates the solution of the optimization problem, as the worst case, g_S for each divided region, S, is generated by the following equation:

$$g_S = \max_{(r,\varphi)\in S} g(\varphi), \tag{6.43}$$

where $g(\varphi)$ denotes the PR antenna factor. $g(\varphi)$ is assumed to be an N_array-element linear uniform array in which the elements are spaced one-half wavelength apart and the phases are zero [74]; $g(\varphi)$ is given as follows:

$$g(\varphi) = \left|\frac{\sin(\pi N_\mathrm{array}\cos\varphi/2)}{N_\mathrm{array}\sin(\pi\cos\varphi/2)}\right|. \tag{6.44}$$

Fig. 6.6 shows $g(\varphi)$ for $N_\mathrm{array} = 10$. Note that in the calculation of the simulated PU OP with Monte Carlo simulation, this work uses $g(\varphi)$; i.e., I_S for each divided region, S, is simulated as follows:

$$I_S = \sum_{z=(r,\varphi)\in\Phi_{S,\mathrm{TX}}} h_z g(\varphi) p_S r^{-\alpha}. \tag{6.45}$$

This work formulates the optimization problems, (6.38) and (6.39), in Python using the Pyomo modeling framework [75] and solve this problems with the open source software, interior point optimizer (IPOPT) nonlinear solver [76, 77].

Finally, Table 6.1 lists the parameters and their values.

6.5.2 Numerical Results

This work presents the results of the first scenario. Figs. 6.7 and 6.8 show the optimized PER in the polar and square grid cases, respectively. These figures demonstrate that a PER is designed, corresponding to the PR antenna pattern shown in Fig. 6.6. In addition, as the area of the divided region is reduced (N_φ is increased), the designed PER shrinks and becomes complex-shaped. Figs. 6.9 and 6.10 show the area of the optimized PER and the simulated PU OP for the area of

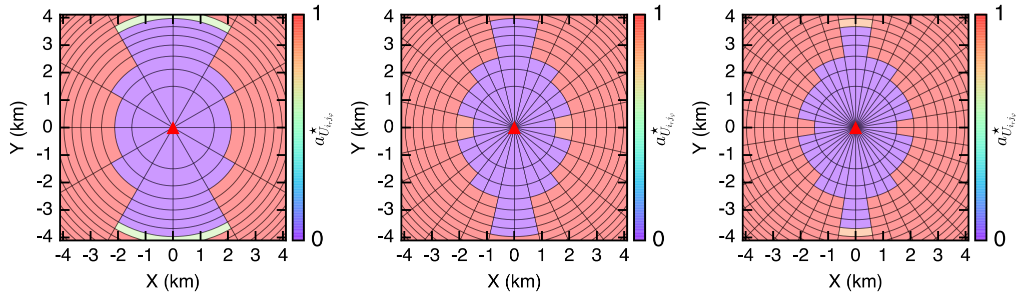

(a) $N_\varphi = 12$. (b) $N_\varphi = 28$. (c) $N_\varphi = 40$.

Figure 6.7: Solution, $(a^\star_{U_{i_r j_\varphi}})$, for the polar grid case, in the first scenario.

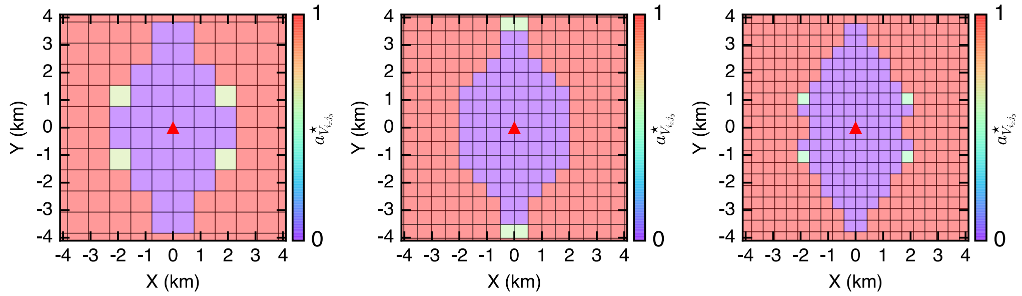

(a) $N_\varphi = 12$. (b) $N_\varphi = 28$. (c) $N_\varphi = 40$.

Figure 6.8: Solution, $(a^\star_{V_{i_x j_y}})$, for the square grid case, in the first scenario.

the divided region, respectively. Fig. 6.9 demonstrates that, in both the spatial grid cases, the area of the optimized PER converges, as the area of the divided region is reduced. Fig. 6.10 shows that the constraint in (6.38) and (6.39) is satisfied, and that the simulated PU OPs in both the spatial grid cases get closer to the target, β_{target}, as the area of the divided region is reduced. From these results, when the area of the divided region is set to be large, the aggregate interference at the PR is underestimated.

This work presents the results of the second scenario. Figs. 6.11a and 6.11b show the optimized PER in the polar and square grid cases, respectively. These figures demonstrate that the optimized PER in each quadrant corresponds to the PR antenna pattern, and the ST density and transmission power, i.e., the smaller the ST density or transmission power, the smaller is the optimized PER. Figs. 6.12 and 6.13 show the area of the optimized PER and the simulated PU OP for the area

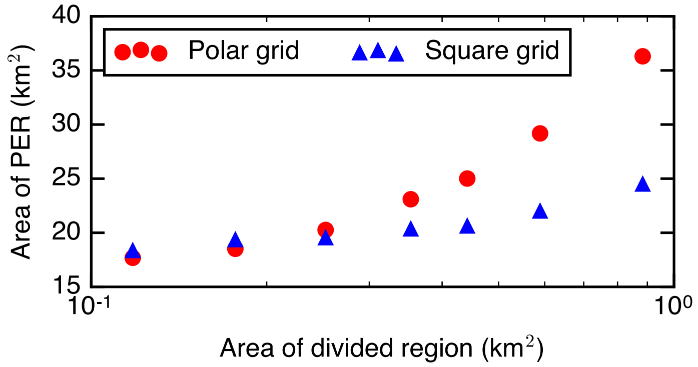

Figure 6.9: PER area for each spatial grid case, in the first scenario.

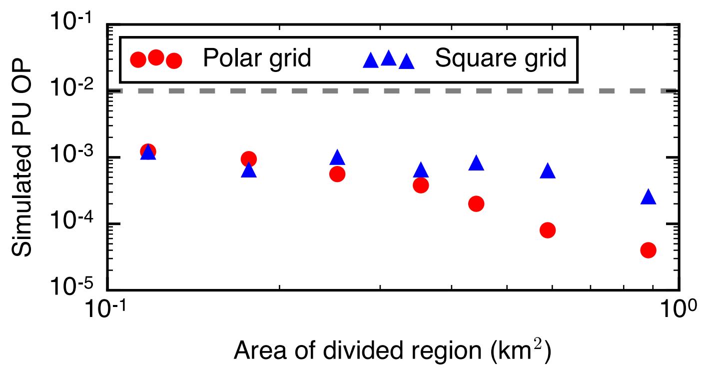

Figure 6.10: Simulated PU OP for each spatial grid case, in the first scenario.

of the divided region, respectively. The trends of the optimized PER area and the simulated PU OP are the same as that of the first scenario.

6.6 Conclusion

This chapter has presented a stochastic geometry analysis and PER design for a spatial grid-based spectrum database system. The purpose of the spatial grid is to utilize the local information, such as the PR antenna pattern, and the ST density and transmission power, in each divided region. Further, polar and square grids were introduced. For these spatial grids, the cumulants of the aggregate interference at a PR from the STs were derived, where the PGFL for the PPP was

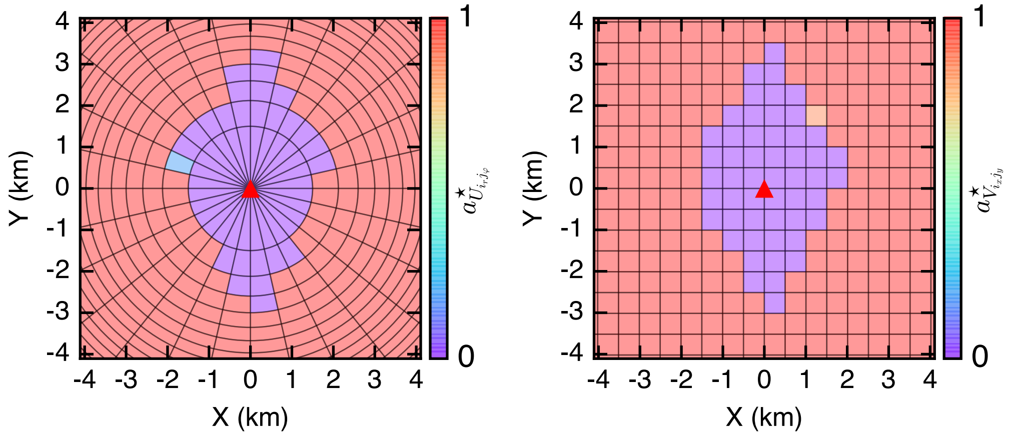

(a) Polar grid. (b) Square grid.

Figure 6.11: Solutions, $(a^{\star}_{U_{i_r j_\varphi}})$ and $(a^{\star}_{V_{i_x j_y}})$, in the second scenario.

used on the assumption that the distribution of the STs in each divided region followed an inhomogeneous PPP. In addition, to obtain the PER as the solution of a continuous optimization problem, the ST ATP in each divided region was introduced. Then, for each spatial grid, the moments of the interference power at a PR from a single ST, which was distributed uniformly in a divided region, was presented. In the polar and square grids, the moments can be expressed as a closed-form for any exponent and for an adjective path-loss exponent, respectively. Finally, the optimization problems to determine the ST ATP in each divided region were formulated and by solving the problem with a nonlinear solver, the optimized PER was designed. Numerical results demonstrated that a PER, corresponding to the local information, was successfully designed and that more detailed local information, due to a reduction in the area of each divided region, led to a smaller and complex-shaped PER.

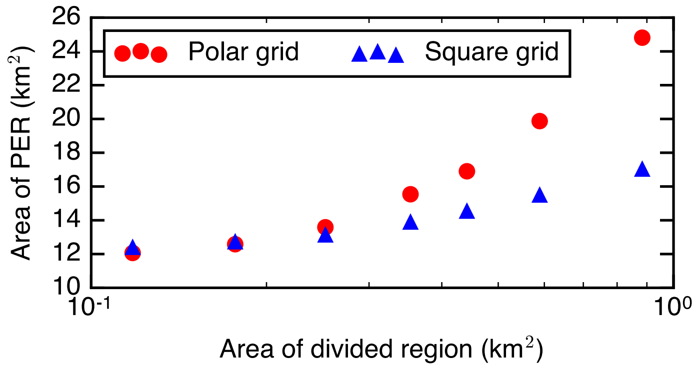

Figure 6.12: PER area for each spatial grid case, in the second scenario.

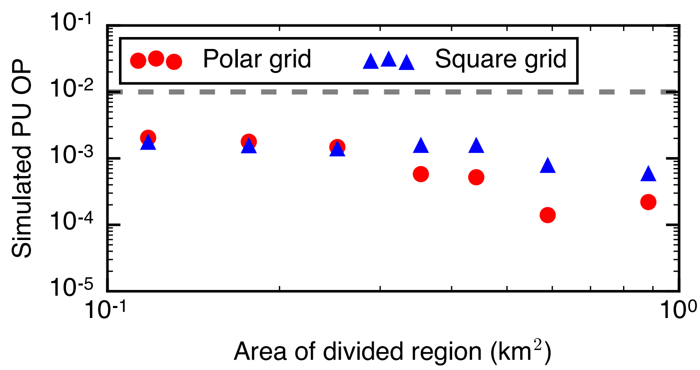

Figure 6.13: Simulated PU OP for each spatial grid case, in the second scenario.

Chapter 7

Conclusion

The theme of this thesis was the coexistence of wireless communication and non-communication systems. Both systems were assumed to use the same spectrum channel for improving spectral efficiency. This thesis focused on two topics. One topic was an MPT system with a WLAN station, i.e., the co-channel operation of MPT and IEEE 802.11-based data transmission. The other topic was a database driven spectrum sharing system, i.e., the operation of a communication SU in the channel allocated to a non-communication PU.

In the first topic, this thesis proposed two schemes. One was a scheduling scheme that allocates time for MPT and IEEE 802.11-based data transmission. In this scheme, on the basis of the time information on data and beacon frame transmissions, and microwave power was transmitted except when these frames were transmitted. The other was a RAS based on exposure assessment with a rectenna output. The devices, on which this scheme was implemented, determined the next PHY data rate using historical data (e.g., data frame loss ratio) corresponding to the assessment result. These proposed schemes were verified by performing the experiments with commercial WLAN devices in a radio frequency anechoic chamber.

In the second topic, this thesis attempted to design and to update a PER, and presented stochastic geometry analysis of the aggregate interference at a PU, and then determined a PER by solving an optimization problem with the analysis results. This work addressed twofold. One was to present a framework for updating a PER and to design a circular PER centered at a PU, and then to analysis the aggregate interference on the assumption that SUs were distributed following a homogeneous PPP. The other was to design a complex-shaped PER by introducing a spatial grid. For polar and square spatial grids, the aggregate interference was analyzed on the assumption that SUs in each divided region were distributed following an inhomogeneous PPP. Numerical results showed that the more detailed database information, such as the PU antenna pattern and SU density and power, led to a smaller PER.

Bibliography

[1] NTT DOCOMO, "5G Radio Access: Requirements, Concept and Technologies," Technical report, NTT DOCOMO White Paper, July 2014.

[2] NGMN Alliance, "NGMN 5G White Paper," Technical report, 5G White Paper, Feb. 2015.

[3] A. Gupta and R.K. Jha, "A survey of 5G network : Architecture and emerging technologies," IEEE Access, vol.3, pp.1206–1232, July 2015.

[4] IEEE, "Part 11: Wireless LAN Medium Access Control (MAC) and Physical Layer (PHY) Specifications," Technical report, IEEE Std 802.11-2012, March 2012.

[5] S. Rangan, T.S. Rappaport, and E. Erkip, "Millimeter-wave cellular wireless networks: Potentials and challenges," Proc. IEEE, vol.102, no.3, pp.366–385, Feb. 2014.

[6] I.F. Akyildiz, W.-Y. Lee, M.C. Vuran, and S. Mohanty, "A survey on spectrum management in cognitive radio networks," IEEE Commun. Mag., vol.46, no.4, pp.40–48, March 2008.

[7] N. Shinohara, "Power without wires," IEEE Microw. Mag., vol.12, no.7, pp.S64–S73, Dec. 2011.

[8] V. Shnayder, B. Chen, K. Lorincz, T.R.F.F. Jones, and M. Welsh, "Sensor networks for medical care," Harvard Univ. TR-08-05, vol.5, p.314, April 2005.

[9] C. Yawut and S. Kilaso, "A wireless sensor network for weather and disaster alarm systems," Proc. ICIEE IPCSIT2011, vol.6, pp.155–159, 2011.

[10] Franck L Lewis, "Wireless sensor networks," Smart Environ. Technol. Protoc. Appl., pp.11–46, John Wiley & Sons, Inc., 2004.

[11] N. Imoto, S. Yamashita, T. Ichihara, K. Yamamoto, T. Nishio, M. Morikura, and N. Shinohara, "Experimental investigation of co-channel and adjacent channel operations of microwave power and IEEE 802.11g data transmissions," IEICE Trans. Commun., vol.E97-B, no.9, pp.1835–1842, Sept. 2014.

[12] A. Al-Fuqaha, M. Guizani, M. Mohammadi, O. Aledhari, and M. Ayyash, "Internet of Things: A Survey on Enabling Technologies, Protocols, and Applications," IEEE Commun. Surv. Tuts., vol.17, no.4, pp.2347–2376, Oct. 2015.

[13] "IEEE 802.11 Task Group ah (TGah) Sub 1 GHz license-exempt operation". `http://www.ieee802.org/11/Reports/tgah_update.htm`

[14] D. Gurney, G. Buchwald, L. Ecklund, S. Kuffner, and J. Grosspietsch, "Geo-location database techniques for incumbent protection in the TV white space," Proc. IEEE 2008 Int. Symp. Dyn. Spectr. Access Networks, pp.232–240, Chicago, IL, Aug. 2008.

[15] M. Barrie, S. Delaere, G. Sukareviciene, J. Gesquiere, and I. Moerman, "Geolocation database beyond TV white spaces? Matching applications with database requirements," Proc. IEEE 2012 Int. Symp. New Front. Dyn. Spectr. Access Networks, pp.467–478, Bellevue, WA, Oct. 2012.

[16] K. Sato, M. Kitamura, K. Inage, and T. Fujii, "Measurement-based spectrum database for flexible spectrum management," IEICE Trans. Commun., vol.E98-B, no.10, pp.2004–2013, Oct. 2015.

[17] M. Vu, N. Devroye, and V. Tarokh, "On the primary exclusive region of cognitive networks," IEEE Trans. Commun., vol.8, no.7, pp.3380–3385, July 2009.

[18] R. Murty, R. Chandra, T. Moscibroda, and P. Bahl, "Sense Less : A Database Driven White Spaces Network," IEEE Trans. Mob. Comput., vol.11, no.2, pp.189–203, Feb. 2012.

[19] R. Dahama, K.W. Sowerby, and G.B. Rowe, "Estimating protection distances in spectrum sharing systems," IEEE Trans. Signal Process., vol.61, no.17, pp.4284–4295, Sept. 2013.

[20] M.S. Ali and N.B. Mehta, "Modeling time-varying aggregate interference in cognitive radio systems, and application to primary exclusive zone design," IEEE Trans. Wirel. Commun., vol.13, no.1, pp.429–439, Jan. 2014.

[21] U. Tefek, S. Member, T.J. Lim, and S. Member, "Interference management through exclusion zones in two-tier cognitive networks," IEEE Trans. Wirel. Commun., vol.15, no.3, pp.2292–2302, March 2016.

[22] S. Bhattarai, A. Ullah, J.M.J. Park, J.H. Reed, D. Gurney, and B. Gao, "Defining incumbent protection zones on the fly: Dynamic boundaries for spectrum sharing," Proc. IEEE 2015 Int. Symp. Dyn. Spectr. Access Networks, pp.251–262, Sept. 2015.

[23] M. Haenggi, Stochastic Geometry for Wireless Networks, Cambridge Univ. Pr., Nov. 2012.

[24] H. ElSawy, E. Hossain, and M. Haenggi, "Stochastic geometry for modeling, analysis, and design of multi-tier and cognitive cellular wireless networks: A survey," IEEE Commun. Surv. Tuts., vol.15, no.3, pp.996–1019, July 2013.

[25] H. ElSawy, A. Sultan-Salem, M.-S. Alouini, and M.Z. Win, "Modeling and Analysis of Cellular Networks using Stochastic Geometry: A Tutorial," IEEE Commun. Surv. Tuts., vol.19, no.1, pp.167–203, Jan. 2017.

[26] J. Hsu, S. Zahedi, A. Kansal, M. Srivastava, and V. Raghunathan, "Adaptive duty cycling for energy harvesting systems," Proc. ACM/IEEE 2006 Int. Symp. Low Power Electron. Des., pp.180–185, New York, USA, Oct. 2006.

[27] A. Kansal, J. Hsu, S. Zahedi, and M.B. Srivastava, "Power Management in Energy Harvesting Sensor Networks," ACM Trans. Embed. Comput. Syst., vol.6, no.4, pp.1–38, Sept. 2007.

[28] T. Ichihara, T. Mitani, and N. Shinohara, "Study on intermittent microwave power transmission to a ZigBee device," Proc. IEEE MTT-S Int. Microw. Symp. Ser. Innov. Wirel. Power Transm., pp.209–212, Kyoto, Japan, May 2012.

[29] D. Maehara, R. Akai, G.K. Tran, K. Sakaguchi, S. Sampei, K. Araki, and H. Iwai, "Experiment on battery-less sensor activation via multi-point wireless energy transmission," Proc. IEEE 24th Annu. Int. Symp. Pers. Indoor Mob. Radio Commun., pp.2336–2340, London, United Kingdom, Sept. 2013.

[30] A. Kamerman and L. Monteban, "WaveLAN-II: A high-performance wireless LAN for the unlicensed band," Bell Labs Tech. J., vol.2, no.3, pp.113–133, June 1997.

[31] G. Holland, N. Vaidya, and P. Bahl, "A rate-adaptive MAC protocol for multi-hop wireless networks," Proc. ACM Spec. Interes. Gr. Mobil. Syst. Users, Data, Comput., pp.236–250, New York, USA, July 2001.

[32] "Madwifi Onoe specification". `http://sourceforge.net/projects/madwifi`

[33] J.C. Bicket, "Bit-rate selection in wireless networks," MIT Master's Thesis, pp.1–50, Feb. 2005.

[34] Q. Pang, V.C.M. Leung, and S.C. Liew, "A rate adaptation algorithm for IEEE 802.11 WLANs based on MAC-layer loss differentiation," Proc. IEEE 2nd Int. Conf. Broadband Networks, pp.659–667, Boston, Massachusetts, USA, Oct. 2005.

[35] J. Kim, S. Kim, S. Choi, and D. Qiao, "CARA: Collision-aware rate adaptation for IEEE 802.11 WLANs," Proc. IEEE 25th Int. Conf. Comput. Commun., pp.146–157, Barcelona, Catalunya, Spain, April 2006.

[36] S. Biaz and S. Wu, "Loss differentiated rate adaptation in wireless networks," Proc. IEEE Wirel. Commun. Netw. Conf. 2008, pp.1639–1644, April 2008.

[37] S. Wu, S. Biaz, and H. Wang, "Rate adaptation with loss diagnosis on IEEE 802.11 networks," Int. J. Commun. Syst., vol.25, no.4, pp.515–528, April 2012.

[38] J. Zhang, K. Tan, J. Zhao, H. Wu, and Y. Zhang, "A practical SNR-guided rate adaptation," Proc. IEEE 27th Int. Conf. Comput. Commun., pp.146–150, Phoenix, AZ, USA, April 2008.

[39] K. Pelechrinis, I. Broustis, S.V. Krishnamurthy, and C. Gkantsidis, "A measurement-driven anti-jamming system for 802.11 networks," IEEE/ACM Trans. Netw., vol.19, no.4, pp.1208–1222, Aug. 2011.

[40] D. Aguayo, J. Bicket, S. Biswas, G. Judd, and R. Morris, "Link-level measurements from an 802.11b mesh network," Proc. ACM Spec. Interes. Gr. Data Commun. Int. Conf., pp.121–132, New York, USA, Aug. 2004.

[41] M. Denkovska, P. Latkoski, and L. Gavrilovska, "Geolocation database approach for secondary spectrum usage of TVWS," Proc. IEEE 19th Telecommun. Forum, pp.369–372, Nov. 2011.

[42] R. Dahama, K.W. Sowerby, and G.B. Rowe, "Approximations for distributions of aggregate interference in spectrum sharing systems," Proc. IEEE 16th Asia-Pacific Conf. Commun., pp.95–100, Oct. 2010.

[43] M. Palola, M. Matinmikko, J. Prokkola, M. Mustonen, M. Heikkilä, T. Kippola, S. Yrjölä, V. Hartikainen, L. Tudose, A. Kivinen, J. Paavola, K. Heiska, T. Hänninen, and J. Okkonen, "Description of finnish Licensed Shared Access (LSA) field trial using TD-LTE in 2.3 GHz band," Proc. IEEE 2014 Int. Symp. Dyn. Spectr. Access Networks, pp.374–375, McLean, VA, USA, April 2014.

[44] M. Palola, M. Matinmikko, J. Prokkola, M. Mustonen, M. Heikkila, T. Kippola, S. Yrjola, V. Hartikainen, L. Tudose, A. Kivinen, J. Paavola, and K. Heiska, "Live field trial of Licensed Shared Access (LSA) concept using LTE network in 2.3 GHz band," Proc. IEEE 2014 Int. Symp. Dyn. Spectr. Access Networks, pp.38–47, McLean, VA, USA, April 2014.

[45] J. Kalliovaara, T. Jokela, R. Ekman, J. Hallio, M. Jakobsson, T. Kippola, and M. Matinmikko, “Interference measurements for Licensed Shared Access (LSA) between LTE and wireless cameras in 2.3 GHz band,” Proc. IEEE 2015 Int. Symp. Dyn. Spectr. Access Networks, pp.123–129, Stockholm, Sweden, Sept. 2015.

[46] ETSI, “Reconfigurable Radio Systems (RRS); Information elements and protocols for the interface between LSA Controller (LC) and LSA Repository (LR) for operation of Licensed Shared Access (LSA) in the 2300 MHz - 2400 MHz band,” Technical report, TS 103 379 - V1.1.1, Jan. 2017.

[47] H.T. Friis, “A note on a simple transmission formula,” Proc. IRE Waves Electrons, vol.34, no.5, pp.254–256, May 1946.

[48] X. Lu, P. Wang, D. Niyato, D.I. Kim, Z. Han, and C. Engineering, “Wireless networks with RF energy harvesting : A contemporary survey,” IEEE Commun. Surv. Tuts., vol.17, no.2, pp.1–34, April 2015.

[49] “mac80211”. http://wireless.kernel.org/en/developers/Documentation/mac80211

[50] W. Yin, P. Hu, J. Indulska, and K. Bialkowski, “Performance of mac80211 rate control mechanisms,” Proc. ACM 14th Int. Conf. Model. Anal. Simul. Wirel. Mob. Syst., pp.427–436, New York, NY, USA, Nov. 2011.

[51] D. Xia, J. Hart, and Q. Fu, “Evaluation of the Minstrel rate adaptation algorithm in IEEE 802.11g WLANs,” Proc. IEEE Int. Conf. Commun., pp.2223–2228, Budapest, Hungary, June 2013.

[52] “PID”. http://linuxwireless.sipsolutions.net/en/developers/Documentation/mac80211/RateControl/PID/

[53] “Minstrel Specification”. http://madwifi-project.org/svn/madwifi/trunk/ath_rate/minstrel/minstrel.txt

[54] T.J. Telecommun. Technol. Council Ministry Posts Telecommun. Deliberation Rep.89, “Radio-radiation protection guidelines for human exposure to electromagnetic fields,” 1997.

[55] "ArduinoBoardFio". http://arduino.cc/en/Main/ArduinoBoardFio

[56] "XBee Wi-Fi". https://www.digi.com/products/xbee-rf-solutions/2-4-ghz-modules/xbee-wi-fi

[57] "Raspberry Pi Model B+". http://www.raspberrypi.org/products/model-b-plus

[58] "ArduinoBoardUno". http://arduino.cc/en/Main/arduinoBoardUno

[59] "Iperf". http://www.iperf.fr

[60] "Wireshark". https://www.wireshark.org

[61] M. Haenggi, J.G. Andrews, F. Baccelli, O. Dousse, and M. Franceschetti, "Stochastic geometry and random graphs for the analysis and design of wireless networks," IEEE J. Sel. Areas Commun., vol.27, no.7, pp.1029–1046, Sept. 2009.

[62] 3GPP, "Evolved Universal Terrestrial Radio Access (E-UTRA); Physical Layer Procedures (Release 10)," Technical report, TR 36.213, April 2015.

[63] D.C. Schleher, "Generalized Gram-Charlier series with application to the sum of log-normal variates," IEEE Trans. Inf. Theory, vol.23, no.2, pp.275–280, May 1977.

[64] M. Timmers, S. Pollin, A. Dejonghe, A. Bahai, L.V. derPerre, and F. Catthoor, "Accumulative interference modeling for cognitive radios with distributed channel access," Proc. IEEE 3rd Int. Conf. Cogn. Radio Oriented Wirel. Networks Commun., pp.1–7, May 2008.

[65] S.A.R. Zaidi, D.C. McLernon, and M. Ghogho, "Outage probability analysis of cognitive radio networks under self-coexistence constraint," Proc. IEEE 44th Annu. Conf. Inf. Sci. Syst., pp.1–6, March 2010.

[66] R.W. Heath, M. Kountouris, and T. Bai, "Modeling heterogeneous network interference using poisson point processes," IEEE Trans. Signal Process., vol.61, no.16, pp.4114–4126, Aug. 2013.

[67] A. Ghasemi and E.S. Sousa, “Interference aggregation in spectrum-sensing cognitive wireless networks,” IEEE J. Sel. Top. Signal Process., vol.2, no.1, pp.41–56, Feb. 2008.

[68] K.L.Q. Read, “A lognormal approximation for the collector’s problem,” Amer. Stat., vol.52, no.2, pp.175–180, May 1998.

[69] S. Sinanović, G. Auer, and H. Haas, “Interference analysis of busy burst enabled interference avoidance,” Proc. IEEE 2010 Glob. Commun. Conf., pp.1–5, Dec. 2010.

[70] F. Paisana, N. Marchetti, and L.A. Dasilva, “Radar, TV and cellular bands: Which spectrum access techniques for which bands?,” IEEE Commun. Surv. Tuts., vol.16, no.3, pp.1193–1220, 2014.

[71] M.K Simon and M.S Alouini, Digital Communication over Fading Channels, Johon Wiley & Sons, Inc., 2004.

[72] J.F. Kenney and E.S. Keeping, Mathematics of Statistics, Pt. 2, 3rd ed. edition, Princeton, NJ: Van Nostrand, 1957.

[73] K.W. Sung, M. Tercero, and J. Zander, “Aggregate interference in secondary access with interference protection,” IEEE Commun. Lett., vol.15, no.6, pp.629–631, April 2011.

[74] W.L. Stutzman and G.A. Thiele, Antenna Theory and Design, 3rd Edition, John Wiley & Sons, Inc., May 2012.

[75] W.E. Hart, C. Laird, J.-P. Watson, and D.L. Woodruff, Pyomo âĂŞ Optimization Modeling in Python, vol.67, Springer Optimization and Its Applications, 2012.

[76] A. Wächter and L.T. Biegler, “On the implementation of a primal-dual interior point filter line search algorithm for large-scale nonlinear programming,” Math. Program., vol.106, no.1, pp.25–57, March 2006.

[77] “Ipopt”. `https://projects.coin-or.org/Ipopt`

Author's Publication List

Journal Papers

1. N. Imoto, S. Yamashita, T. Ichihara, K. Yamamoto, T. Nishio, M. Morikura, and N. Shinohara, "Experimental investigation of co-channel and adjacent channel operations of microwave power and IEEE 802.11g data transmissions," IEICE Trans. Commun., vol.E97-B, no.9, pp.1835–1842, Sept. 2014.

2. S. Yamashita, N. Imoto, T. Ichihara, K. Yamamoto, T. Nishio, M. Morikura, and N. Shinohara, "Implementation and feasibility study of co-channel operation system of microwave power transmissions to IEEE 802.11-based batteryless sensor," IEICE Trans. Commun., vol.E97-B, no.9, pp.1843–1852, Sept. 2014.

3. S. Yamashita, K. Sakaguchi, Y. Huang, K. Yamamoto, T. Nishio, M. Morikura, and N. Shinohara, "Rate adaptation based on exposure assessment using rectenna output for WLAN station powered with microwave power transmission," IEICE Trans. Commun., vol.E98-B, no.9, pp.1785–1794, Sept. 2015.

4. S. Yamashita, K. Yamamoto, T. Nishio, and M. Morikura, "Knowledge-based reestablishment of primary exclusive region in database-driven spectrum sharing," IEICE Trans. Commun., vol.E99-B, no.9, pp.2019–2027, Sept. 2016.

5. S. Yamashita, K. Yamamoto, T. Nishio, and M. Morikura, "Performance analysis of secondary networks with multiple primary users for spectrum

database system," IEICE Commun. Express, vol.6, no.5, pp.225–230, May 2017.

International Conference Papers

1. N. Imoto, S. Yamashita, K. Yamamoto, and M. Morikura, "Experiment of power and data transmission scheduling for single wireless LAN sensor," Proc. the 2013 International Symposium on Electromagnetic Theory (URSI EMTS), Hiroshima, May 2013.

2. S. Yamashita, N, Imoto, T. Ichihara, K. Yamamoto, M. Morikura, and N. Shinohara, "Co-channel operation of microwave power and IEEE 802.11-based data transmissions: A feasibility study," Proc. IEEE the 19th Asia-Pacific Conference on Communications (APCC2013), pp.115–159, Bali, Indonesia, Aug. 2013.

3. N. Imoto, S. Yamashita, T. Ichihara, K. Yamamoto, M. Morikura, and N. Shinohara, "Experiment of microwave power and data transmission scheduling for IEEE 802.11-based sensor networks," Proc. IEEE the 28th Annual International Symposium on Personal, Indoor and Mobile Radio Communications (PIMRC2013), London, UK, Sept. 2013.

4. K. Sakaguchi, S. Yamashita, Y. Huang, K. Yamamoto, T. Nishio, M. Morikura, and N. Shinohara, "Experiment of power supply method for WLAN sensor using both energy harvesting and microwave power transmissions," Proc. the 14th International Conference on Micro and Nanotechnology for Power Generation and Energy Conversion Applications (PowerMEMS2014), Awaji Island, Hyogo, Japan, Nov. 2014.

5. S. Yamashita, K. Yamamoto, T. Nishio, and M. Morikura, "Knowledge-based update of primary exclusive region for database-driven spectrum sharing towards 5G," Proc. IEEE Wireless Communications and Networking Conference (WCNC) 2016 International Workshop on Smart Spectrum (IWSS), pp. 473–476, Doha, Qatar, April 2016.

6. S. Yamashita, K. Yamamoto, T. Nishio, and M. Morikura, "Performance analysis in secondary networks with multiple primary users for

database-driven spectrum sharing," Proc. the 13th IEEE Vehicular Technology Society Asia Pacific Wireless Communications Symposium (APWCS), Tokyo, Japan, Aug. 2016.

7. S. Yamashita, K. Yamamoto, T. Nishio, and M. Morikura, "Optimization of primary exclusion region in spatial grid-based spectrum database using stochastic geometry," Proc. IEEE International Conference on Communications (ICC2017), Paris, France, May 2017.

8. S. Yamashita, K. Yamamoto, T. Nishio, and M. Morikura, "Stochastic geometry analysis of spatial grid-based spectrum database," Proc. the 85th IEEE Vehicular Technology Conference (VTC2017-Spring), Sydney, Australia, June 2017.

9. K. Yoshikawa, S. Yamashita, K. Yamamoto, T. Nishio, and M. Morikura, "Resource allocation for 3D drone networks sharing spectrum bands," Proc. the 86th IEEE Vehicular Technology Conference (VTC2017-Fall), Toronto, Canada, Sept. 2017.

Technical Meeting Papers

1. N. Imoto, S. Yamashita, K. Yamamoto, M. Morikura, "Experiment of data and power transmission scheduling for single wireless LAN station," IEICE Technical Report, USN2012-57, pp. 3–7, Jan. 2013.

2. S. Yamashita, N. Imoto, T. Ichihara, K. Yamamoto, M. Morikura, and N. Shinohara, "Energy-aware transmission schedulingfor batteryless wireless LAN using microwave power transmission," IEICE Technical Report, WPT2012-48, pp.40–45, March 2013.

3. S. Yamashita, N. Imoto, T. Ichihara, K. Yamamoto, M. Morikura, and N. Shinohara, "Experiment on charge and communication schedulingfor single wireless LAN terminal using microwave power transmission," IEICE Technical Report, ASN2013-16, pp.85–90, May 2013.

4. N. Imoto, S. Yamashita, T. Ichihara, K. Yamamoto, T. Nishio, M. Morikura, and N. Shinohara, "Experimental investigation of time and

frequency division of microwave power transmission for wireless LAN communications," IEICE Technical Report, WPT2013-40, pp. 29–34, March 2014.

5. S. Yamashita, K. Yamamoto, T. Nishio, M. Morikura, and N. Shinohara, "Experiment on power and data transmission scheduling for wireless LAN terminal powered with microwave power transmission," IEICE Technical Report, SR2014-10, pp.65–68, May 2014.

6. K. Sakaguchi, S. Yamashita, K. Yamamoto, T. Nishio, and M. Morikura, "A study of powering WLAN station using both energy harvesting and microwave power transmission," IEICE Technical Report, ASN2014-19, pp.63–66, May 2014.

7. S. Yamashita, K. Sakaguchi, Y. Huang, K. Yamamoto, T. Nishio, M. Morikura, and N. Shinohara, "Experiment on rate adaptation scheme with rectenna for wireless LAN sensor receiving microwave power," IEICE Technical Report, WPT2014-97, pp.21–24, March 2015.

8. K. Yamamoto, S. Yamashita, T. Nishio, and M. Morikura, "[Invited Talk] ENTERPRICE M2M network consisting of enourmous number of terminals," IEICE Technical Report, SR2015-10, pp. 59–63, May 2015.

9. S. Yamashita, K. Yamamoto, T. Nishio, and M. Morikura, "Auxiliary update of primary exclusive region for database-driven spectrum sharing," IEICE Technical Report, SR2015-80, pp.57–61, Jan. 2016.

10. S. Yamashita, K. Sakaguchi, Y. Huang, K. Yamamoto, T. Nishio, M. Morikura, and N. Shinohara, "Experiment on coexistence scheme for wireless LAN system with microwave power transmission," IEICE Technical Report, WPT2015-92, pp.85–90, March 2016.

11. S. Yamashita, K. Yamamoto, T. Nishio, and M. Morikura, "Secondary network analysis with multiple primary users for database-assisted spectrum sharing system," IEICE Technical Report, SR2016-95, pp. 25–27, March 2017.

12. K. Yoshikawa, S. Yamashita, K. Yamamoto, T. Nishio, and M. Morikura, “Resource allocation for 3D drone networks operating in licensed spectrum,” IEICE Technical Report, RCS2017-06, pp. 103–107, June 2017.

Local Conference Papers

1. N. Imoto, S. Yamashita, T. Ichihara, K. Yamamoto, M. Morikura, and N. Shinohara, “Experiment of wireless LAN frame transmission during microwave power transmission,” Proc. IEICE Gen. Conf., B-19-3, p.547, March 2013.

2. S. Yamashita, N. Imoto, T. Ichihara, K. Yamamoto, M. Morikura, and N. Shinohara, “Experiment of energy-aware transmission scheduling for batteryless wireless LAN using microwave power transmission,” Proc. IEICE Gen. Conf., B-19-1, p.545, March 2013.

3. K. Sakaguchi, S. Yamashita, N. Imoto, K. Yamamoto, T. Nishio, and M. Morikura, “Energy-aware power transmission scheduling using multiple power sources,” Proc. IEICE Gen. Conf., B-18-45, p.613, March 2014.

4. S. Yamashita, N. Imoto, T. Ichihara, K. Yamamoto, T. Nishio, M. Morikura, and N. Shinohara, “Feasibility study of battery-less WLAN sensor using microwave power transmissions,” Proc. IEICE Gen. Conf., BCS-1-16, pp.44–45, March 2014.

5. K. Sakaguchi, S. Yamashita, Y. Huang, K. Yamamoto, T. Nishio, M. Morikura, and N. Shinohara, “Experiment of power supply method for WLAN sensor operated with microwave power transmission and energy harvesting,” Proc. IEICE Commun. Conf., B-21-14, p.449, Sept. 2014.

6. S. Yamashita, K. Yamamoto, T. Nishio, M. Morikura, and N. Shinohara, “Proposal of rate control algorithm for wireless sensor powered with microwave power transmission,” Proc. IEICE Commun. Conf., B-18-36, p.394, Sept. 2014.

7. S. Yamashita, K. Sakaguchi, Y. Huang, K. Yamamoto, T. Nishio, M. Morikura, and N. Shinohara, “Experiment on rate adaptation scheme

using rectenna for WLAN station powered with microwave power transmission," Proc. IEICE Gen. Conf., B-21-18, p. 619, March 2015.

8. S. Yamashita, K. Sakaguchi, Y. Huang, K. Yamamoto, T. Nishio, M. Morikura, and N. Shinohara, "Experiments of rectenna-output-based rate adaptation scheme for WLAN station using microwave power transmission," Proc. IEICE Commun. Conf., B-18-12, p.346, Sept. 2015.

9. S. Yamashita, K. Yamamoto, T. Nishio, and M. Morikura, "Reestablishment of primary exclusive region in database-assisted spectrum sharing," Proc. IEICE Gen. Conf., B-17-16, p.619, March 2016.

10. T. Nakamura, S. Yamashita, K. Yamamoto, T. Nishio, and M. Morikura, "Network simulation of interference to primary user in database-assisted spectrum sharing system," Proc. IEICE Commun. Conf., B-17-26, p.425, Sept. 2016.

11. S. Yamashita, K. Yamamoto, T. Nishio, and M. Morikura, "Path-loss evaluation with terrain effects for designing primary exclusive region," Proc. IEICE Commun. Conf., B-17-25, p.424, Sept. 2016.

12. S. Yamashita, K. Yamamoto, T. Nishio, and M. Morikura, "Spectral efficiency analysis of secondary users with multiple primary users in database-driven spectrum sharing System," Proc. IEICE Gen. Conf., B-17-24, March 2017.

13. K. Yoshikawa, S. Yamashita, K. Yamamoto, T. Nishio, and M. Morikura, "Stochastic geometry analysis of interference in drone networks," Proc. IEICE Gen. Conf., B-17-25, March 2017.

14. K. Yoshikawa, S. Yamashita, K. Yamamoto, T. Nishio, and M. Morikura, "Stochastic geometry analysis of outage probability in drone networks with limited height," Proc. IEICE Gen. Conf., B-17-20, Sept. 2017.

Awards

1. IEEE VTS Tokyo Chapter 2017 Young Researcher's Encouragement Award